Lehigh University

INSTITUTE OF RESEARCH

Technical Report 4

DENSITY MEASUREMENT IN SHOCK TUBE FLOW WITH THE CHRONO-INTERFEROMETER

by

JOHN E. MACK

Submitted by
R. J. Emrich
15 April 1954

Project NR 061-063
Contract N7onr39302
Office of Naval Research

Reprinted from The Review of Scientific Instruments, Vol. 24, No. 11, 1069–1070, November, 1953
Printed in U. S. A.

Ring-Shaped Piezoelectric Gauge for Shock Tube*

R. A. Shunk, A. I. Dranetz,† and P. P. Rudenstein
Lehigh University, Bethlehem, Pennsylvania
(Received March 12, 1953)

TRANSIENT pressures in fluids have been studied by piezoelectric elements having a disk or slab shape.[1] A piezoelectric element which conforms to the curved wall of a shock tube has been constructed of barium titanate ceramic; this material can be molded into various shapes and the orientation of its piezoelectric axes chosen at will. Minimum disturbance of the flow, a large sensitive area, and simplicity of mounting result from the symmetry of the ring-shaped element whose inside diameter is the same as that of the shock tube.

The mount for the piezoelectric element is shown in Fig. 1. The gauge mount can be inserted between flanges at any point in the shock tube. The $1\frac{3}{8}$-in. i.d.$\times 1\frac{5}{8}$-in. o.d.$\times \frac{1}{4}$-in. ceramic element is of Glennite No. 103, made by the Gulton Manufacturing Corporation. Silver platings on the inside and outside surfaces serve as electrodes both for initially polarizing the ceramic in the radial direction and for pickup electrodes when it is used as a piezoelectric element. The outside electrode is electrically insulated from the duralumin mount by a Lucite ring and by $\frac{1}{32}$ in. thick Neoprene rings. The latter are gas seals which also help to damp the free vibrations of the piezoelectric element.

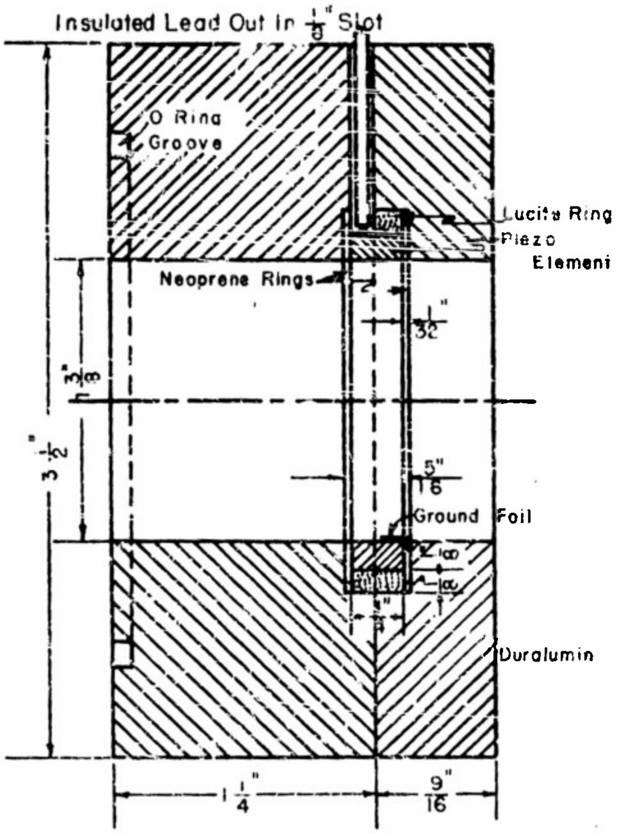

FIG. 1. Mount for ring-type piezoelectric element. "O" rings form gas seals where the mount is bolted between flanges of the shock tube. ⅛ inch diameter hardened steel pins are used at all joints for alignment. The inner electrode is grounded with 0.003-inch gold foil soldered to silver plating and pressed between duralumin mount and rubber seal.

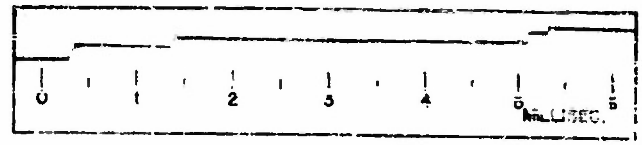

FIG. 2. Oscillographic record of potentials appearing across two gauges and a condenser connected in parallel as two overtaking shocks pass. The sudden increases in pressure with the arrival of each shock at a gauge cause damped vibrations having the natural frequency of the element.

The approximate characteristics observed for the three gauges which have been built are

dc leakage resistance—>200 megohms,
capacity—0.005 μf,
sensitivity—1000 $\mu\mu$ coulomb/psi
natural frequency—4×10^4 sec^{-1}
damping of natural vibrations—half amplitude—in 75 μsec.

Pressures above 60 psi have not been used so the ultimate strength of the element is not known. The electrical behavior of the element is such that it does not have a capacitance in the ordinary sense; the value given was obtained by momentarily shunting the element across a charged 0.03 μf condenser and noting the change in potential difference with an electrometer.

The dc amplifiers are used in recording the transient potentials appearing across the gauge. The input amplifier has a floating input grid so that the input impedance is greater than 10^8 ohms and shunting capacitors of 0.05 μf or greater may be used to permit recording during 30 msec intervals without an observable electrical transient. RC coupling with 4 second time constant is used to a dc cathode-ray deflection amplifier. The cathode-ray spot is recorded on 35-mm film in a rotating drum.

Figure 2 is a portion of a record. In this example, two gauges 2 in apart in the shock tube are in parallel with a 0.1 μf capacitor. Two shocks, one overtaking the other, are both recorded at each gauge.

The reproducibility of records obtained by successive trials with identical starting conditions is within the 2–3 percent accuracy with which the deflections on the film can be measured. However, the proportionality of deflection on the film to pressure in the shock tube has not been demonstrated. This gauge suffers, in common with all piezoelectric gauges, the disadvantage that it cannot be calibrated statically. This and three other types of pressure gauge have confirmed a continuing rise in pressure of the gas in the shock tube after the shock passes.

Thus, even though the pressure jump across the shock is known from shock velocity measurements, so that the initial rise can be calibrated, it is not possible to calibrate the long-time characteristic of the gauge in the shock tube by assuming constant pressure in the flow following the shock. An observed temperature sensitivity of the gauge has been reduced, probably to a negligible level, by covering the inner surface with Scotch Electrical Tape.

* Supported by the U. S. Office of Naval Research.
† Gulton Manufacturing Corporation, Metuchen, New Jersey.
[1] A. B. Arons and R. H. Cole, Rev. Sci. Instr. 21, 31 (1950).

DENSITY MEASUREMENT

IN SHOCK TUBE FLOW WITH

THE CHRONO-INTERFEROMETER

by

John E. Mack

Technical Report No 4

Project NR 061-063

issued under contract N7onr39302

between the Office of Naval Research

and the Institute of Research,

Lehigh University

This report which comprises the Ph.D. thesis of the author describes the design, development, and testing of a new instrument -- the chrono-interferometer -- for transient flow measurements, and presents an extensive set of measurements made of gas density throughout shock tube flows. This work constitutes a part of a program of study of transient flow of gases in a tube, jointly supported by ONR and the Physics Department. The research reported herein was performed from September 1951 to February 1954.

R. J. Emrich

C. W. Curtis

ABSTRACT

A new instrument measuring absolute gas densities in unsteady flows as a function of time has been developed. The instrument is best suited to the study of one-dimensional flows without steep density gradients; its chief advantage lies in the absence of any essential limitation to the extent of a flow which it can record. By studying the density variation in space and time throughout primary shock tube flows in a 3.5 cm diameter tube, it has been found that 1) the gas density increases within the hot gas by as much as 50% of the density increase across the shock, 2) the cold front spreads out, eventually occupying a space along the tube equal to 60 tube diameters, and 3) the density decreases within the rarefaction in the chamber by only 80% of the decrease which would occur in the centered isentropic wave ordinarily assumed in the ideal shock tube theory.

CONTENTS

I Introduction

Predictions of the gas flow in a shock tube are customarily based on two simplifying assumptions. First, it is supposed that immediately upon bursting the diaphragm which initially divides the tube into the high pressure chamber and the low pressure channel, a shock and a rarefaction form at the diaphragm position. At this instant and at this position, the shock and the rarefaction are taken to be plane and fully developed. Second, by assuming that the subsequent flow is one dimensional, adiabatic, and inviscid, interactions with the walls of the tube are neglected. It is considered that the flow is uniform and steady between the shock and rarefaction with a contact surface moving with the gas from the diaphragm position. The shock progresses down the tube with a constant speed.[1]

Under conditions at which shock tubes are usually operated, calculations based upon the idealized theory agree reasonably well with experimental results. It is generally recognized, however, that the agreement is not exact. Measurements have shown that the shock velocity[2,3,4,5] and the density change across the shock[2] are less

---

1. The mathematical treatment of the idealized shock-tube flow is summarized in appendix C.
2. Bleakney, Weimer, and Fletcher, Rev. Sci. Instr. 20, 807 (1949)
3. R. J. Emrich and C. W. Curtis, J. Appl. Phys. 24, 360 (1952)
4. R. N. Hollyer, Jr., Engineering Research Report TO IV, University of Michigan (1953)
5. R. K. Lobb, Institute of Aerophysics Report No. 8, University of Toronto (1950)

than predicted by theory. The shock velocity is not constant as the shock travels down the tube.[3] It has been demonstrated that the region of flow between the shock and rarefaction is not uniform and steady[4,5,6].

Further study of the processes taking place in the shock tube requires more detailed measurements throughout the entire extent and duration of the flow. Of the pertinent variables which may be used to specify the flow -- temperature, pressure, density, particle velocity, shock velocity, and Mach number -- only shock velocity and density have been demonstrated to be susceptible to absolute measurement. Shock velocity measurements, however, only give information on the flow directly behind the shock. Therefore the second variable susceptible to absolute measurement, the density, was measured by optical interferometry for the further study of shock-tube flow which is presented in this thesis.

To find gas density by interferometric means throughout the entire extent and duration of the flow, measurement can be made either over a region in space at a given time or over a period of time at a given position. The first of these methods has been applied to the study of a wide range

- -

6. F. W. Geiger and C. W. Mautz, Engineering Research Institute Report TO IV, University of Michigan (1949)

of problems[2], but the measurement throughout the large extent and duration of the shock-tube flow is performed more efficiently over a period of time at a fixed position. The new instrument designed to perform this function has been termed the "chrono-interferometer".

The 13 meter long shock tube previously used in the shock velocity loss studies[3] and studies of shock formation and growth[7] was available. This tube is constructed of 1-3/8 inch diameter brass and Lucite tubing in interchangeable sections. The sections of tubing, which are bolted together at flanges and sealed with "O" ring gaskets, are supported by clamps fixed to a heavy five-inch steel beam. Light stations for shock detection, and two recording oscillographs with accurate time bases over 30 millisecond intervals were also available. A chrono-interferometer was constructed to observe density variations in this shock tube; the variations were recorded on one of the oscillographs.

This thesis is divided into two parts: the design, construction, and testing of the instrument comprise part A, while the density measurements in the shock-tube flow are presented in part B.

- -

7. A. B. Laponsky, Institute of Research Report TR 1, Lehigh University (1951). See also A. B. Laponsky and R. J. Emrich, J. Appl. Phys. 24, 1383 (1953)

A schematic diagram of the chrono-interferometer constructed is shown in Fig. 1. This instrument employs the Michelson arrangement of optical parts. After passing through the shock tube, the light beam in one arm of the instrument combines with the beam in the other arm to produce a single fringe across the entire field. The size of the field is determined by the 1/8" diameter of the windows W; their size was chosen such that sufficient light passes to operate the phototube without excessive deformation of the interior shock-tube surface. The resultant light intensity on the phototube depends upon the relative phase of the interfering beams; the intensity varies with the index of refraction, and hence with the density of the gas in the tube. A time record of the phototube's output is made on an oscillograph.

The time dependence of density in shock-tube flow was measured at four positions in the channel and at four positions in the chamber. These measurements extended only over the primary flow, that is over that portion of the flow unaffected by reflections from the closed ends of the shock tube. The maximum duration of primary flow was achieved for each of the four positions by arranging the shock tube as shown in Fig. 2. Measurements of channel and chamber flow were accomplished by arranging the higher

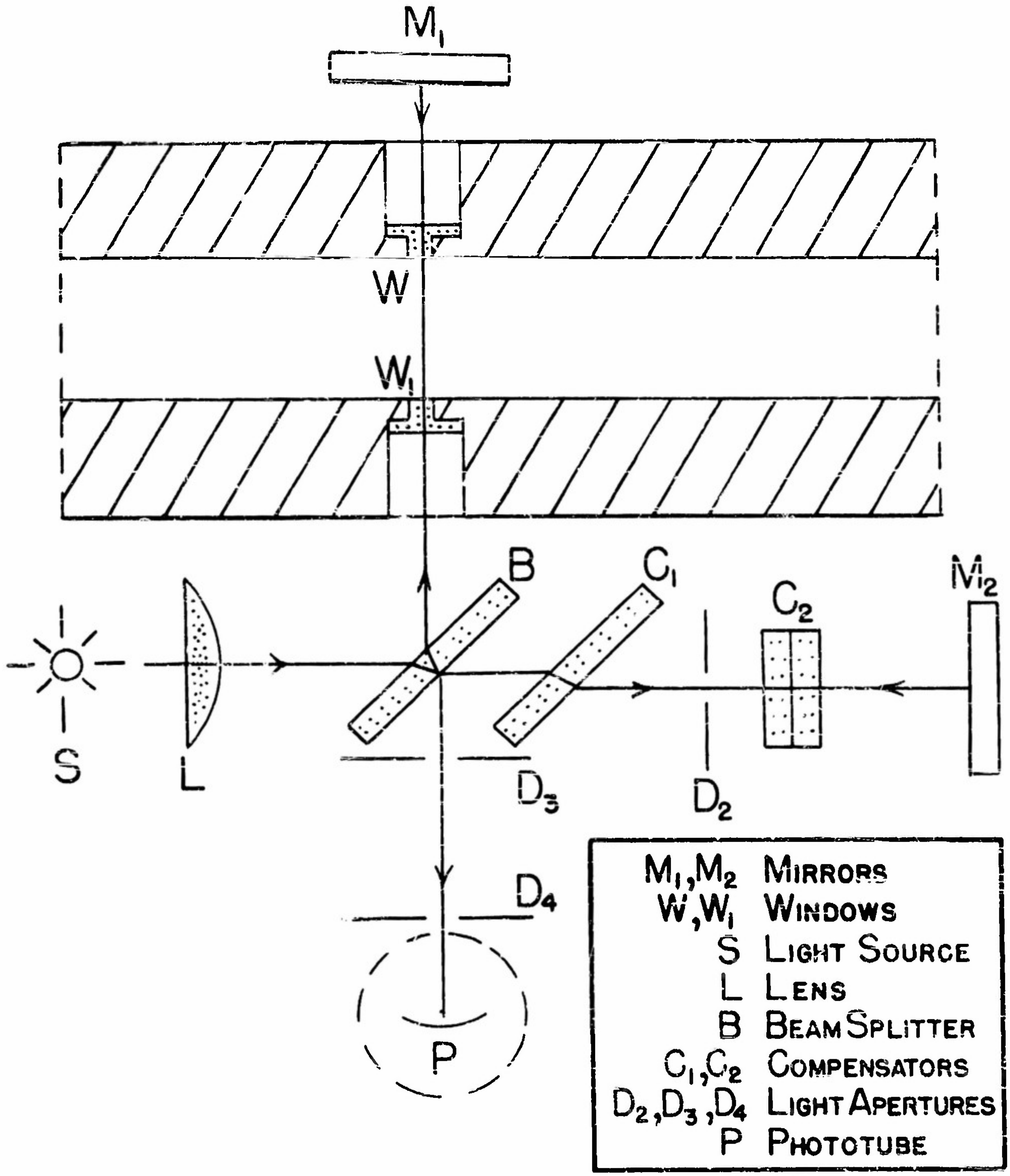

Fig. 1 Schematic Diagram of Chrono-interferometer

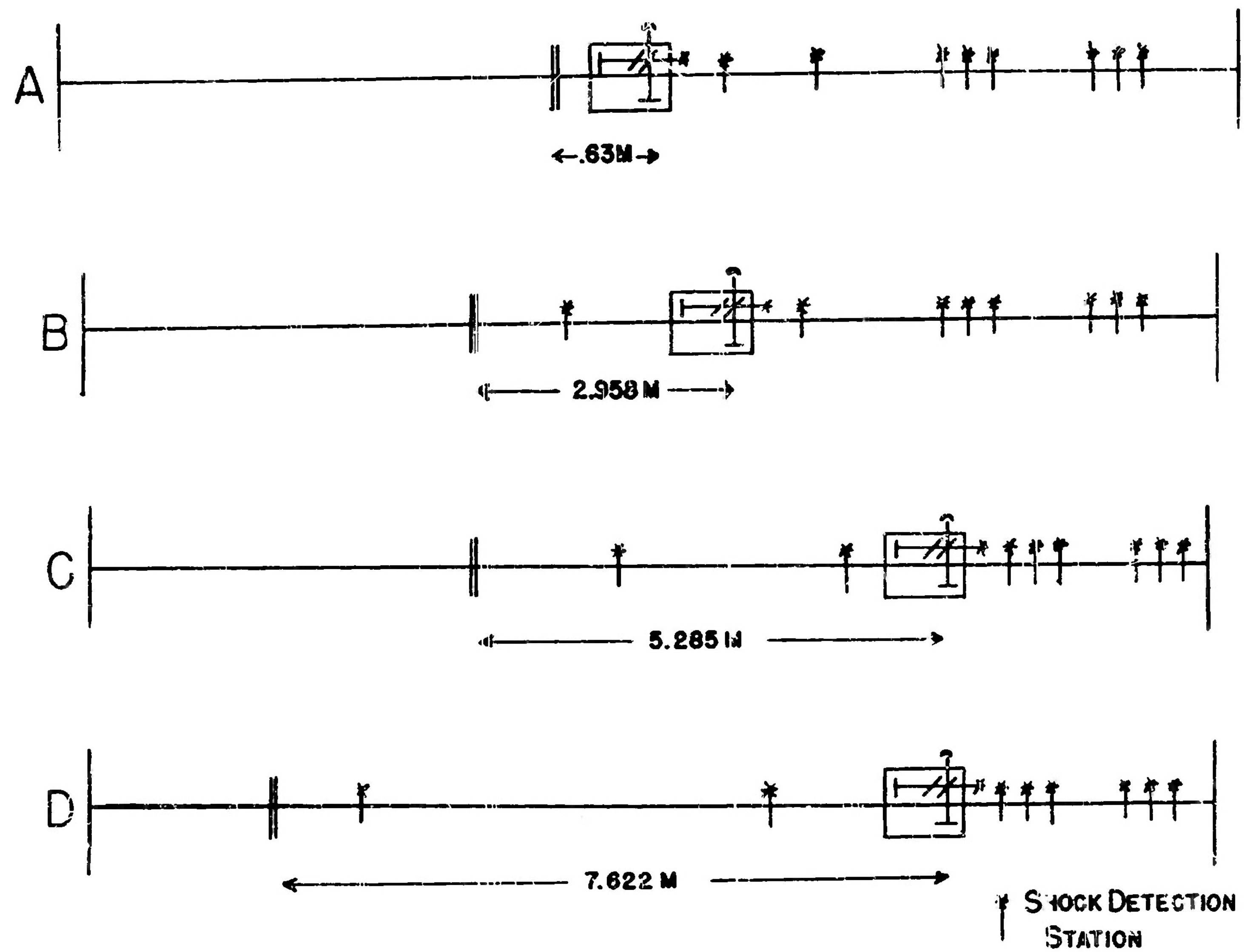

FIG. 2 ARRANGEMENT OF SHOCK TUBE AND INTERFEROMETER TO OBTAIN MAXIMUM DURATION OF PRIMARY FLOW

initial pressure across the diaphragm on the left hand and right hand sides respectively. Flows in nitrogen resulting from initial diaphragm pressure ratios of approximately 2, 10, and 50 were measured at each position. The flows studied include cases in which the hot gas and the cold gas are each either subsonic or supersonic.

PART A. THE CHRONO-INTERFEROMETER

II Design and Construction of the Instrument

2.1 General Features.

Photographs of the interferometer constructed for use on the 1-3/8 inch diameter shock tube are shown in Figs. 3 and 4. The instrument is supported from below by the steel beam on which the shock tube is mounted. The Michelson arrangement of components is employed. One of the interfering beams passes through the shock tube and recombines with the other interfering beam to produce a single fringe over the instrument's field, which is limited by 1/8" diameter windows in the shock tube. The relative phase of the interfering beams is dependent upon the index of refraction -- and hence the density -- of the gas in the tube. The measurement of the gas density during the transient shock-tube flow is obtained by photoelectrically recording the variations of the fringe pattern's light intensity on an oscillograph. The alternative method of recording an interference pattern directly on moving film has been employed elsewhere [8, 9, 10]; the oscillographic recording of a phototube signal has the advantage that a

---

8. R. Ladenburg, J. Winckler, and C. C. Van Voorhis, Phys. Rev. 73, 1367 (1948)
9. J. Winckler, Rev. Sci. Instr. 19, 307 (1948)
10. D. Bershader, Rev. Sci. Instr. 20, 260 (1949)

FIG. 3 THE CHRONO-INTERFEROMETER

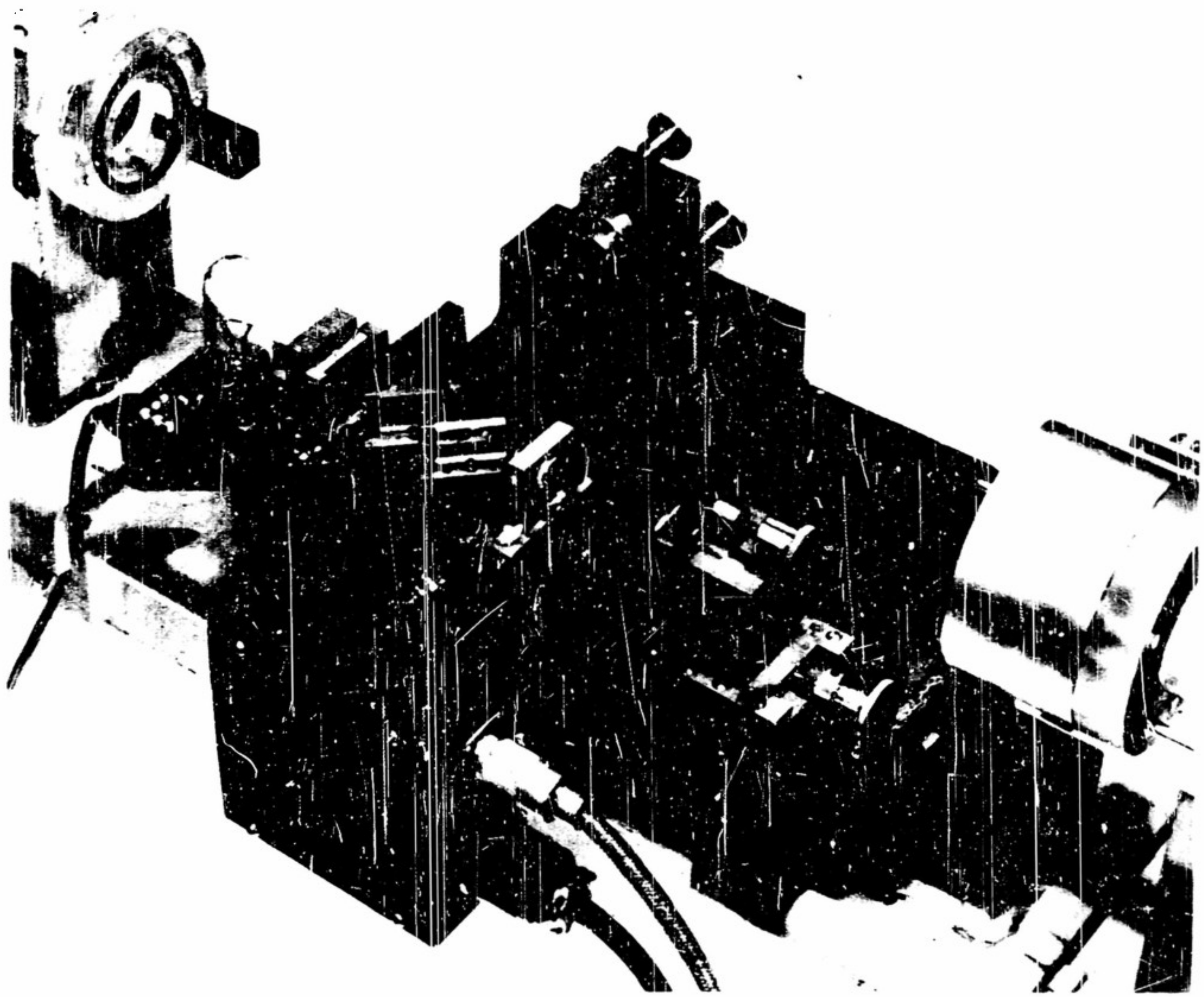

FIG. 4 INTERFEROMETER WITH SHOCK TUBE WINDOW SECTION REMOVED TO SHOW BASIC ELEMENTS

higher writing speed is possible, since the writing speed does not depend upon the intensity of the interfering beams.

2.2 Design.

In the chrono-interferometer the light intensity should be high, the relative phase of the interfering beams should be constant over the field of view, and the extraneous light on the phototube should be minimized.

The requirement of high intensity suggests an interferometer which can be used with an extended source. The Michelson arrangement was chosen mainly for its simplicity and because double sensitivity to changes in gas density is provided by the double passage of one interfering beam through the shock tube. The Michelson interferometer's inability to localize fringes[9] at any desired position is no restriction since the instrument is used with a single fringe adjustment. Light is furnished by a G.E..10v/7.5A/T8 sound reproducer lamp operated with direct current. A Western Union K100 concentrated arc source was also investigated as a possible source. In the current application, the higher radiancy of this source is not needed; furthermore the inherent instability of the arc was found to result in slowly varying changes in light intensity which are recorded by the phototube as spurious fringe shifts. To include the maximum amount of light available from the source in the interfering beams, the short focal length lens designated by L in Fig. 1 produces an image of the incandescent filament larger than W_1 somewhere between the entrance and exit windows of the instrument. The window W_1, together with its equivalent opening in the diaphragm D_2, determines the stop of the system. After reflection at the mirrors, these same stops limit the angles that the rays make with the optic axis. The cone of limiting rays that can pass the stops is completely intercepted by the lens L. The light source is made monochromatic by a 1 inch square Baird interference-film filter which has a half-intensity width of 150 Å centered about 5460 Å.

Since this instrument is designed for use on a shock tube of circular cross-section, the window openings in the tube wall had to be kept small to minimize distortion of the inner cylindrical surface of the tube. Small stops are also necessary so that the gas density very as little as possible over the cross-section of flow at any instant during the measurement. A lower limit to the stop size is set by the radiancy of the source and the sensitivity of the phototu . The choice of 1/8" diameter is a compromise to satisfy light intensity requirements and minimal distortion of the shock tube. The amount of light transmitted through the 1/8" diameter openings spaced effectively four inches apart is sufficient for operation of a 931A photo-multiplier tube with a signal to noise ratio of ten. R. A. Shunk has shown that slits as narrow as 1/32" can be used to stop down the interferometer field before phototube noise exceeds signal from changing fringe intensity.

The phase difference of the interfering rays in the emergent beam of light can be made essentially constant over the illuminated surface of the phototube without the use of an extra lens. It has been shown that the criterion for a constant phase over the phototube surface is that the instrument be adjusted for a single fringe over its field[11]. Since the single fringe adjustment is used in the chrono-interferometer, no lens is needed to focus the fringe on the phototube.

In order to minimize scattered light falling on the phototube, covers are placed over the light source, the interferometer, and the phototube, non-reflecting coatings are used on the shock-tube windows (W), and their compensating elements (C_2), and the diaphragms D_3 and D_4 (Fig. 1) are used to collimate the emergent interfering beams. The cover over the light source is provided with a forced air draft to remove the heat given off by the lamp. A sheet

11. C. W. Curtis, R. J. Emrich, and John Mack, "A Chrono-Interferometer for Measuring Gas Density During Transient Flow.", Rev. Sci. Instr. (To be published)

metal case (not shown in Figs. 3, 4) completely covers the interferometer to serve the dual purpose of a dust cover and a draft shield to eliminate thermal air currents in the outside interferometer beam.

2.3 Optical Components.

Although the use of small stops means that small optical components can be used, the requirement of single fringe adjustment imposes a restriction of high optical quality on the components. The basic Michelson components -- the beam splitter B, its compensator C_1, and the mirrors M_1 and M_2 (Fig. 1) -- were purchased from Gaertner Scientific Co., Chicago, Ill. The catalog specifications of these components are: "a pair of 15 x 25 x 5 mm thick matched plates, flat to 1/10 wavelength parallel to 1/4 wavelength; 2 pyrex mirrors, front surfaces aluminized, flat to 1/10 wavelength, 19 mm in diameter." The flatness of these components was not checked directly; however, the surfaces of the matched plates were found to be parallel only to 1 1/2 wavelength over their surfaces.

The shock-tube windows and their compensators were constructed to our specifications by Perkin-Elmer Corp., Norwalk, Conn. These windows are plug shaped (Fig. 1) and mounted with the inside surface tangent to the shock tube's wall. The special shock tube section for mounting these windows is described in section 2.4. These components were specified to be cut from the same piece of glass, flat to 1/4 wavelength, parallel to 1 wavelength over 1/8" of surface, and each element to have non-reflecting coatings at 5460 Å. Flat windows without the plug to fill the 0.060" deep recess in the shock tube wall were employed in early tests of the instrument. These recesses affected the flow (Sec. 3.4). Plug shaped windows of Lucite were also tried; however, the Lucite used was not sufficiently homogeneous to permit the attainment of a single fringe even in a 1/8" diameter field.

The quality of an interferometer's optical components is readily judged by the quality of its white-light-fringes and the nature of the single fringe obtainable. Equal dispersion in each interferometer arm will result in a white-light-fringe pattern which has good color symmetry centered about a dark central fringe[12]. The size of the single fringe obtained is also a measure of flatness of components. With the Gaertner components a single fringe can be obtained over the entire field, approximately 12 mm in diameter. With the

- -

12. Normally one might expect the central or zeroth fringe to be white, as the two interfering beams should be in phase for all wavelengths at the point of zero path difference. In the Michelson arrangement one interfering beam undergoes internal reflection and the other external reflection at the beam splitter, with a consequent phase difference of π; the zeroth fringe is dark.

Perkin-Elmer windows and their compensators in place a single fringe is readily obtained over the 1/8" diameter field. The white light pattern is well defined, and the color is symmetric about a dark central fringe. Eight colored fringes are distinguishable on each side of the zeroth fringe. A close examination of the zeroth fringe with the single fringe adjustment shows that a purplish tinge exists in parts of the field. This is presumably due to a lack of perfect compensation.

2.4. Mechanical Construction.

The principal problem of mechanical design is to provide supports for the optical components which will allow delicate adjustment and yet remain free of vibration during a measurement.

All the optical components, with the exception of the shock-tube windows, are held in heavy mounts which in turn are bolted to a heavy iron casting. The window mounting is discussed later in this section. The plan drawing of the interferometer (Fig. 5) depicts the arrangement of components on the casting. The mounting surfaces of the casting are milled flat to 0.001". Fig. 4, a photograph of the interferometer bed with the window section and the various light and draft shields removed, shows the arrangement of optical elements on the casting. The casting is supported by two

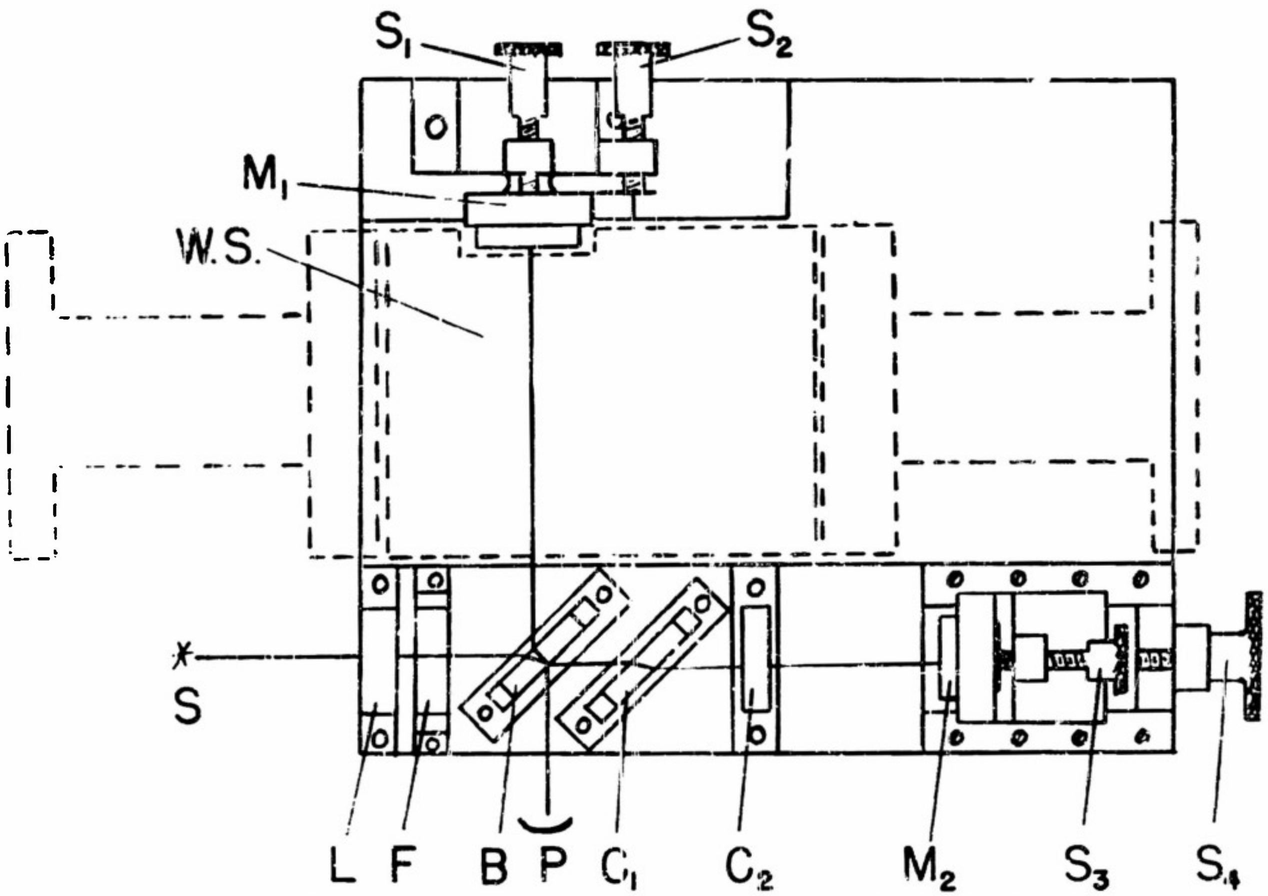

S_1	Horizontal Axis Inclination Screw	F	Filter
S_2	Vertical Axis Inclination Screw	B	Beam Splitter
M_1, M_2	Mirrors	C_1, C_2	Compensators
W.S.	Window Section (Shown dashed)	S_3	Horizontal Axis Inclination Screw
S	Light Source	S_4	Path Length Screw
L	Lens	P	Phototube

Fig. 5 Plan View of Interferometer

pieces of 1/4 inch flexible conveyor belting attached to clamps on the steel beam as shown in Fig. 4. Originally the shock-tube window section was designed to be bolted rigidly to the casting which in turn was to be rigidly fastened to the steel beam. It was found that vibrations were induced in the optics during a measurement and that these vibrations could be eliminated by removing all direct contact between the shock tube and the interferometer bed. (Sec. 3.4)

The light source is mounted at the side of the casting by a bracket permitting slight adjustment for alignment. The lens and filter for the source are fixed in front of the beam splitter on the casting. The window compensators and the diaphragm D_2 (Fig. 1) are mounted on a common holder (Fig. 5) in front of the mirror M_2. The phototube socket is mounted in a sheet metal box which is bolted to the casting on the side of the emergent beam. The sheet metal box contains electronic components associated with the phototube.

The Michelson components -- the beam splitter, its compensator, and the two mirrors -- are each clamped at three points in their mounts. The beam splitter and its compensator are adjusted by tilting their mounts with shims. In order to adjust the interferometer to the zeroth fringe, a fine screw S_4 is provided to translate the mount of mirror

M_2 along machined ways parallel to the optic axis. The final adjustment of the interferometer is accomplished in the mirror mounts which provide slight rotations of the mirrors; these rotational adjustments operate on the principle of working a weak spring against a strong spring. The details of the mount for mirror M_1 are given in Fig. 6. The adjusting screws S_1 and S_2 acting against steel spring arms rotate the mirror by bending the strong central support. The movable mirror M_2 has a rotational adjustment S_3 which operates on the same principle. This latter adjustment provides extra flexibility which, although unnecessary, has proven to be convenient.

The windows are mounted in a duraluminum section which can be inserted at any joint of the 1-3/8" diameter tube to form a part of the shock tube. The mounting of the windows is indicated in the cross sectional drawing Fig. 7. The inner surfaces of the windows are flush with the shock tube's inside surface at the section shown. The shock tube wall curves away from the flat 1/8" diameter windows leaving a maximum recess in the shock tube surface of 0.0045". Each window is pressed against the duraluminum section by a brass insert and a Neoprene gasket as shown. The gas seal furnished by the Neoprene gaskets is adequate over the pressure range from vacuum to 75 psi. Special flanged sections of tubing are joined to each end of the window section. These sections

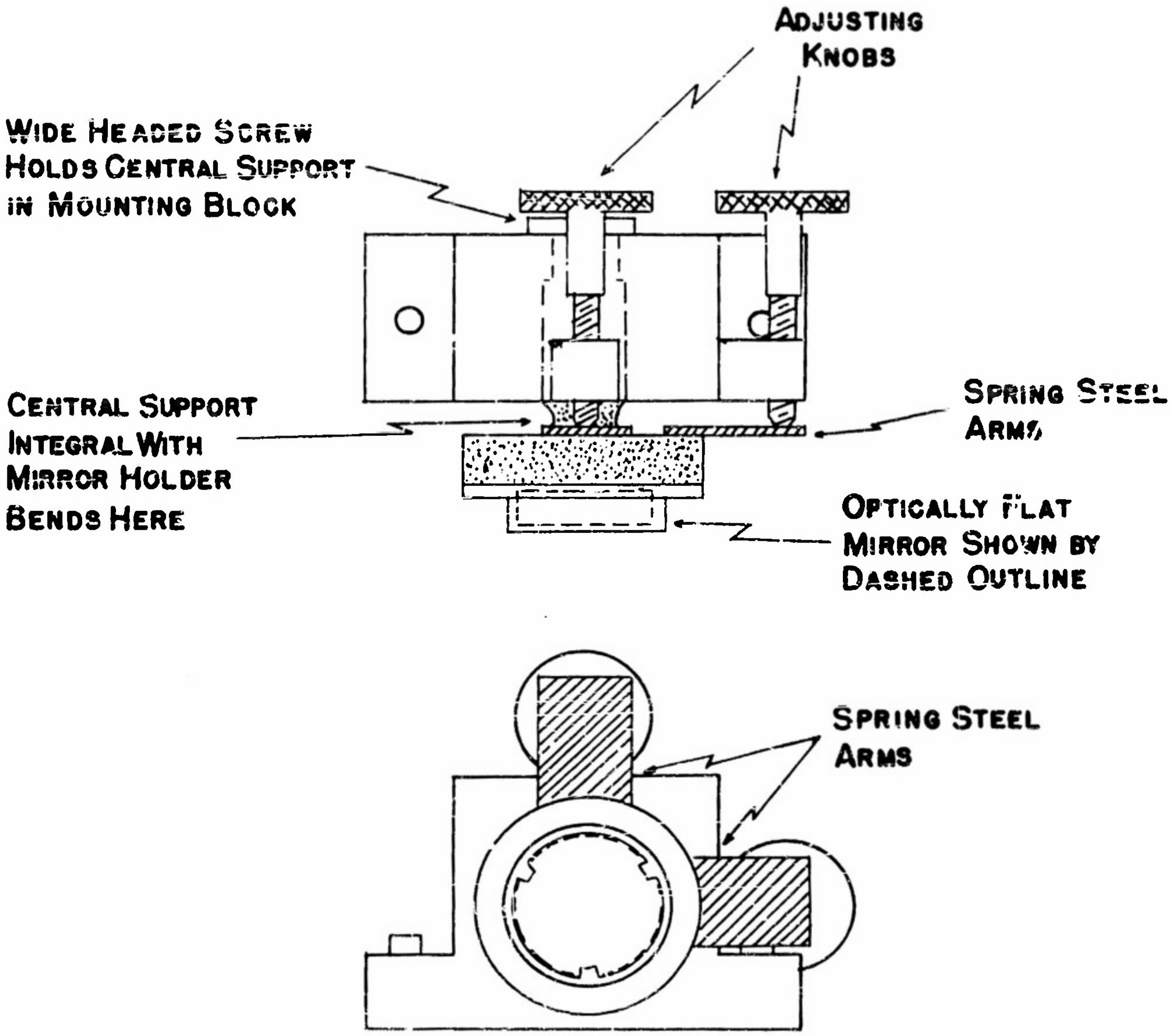

FIG. 6 MOUNT FOR MIRROR M_1 PERMITTING FINE ANGLE ADJUSTMENT

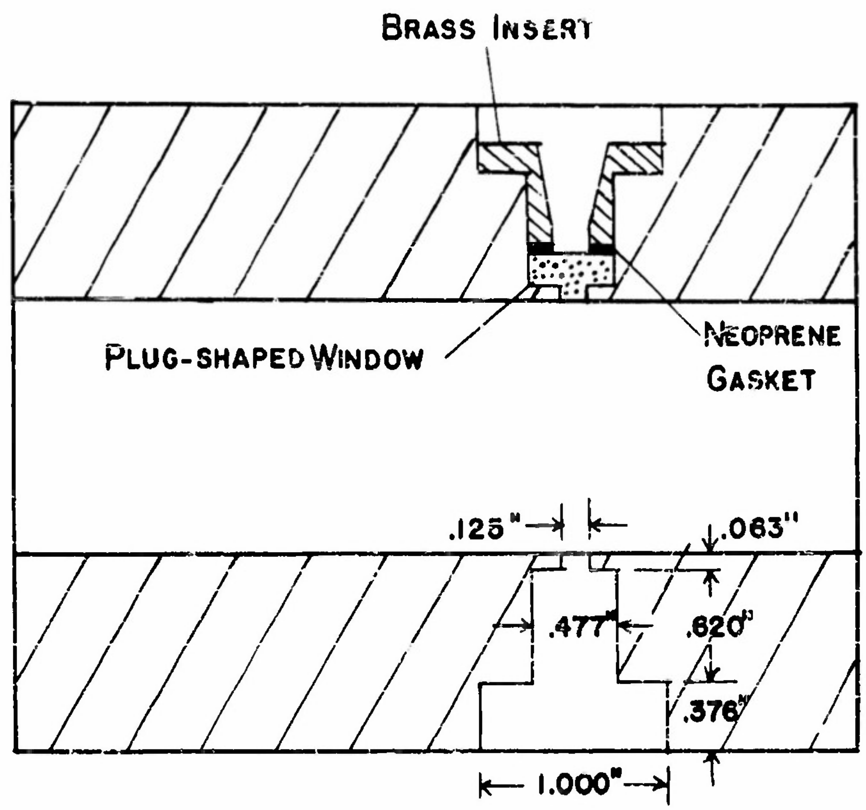

FIG. 7 SHOCK TUBE SECTION FOR MOUNTING OF CHRONO-INTERFEROMETER WINDOWS

allow rotation of the window section to permit optical alignment without disturbing the remainder of the shock tube.

The range of adjustment of optical components has been purposely sacrificed for rigidity of mount. This requires careful initial alignment of the interferometer elements. The alignment procedure consists of five steps: 1) the alignment of beam splitter and mirrors before the shock tube windows and their compensators are put in place, 2) the location of the zeroth fringe position, 3) the adjustment of the compensating plate (C_1), 4) the positioning of the windows, and their compensators, and 5) the alignment of the light source, phototube, and the auxiliary apertures.

The first step positions the beam splitter at 45° to the mirrors, and makes certain that the final fringe adjustments can be made within the range of the fine mirror adjustments. The second step assures that the optical path lengths in the two arms are sufficiently near to each other so that subsequent adjustments can be made with visible fringes using light passed by the wide band filter. The third step provides equal dispersion of the light in the two arms and is also necessary to permit adjustment to a single fringe pattern. Step four aligns the shock tube windows centrally on the optic axis. The last step minimizes scattered light and selects the light contributing to the fringe pattern on the phototube surface.

The third step is somewhat difficult and will be described in more detail; its importance is not emphasized in most descriptions of the Michelson interferometer, and techniques for achieving optical parallelism of the beam splitter and its compensator are not usually suggested. Two equally satisfactory techniques have been developed. One consists in using the two plates as though they were elements of a Jamin refractometer (Fig. 8a); the compensating plate is tilted until white-light-fringes appear and then adjusted for a single fringe. The second technique employs the circular Fabry-Perot fringes seen with monochromatic light in each of the plates viewed normally (Fig. 8b); the compensator is tilted until the centers of the two patterns coincide.

2.5 Recording Equipment

The phototube pickup and transducer circuit is shown in Fig. 9. In order to record steady or slowly changing transient flows, long period response of the phototube output is needed. Therefore the voltages for the 931A are obtained from electronically regulated power supplies. The dynode voltages are furnished by a series of resistors connected across a regulated negative supply variable from -400v to -1000v[13]. With the amount of light available a maximum signal to noise ratio of ten to one is obtained

---

13. B. H. Zimm, J. Chem. Phys. 16, 1099 (1948)

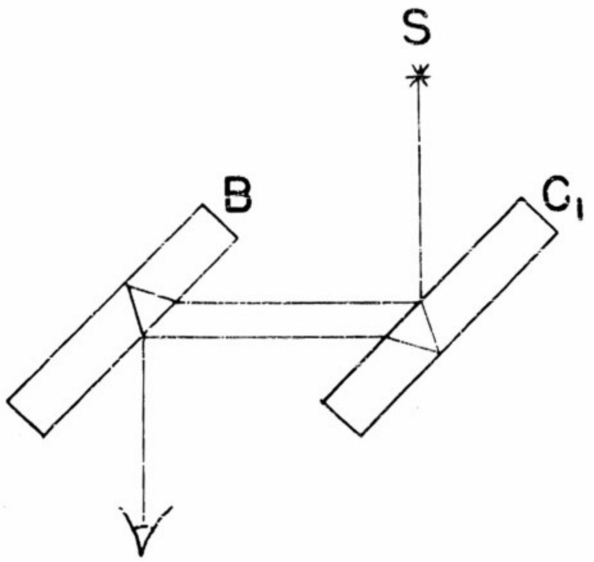

(A) Jamin Refractometer Technique

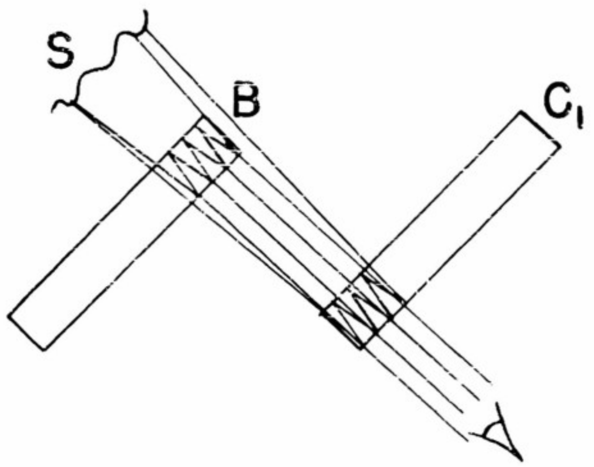

(B) Fabry-Perot Fringe Technique

Fig. 8 Techniques for Adjusting Beam Splitter and Compensating Plate to Accurate Parallelism

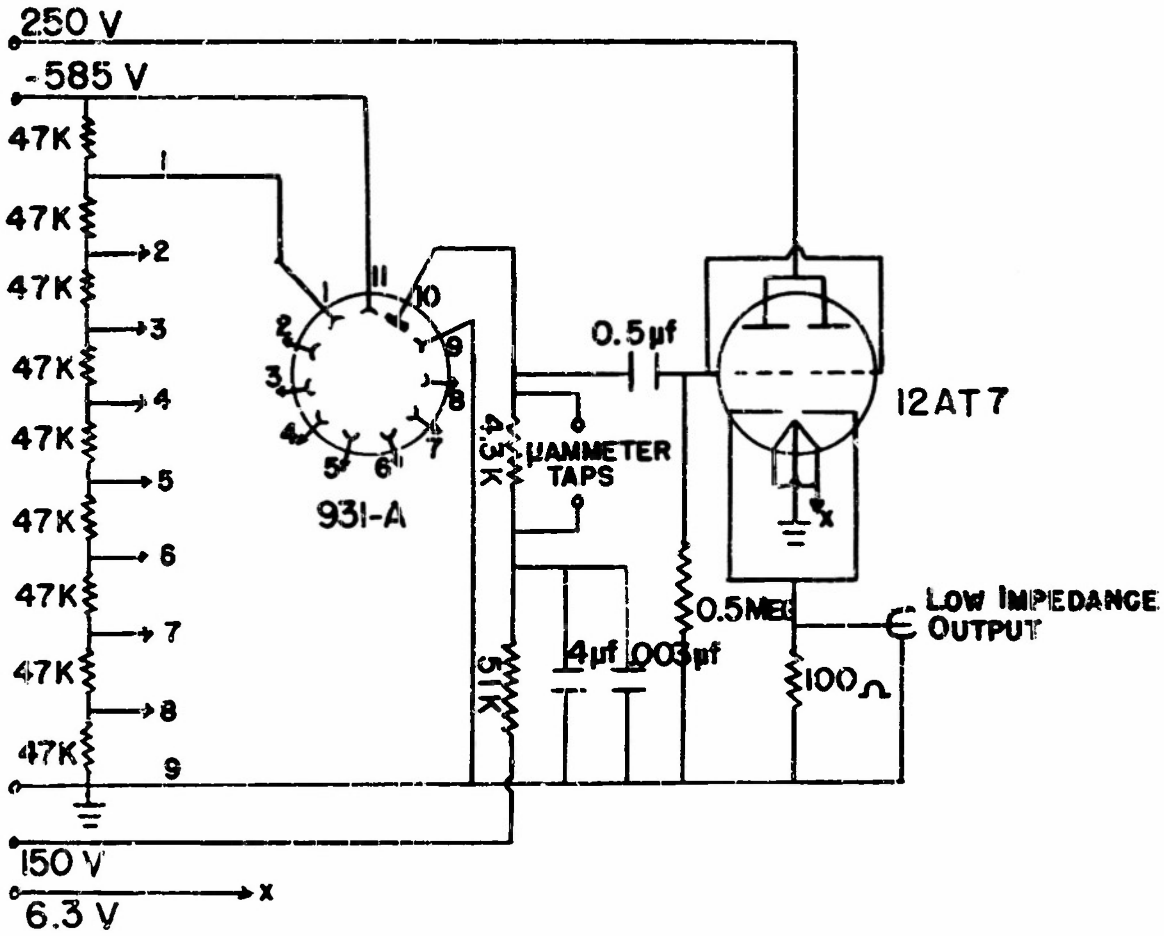

Fig. 9 Phototube Pickup and Transducer

using 65 volts per dynode stage. The 931A anode supply voltage of 150v is furnished by a separate electronically regulated supply.[14] The phototube anode load value is chosen to develop a signal size sufficient to drive a 12AT7 cathode follower stage over its linear range. The signal at the phototube anode is applied to the grid of the cathode follower stage by RC coupling with a 0.25 second time constant. The cathode follower is mounted next to the phototube (Figs. 3, 4). The variation of the resultant intensity of the interfering beams from a maximum to a mimimum produces a change of approximately 0.1 volt at the output of the cathode follower. This signal is transmitted by coaxial cable to the deflection amplifier of a cathode ray oscillograph.

The oscillograph used to record the interferometer signal employs a Dumont 3JP15 cathode ray tube. The deflection amplifier sensitivity is 0.08 v/inch. Instead of using a single sweep across the tube face to provide a time base, a more extended time base is obtained by focusing the image of the cathode ray spot on 35 mm film held in a rotating drum. The 42.5 cm diameter drum rotates at 1800 rpm; this rotation yields a time base of 25 μsec/mm on the film. The cathode ray spot is intensified by an initiator pulse at the beginning of an experiment and remains on for one drum revolution

---

14. Elmore and Sands, Electronics, p. 317 Model 50, McGraw-Hill, N. Y. (1949)

or about 30 milliseconds. The oscillograph has a second cathode ray tube with separate deflection amplifier and separate optical system which focusses the cathode ray spot on the same 35 mm film. Thus two recording channels are available for simultaneous recording of time dependent information. A crystal controlled oscillator supplies time markers for either or both channels.

In order to observe very slow changes in the intensity of the interfering beams an external microammeter is temporarily shunted across the phototube load resistor as indicated in Fig. 9.

III Density Measurement with the Chrono-Interferometer

3.1 Basic Interferometric Equation.

The variation of fringe intensity is interpreted as a density change in the shock tube gas which lies in one arm of the interferometer. This interpretation is dependent upon the relationship between density and index of refraction of a transparent medium. The relationship between refractive index and fringe shift for a transparent medium inserted in one arm of a Michelson interferometer is readily established. If the fringe shift of s fringes is observed when the gas of refractive index n enters the evacuated space of thickness d, and if the light source is monochromatic with a wavelength λ, then

$$s\lambda = (n-1)2d \tag{3.1}$$

In their work on the refraction and dispersion of air, Barrell and Sears[15] point out that three expressions have been proposed for the relationship betwoen index of refraction, n, and density ρ, for a transparent medium at a particular wavelength.[15] These expressions in historical order are:

---

15. H. Barrell and J. E. Sears, Phil. Trans. A238, 1 (1939)

I	$\frac{n^2-1}{\rho} = \text{const.}$	Newton-Laplace
II	$\frac{n-1}{\rho} = \text{const.}$	Gladstone-Dale
III	$\frac{n^2-1}{(n^2+2)\rho} = \text{const.}$	Lorentz-Lorenz

Newton found (I) to be true for a large number of liquids, and Laplace inferred (I) on the basis of the undulatory theory of light. Gladstone and Dale[16] put forth (II) as an empirical expression in agreement with measurements on the refractivity of water, alcohol, carbon disulphide, and other liquids at different temperatures. H. A. Lorentz and F. Lorenz derived expression (III) independently on theoretical grounds. Lorentz based his deductions on his own electron theory considered in relation to Maxwell's system of equations for the electromagnetic theory of light. A short time later Lorenz deduced expression (III) by considering the passage of light through a medium consisting of spherical molecules immersed in an ether having the properties of an elastic solid.

The refractivity of gases at normal densities is small, and the expressions (I) and (III) reduce in first approximation to the Gladstone-Dale expression (II). Furthermore, as (n^2-1) differs from $2(n-1)$ only by a term $(n-1)^2$, then

---

16. T. H. Gladstone, and T. P. Dale, Phil. Trans. 153, 317 (1863)

for air where $n-1 = 3 \times 10^{-4}$, differences in n-1 of the order of $9/2 \times 10^{-8}$ would have to be detected in order to distinguish between expressions (I), (II), and (III). The Gladstone-Dale relationship has been found to be correct for dry air at 20°C to within 0.1% over a pressure range of 1-20 atmospheres.[17]

On the basis of the Gladstone-Dale relationship the number of periodic changes in intensity of a single fringe pattern, i.e. the fringe shift, varies linearly with the gas density. On combining equations (II) and (3.1) we obtain

$$\Delta\rho = \frac{\lambda}{2dK} \Delta S = L \,\Delta S \tag{3.2}$$

where K is the Gladstone-Dale constant for the gas at the wavelength λ, and d is the distance in the interferometer arm over which the density change occurs. The constant $L = \frac{\lambda}{2dK}$ is a measure of the instrument's sensitivity.

Equation (3.2) is strictly valid for a monochromatic source. In measurements made with the currently described instrument no marked deviation in fringe spacing with density change has been noted for as many as 120 fringes on one side of the zeroth fringe when using the 150 Å band, interference-film, filter. The center of the filter's

---

17. Gale, Phys. Rev. 14, 1 (1902)

transmission band 5460 Å will be used for λ in considering equation (3.2).

3.2 Interferometer Calibration.

In order to test the performance of the interferometer the constant L was determined experimentally for air, nitrogen, and helium. The procedure followed was to obtain a fringe count with the external microammeter shunted across the photo-anode load (Sec. 2.5) while the gas was slowly admitted to or exhausted from the shock tube over a measured isothermal pressure interval. For an isothermal process involving an ideal gas

$$\Delta\rho = \frac{\Delta P}{\frac{RT}{M}} = L\ \Delta S,$$

so that

$$L = \frac{M}{RT_1}\left(\frac{\Delta P}{\Delta S}\right)_1 \quad ;$$

where the subscript i denotes on isothermal process. Most of the calibration runs were carried out with the interferometer mounted on the shock tube with the entire tube acting as a pressure chamber. Since even small amounts of air would lead to easily detectable contamination of helium, the instrument was demounted from the tube and the window section with a short section of Lucite tubing served as a test section for runs in helium. This small section could be evacuated to a pressure below 0.3 mm of mercury. The pressure measurements were made with a dead weight pressure gauge, and a vacuum referenced mercury manometer. The ambient temperature was measured with a 0-50°C thermometer in good thermal contact with the window section of the shock tube.

Calibration runs with room air reflect the day to day variation in water vapor content. This effect is very large; daily variations of 15% were noted in the slopes of graphs of pressure plotted against fringe shift. This experience with room air indicated the advisability of confining the use of the interferometer to gases of known composition. All subsequent experiments were carried out with commercially prepared nitrogen and helium.

The data from the calibration runs in nitrogen are plotted in Fig. 10. Each point on this graph represents a separate run, and all the experimental points have been reduced to a standard temperature (25°C) assuming ideal gas behavior. The Gladstone-Dale constant for nitrogen is calculated from the slope of the graph in Fig. 10. The formula for the calculation of K is deduced from the basic equation (3.2)

$$K = \frac{RT_1 \lambda}{M \rho_{Hg}\, g\, 2d \left(\frac{\Delta P}{\Delta S}\right)_1}$$

From Fig. 10.

$$\left(\frac{\Delta P}{\Delta S}\right)_1 = 2.182 \ \frac{\text{cm of Hg}}{\text{fringe}}$$

$R = 8.3136 \times 10^7$ ergs/mole°

$2d = 6.985$ cm

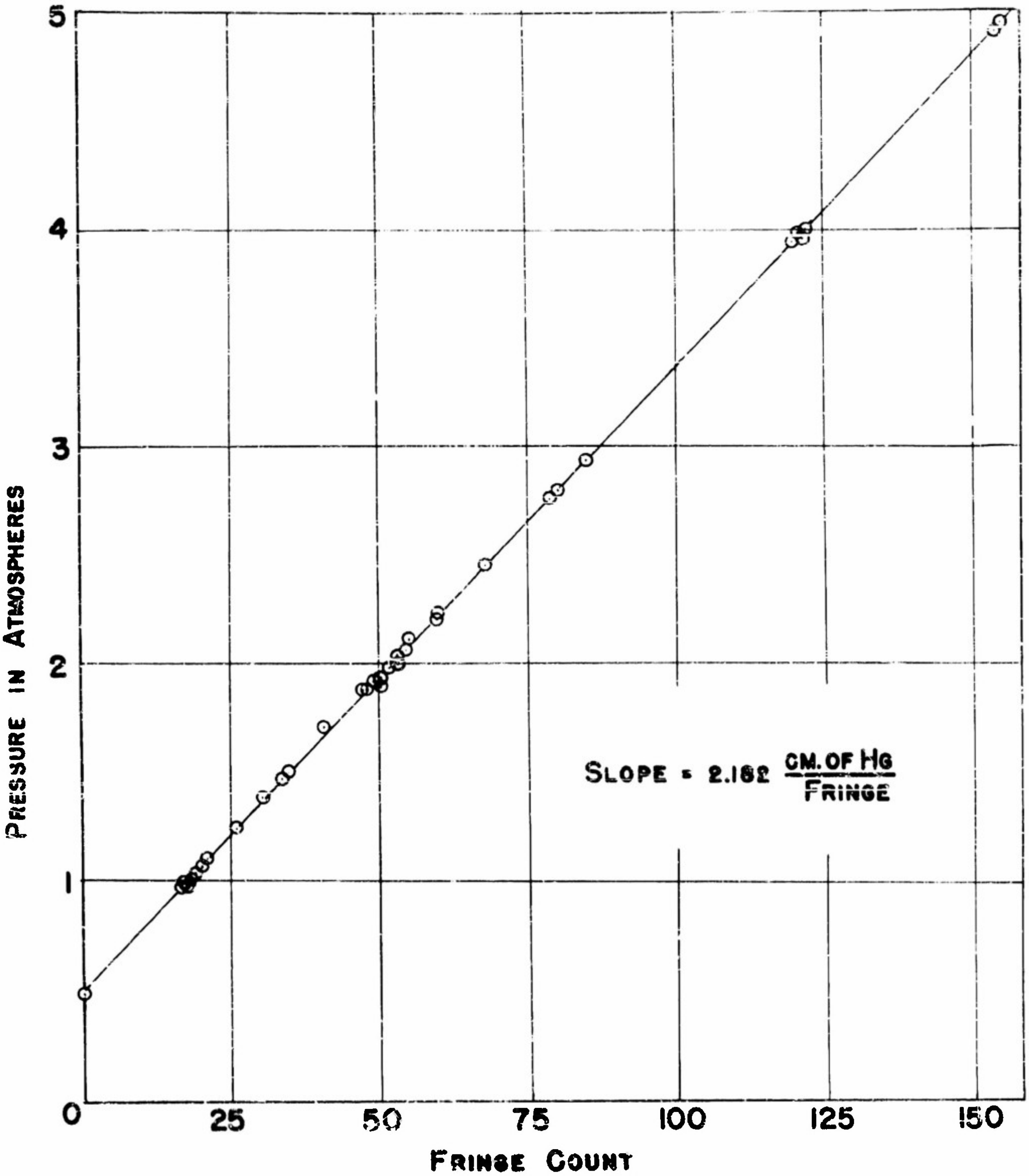

Fig. 10 Interferometer Calibration with N_2 at 25°C

$M = 28.016$ gm for N_2 $\qquad$ $T = 298.2^{\circ}K$

$\rho_{Hg} = 13.595$ gm/cc for Hg. $\qquad$ $\lambda = 5460$ Å

$g = 980.1 \text{ cm/sec}^2$

On substituting the above values into the formula for K we obtain

$$K = 0.2379 \frac{cm^3}{gm} \text{ for nitrogen.}$$

The estimated experimental errors for the Gladstone-Dale constant determinations in nitrogen and helium are given in Table I.

TABLE I

EXPERIMENTAL ERRORS IN DETERMINATION OF THE GLADSTONE-DALE CONSTANT K

Quantity	Percent Error N_2	Percent Error He
d	0.02%	0.02%
T_1	0.1 %	0.1 %
ΔP_1	0.02%	0.05%
ΔS_1	0.3 %	0.6 %
K	0.4 %	0.8 %

The results of the interferometer calibrations are summarized in the table below in which the measured values of K are compared with values of K calculated from the values of density and refractivity in the International Critical Tables.

TABLE II

GLADSTONE-DALE CONSTANT K FOR N_2 AND He at 5460 Å

Gas	I.C.T. K	Experimental K
Nitrogen	0.2385 cc./gm.	(0.2379$\pm$0.0009) cc./gm.
Helium	0.1963 cc./gm.	(0.201$\pm$0.002) cc./gm.

The percentage deviation from the handbook value of K for He is 2%, which is outside the estimated experimental error. The commercially prepared helium is stated by the supplier to be [illegible].8% pure, although the impurities are not given; it is unlikely that these impurities could account for an appreciable amount of the 2% deviation. The difference observed could be attributed to an undetected source of contamination in the chambers, hoses, valves, and gauges used to introduce and measure the pressure of the helium.

The constants L for N_2 and He are

$$L_{N_2} = 3.285 \times 10^{-5} \text{ gm/cc/fringe},$$

$$L_{He} = 3.89 \times 10^{-5} \text{ gm/cc/fringe}.$$

Thus, for example, an isothermal pressure change of one atmosphere will cause the following fringe shifts in N_2 and He.

$$\Delta S_{N_2} = 34.8 \text{ fringes},$$

$$\Delta S_{He} = 4.19 \text{ fringes}.$$

The calibration runs in nitrogen justify the applicability of the Gladstone-Dale relationship to measurements made with the chrono-interferometer over a pressure range from 1/2 to 5 atmospheres to within 0.4%.

3.3 Measurement in Transient Flows.

The oscillographic traces in Fig. 11 illustrate the types of record obtained with the chrono-interferometer when studying shock-tube flows. An undisturbed portion of the trace to the left corresponds to a constant gas density preceding the arrival of a wave at the interferometer. Fig. 11a is the response to flow in the chamber and Fig. 11b is the response to flow in the channel. There is a background of phototube noise present throughout the trace; it is spurious and is to be disregarded. The auxiliary trace in Fig. 11b shows timing markers at 100 microsecond intervals.

Fig. 11a illustrates the time variation of intensity of the interfering beams when the gas density continually decreases during the passage of a rarefaction. A change from one maximum to the next represents a change of 2π

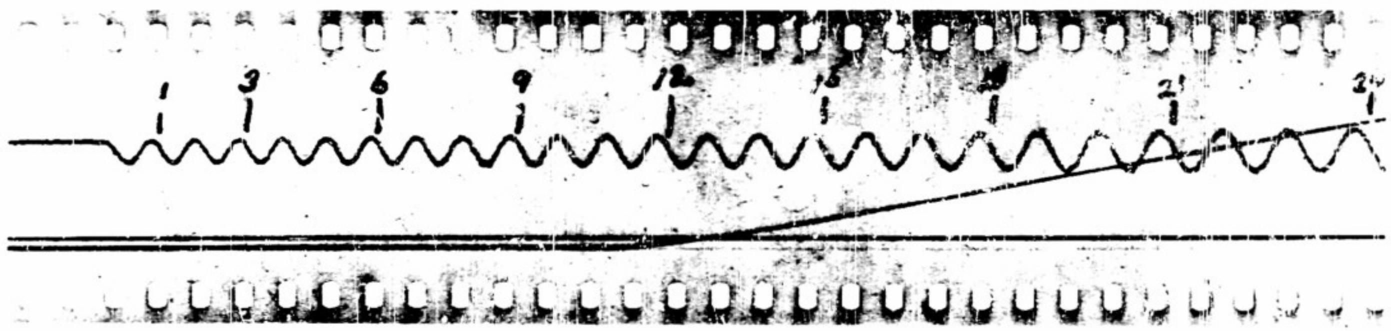

← 1 MSEC →　　　INCREASING TIME →

(A) RESPONSE TO A RAREFACTION

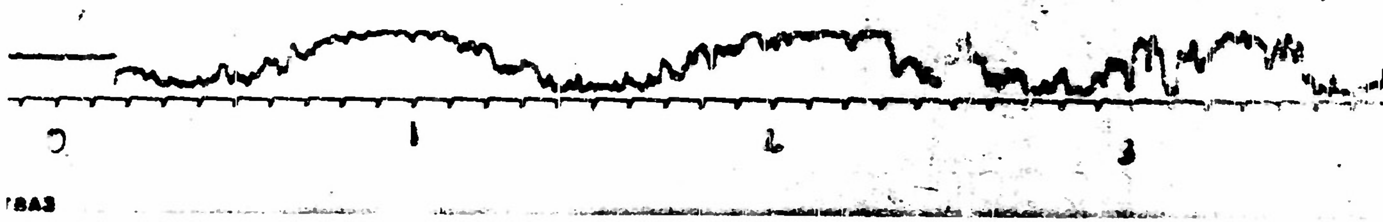

← 1 MSEC →　　　INCREASING TIME →

(B) RESPONSE TO A SHOCK AND THE HOT GAS REGION OF FLOW

FIG. 11 TYPICAL RECORDS OBTAINED WITH CHRONO-INTERFEROMETER IN FLOWS PERMITTING THE USE OF MONOCHROMATIC LIGHT radians in the relative phase of the interfering beams, and is referred to as a shift of one fringe. The fringe shift as a function of time is read off the record, and the density change with time is calculated from the fringe shift using the basic interferometric equation (3.2).

With strictly monochromatic light the amplitude of successive fringes would be the same and there would be no way to distinguish between an increase and a decrease in the gas density. This ambiguity in the sense of the density change is circumvented when the light source contains a wide band of wavelengths so that the amplitude of fringes decreases in going away from the zeroth fringe. This effect is evident in the record shown in Fig. 11a, where the fringe amplitude increases with time. This indicates a continual decrease in density since the zeroth fringe was set to correspond to a density below the starting density.

Whenever the density gradient in the flow becomes steep, the variation over the cross-section of the interfering light beam produces an appreciable difference in the optic paths of extreme rays. R. A. Shunk has demonstrated that compression waves with successively higher gradients lead to smaller amplitude fringes as the difference in optic path across the field approaches 1/2 wavelength. For sufficiently large density gradients the single fringe pattern washes out. Across a shock, the density changes discontinuously by an amount which may correspond to a shift of several fringes plus a fraction. With the passage of a shock the instrument detects the fractional fringe change only; the shock appears as an abrupt change in intensity. Such a change is evident in the record of Fig. 11b.

Fig. 11b is the response of the interferometer to the channel flow in the shock tube as a shock and the hot gas behind the shock pass. The slow oscillations appearing on the record after the shock passage represent a gradual increase in the average density of the gas. The more rapid, irregular fluctuations which increase in amplitude with time are believed to be fluctuations in the flow and are not due to mechanical vibrations of the instrument (Sec. 3.4). The time dependence of density in the region behind the shock is obtained by measuring the fringe shift as a function of time following the abrupt signal which occurs as the shock passes; the basic interferometric equation (3.2) relates fringe shift to density change. The total density change from the value in the undisturbed channel gas requires an auxiliary measurement of the density at the shock discontinuity. The auxiliary measurement in the presently reported work consisted of a determination of shock speed.

It is found as shock tube flow develops at some position in the tube that the rapid, irregular fluctuations may attain a magnitude which exceeds a half fringe. Whenever these signals exceed a half fringe a reliable fringe count in time can no longer be made. In order to extend the measurement of density in time it becomes necessary to make use of another method of determining fringe shift referred to as the white-light-fringe technique.

When the wide-band filter is removed from the incident beam so that the full spectrum of white light falls on the phototube, there will be no fringes and no variation of intensity except when the gas density changes through the region of white-light-fringes. Fig. 12a shows the interferometer response to the appropriate small portion of a rarefaction when using a white light source. The record shows that the fringes have an amplitude symmetry about a central fringe. The amplitude of successive half fringes reaches 1/10th the central fringe amplitude at the fifth fringe on either side of the zeroth fringe; the density change corresponding to five white-light-fringes is not measurably different from that causing an equal fringe shift with the monochromatic filter in place.

The white-light-fringe technique for obtaining density measurements in noisy flows consists of the following procedure. The interferometer is adjusted so that the

Increasing Time ⟶

(A) White Light Response to a Portion of a Rarefaction

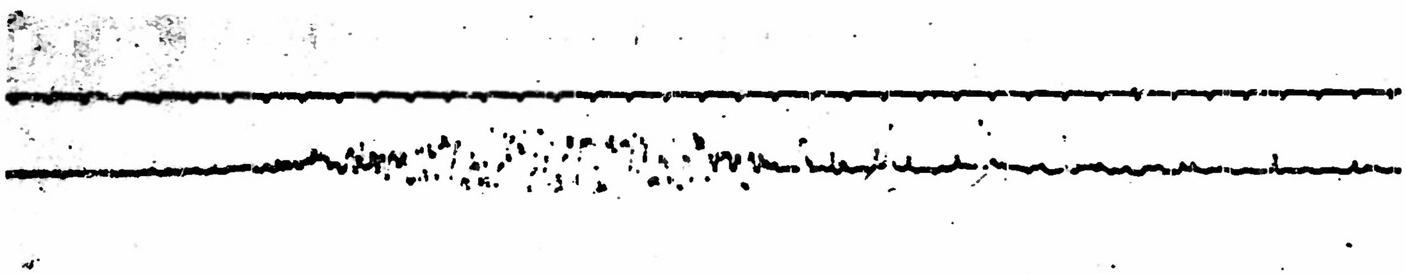

Increasing Time ⟶

(B) White Light Response to the Noisy Cold Front Region of Flow

Fig. 12 Typical Records Obtained with Chrono-interferometer Using White Light. Timing Pulses Occur at 100 μsec Intervals.

zeroth fringe will occur at a density value existing within the region of noisy flow. The density at which the zeroth fringe exists is measured either by recording the static pressure and temperature or by slowly admitting gas to increase the density from a reference density to the zeroth fringe density while counting fringes with the monochromatic filter in place. The shock tube flow to be studied is then generated while the interferometer is recording with a white-light-fringe response to a noisy flow region. The density over a limited duration of the flow can be found by noting the amplitude of the response as a function of time. In view of the large fluctuations present when this technique is resorted to, the density is determined only within extreme values and average density values must be inferred by making repeated experiments with different zeroth-fringe settings. The observation of density by this technique is not capable of the high accuracy obtained with the monochromatic light, both for the reason just mentioned and because the reproducibility of flows initiated from the same starting conditions is assumed. In Fig. 12b the large amplitude pulses appearing in the right half with only upward deflection are due to the interception of the light beam by fragments of the shattered diaphragm.

The white-light-fringe technique can be used to determine the density change across a shock discontinuity. However inaccuracies in the determination of the zeroth fringe density, and in the measurement of fringe amplitude lead to an error of $\pm$ 1 fringe.

3.4 Tests of the Chrono-Interferometer

To make certain that the deflections observed on the oscillograph record accurately represent density changes during a measurement, the instrument was subjected to a series of tests. In particular, the sensitivity of the instrument to mechanical vibrations and the effect of the windows on the flow were investigated. The tests are summarized in this section.

a) Vibration Tests.

One attempt in design of the instrument to obtain freedom from mechanical vibration consisted of fastening all parts together rigidly; the window section was bolted rigidly to the casting which in turn was rigidly fastened to the beam supporting the shock tube. Records of channel flow taken with this mounting revealed deflections from signals reaching the instrument ahead of the shock. These signals were attributed to induced mechanical vibrations of optical elements. This was shown by taking a record as a shock was reflected from a solid plate before reaching the interferometer. Since no gas could leak past the plate, any signal observed in this manner is due to induced mechanical vibrations of optical elements. A small amplitude 1000 cps signal appeared on the record before the shock reflection, after reflection the signal amplitude increased to a half fringe and the signal frequency changed to 5000 cps which degenerated to a 2000 cps signal in 6 msec. The half-fringe amplitude of the signal was maintained for the remaining 20 msec of the record.

The successful design of the mounting to free the instrument from mechanical vibrations consisted in isolating the interferometer bed from both the supporting beam and the shock tube. The bed was effectively isolated from the beam by using two pieces of 1/4 inch thick rubberized fabric (conveyor belting) for support. The window section was supported by the adjoining shock-tube sections so that no part touched the bed. When a similar test by shock reflection ahead of the interferometer was applied with this mounting, no signal appeared on the record prior to shock reflection. Shortly after reflection a 1000 cps signal appeared on the record whose amplitude was less than 1/10th of a fringe. Since the shock reflection test produced vibrations much more severe than those experienced in normal shock-tube operation; the appearance of only this small signal is considered to signify absence of mechanical vibrations in normal operation.

The degree of vibration sensitivity of the interferometer mounting and the mountings of optical elements is illustrated by observing the phototube output signals due to vibrations caused by hammering the support beam and the shock tube, and by tapping the various mounts. A sharp hammer blow on the support beam near the interferometer or on the window section of the shock tube is required to produce a half fringe amplitude signal. At a distance of seven meters from the instrument a heavy hammer blow is required on either the beam or the tube to produce a half fringe signal. Light tapping of any of the optical reflecting elements with a pencil produces a half-fringe signal. The compensating elements are relatively insensitive. The predominant vibration frequencies observed are: 1000 cps for the movable mirror M_2, 2000 cps and 2700 cps for the fixed mirror M_1, and 2700 cps and 1000 cps for the beam splitter. The high frequency of the vibrations observed explains why the flexible coupling of the massive interferometer base to the support beam does not transmit vibrations to the optical elements; at the low frequencies transmitted through the flexible belting, the interferometer base and optical elements all move as a rigid whole.

b) Window Tests

Initially a pair of plane windows was mounted in the shock-tube window sections (Fig. 7, Sec. 2,4). Without plug-shaped windows in the window section a cavity 1/8" in diameter and 0.063" deep is present on each side of the tube. Records of channel flow with these cavities in the tube wall showed a high frequency, large amplitude fringe variation after the shock arrived. The high frequency signal damped rapidly in a few milliseconds and a regular variation in fringe intensity with small, rapid, irregular fluctuations superimposed followed. The high frequency signal did not appear on records taken with the plug-shaped windows. The high frequency signal observed with the plane windows is attributed to a disturbance in the gas within the small cavities or to disturbances propagated from these cavities into the main flow.

The typical records reproduced in Fig. 13 illustrate the effects which have been described. Trial 467 shows both the high frequency signal after the shock arrived when the cavities were in the tube wall and the small signals arriving ahead of the shock when the rigid mounting of the instrument is used. Trials 585 and 590 show respectively the effects of introducing the flexible mount and of filling the cavities in the tube wall with the plug-shaped windows. The high frequency signal completely disappears

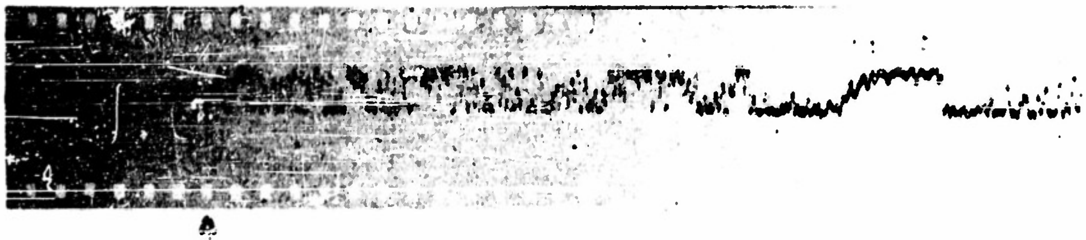

SHOCK ARRIVAL INCREASING TIME ⟶

TRIAL 467 N_2 GAS CHANNEL FLOW 5.12 M FROM DIAPHRAGM
$P_2/P_0 = 3.66$ RIGID MOUNTING PLANE WINDOWS

SHOCK ARRIVAL INCREASING TIME ⟶

TRIAL 585 N_2 GAS CHANNEL FLOW 4.55 M FROM DIAPHRAGM
$P_2/P_0 = 3$ FLEXIBLE MOUNTING PLANE WINDOWS

SHOCK ARRIVAL INCREASING TIME ⟶

TRIAL 590 N_2 GAS CHANNEL FLOW 4.55 M FROM DIAPHRAGM
$P_2/P_0 = 3$ FLEXIBLE MOUNTING PLUG-SHAPED WINDOWS

FIG. 13 TESTS OF INTERFEROMETER MOUNTING AND SHOCK TUBE WINDOWS when the plug-shaped windows are used. The relatively high phototube noise level on the records of Fig. 13 was present during the early stages of development of the instrument. The removal of extraneous light from the phototube by diaphragms (Sec. 2.2) results in the lower level of phototube noise seen in the other records presented in this thesis.

After the cavities in the window section were filled by the plug-shaped windows causing the high frequency fluctuations right after shock arrival to vanish, there still remain irregular fluctuations in fringe intensity on records taken to observe rapid flow in the channel. These fluctuations are most marked as the cold gas flows past the interferometer. Smaller fluctuations occur immediately after shock arrival and during the passage of the hot gas. It is important to show that all these remaining fluctuations, examples of which may be seen in Figs. 11b and 14a, are not due to vibrations induced in mirrors, windows, and compensating plates but are due to fluctuations in the gas flow itself. As primary evidence, the complete absence of these fluctuations prior to the shock arrival at the interferometer is cited. Furthermore, oscillations of the same character do not occur whenever the interferometer components are purposely set into oscillation. If the fluctuations are

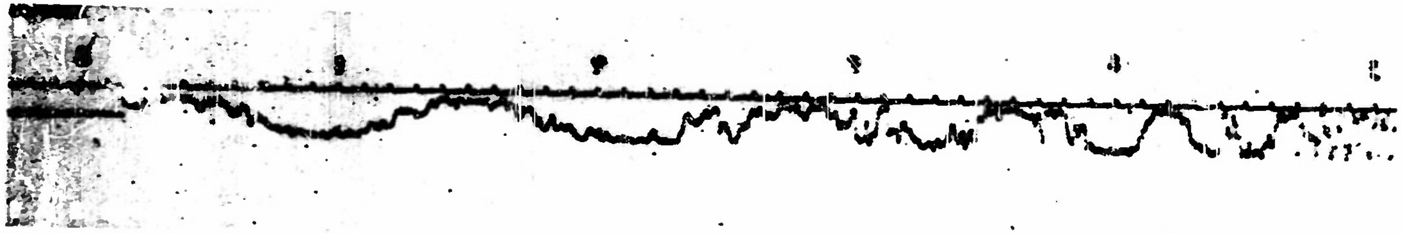

(A) TRIAL L 114 NITROGEN INTO NITROGEN - NORMAL OPERATION INCREASING TIME ⟶

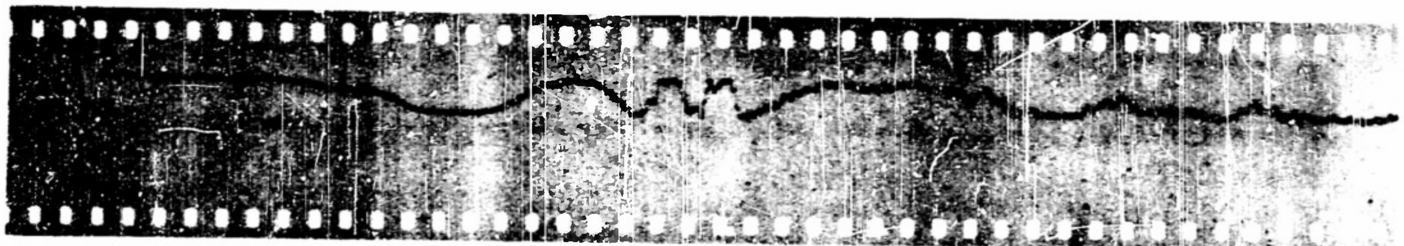

(B) TRIAL L 269 HELIUM INTO HELIUM - NORMAL OPERATION INCREASING TIME ⟶

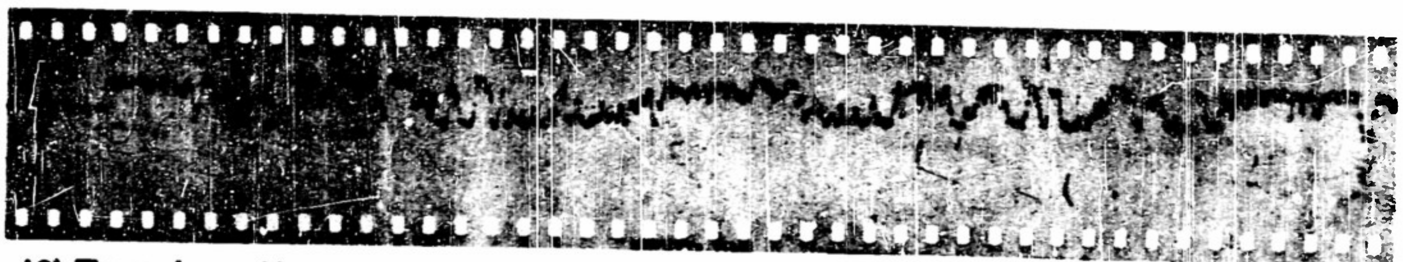

(C) TRIAL L 181 NITROGEN INTO NITROGEN - TRIPPED FLOW INCREASING TIME ⟶

FIG. 14 RECORDS DEMONSTRATING THAT FLUCTUATIONS ARE NOT DUE TO SHOCK INDUCED WINDOW VIBRATIONS. THE PRESSURE DIFFERENCE ACROSS THE SHOCKS CALCULATED FROM P_c/P_0 BY IDEAL THEORY IS 21 lb/in^2 IN ALL CASES.

caused by mechanical vibrations set up as the shock passes the windows, one would expect their amplitude to depend only on the pressure change across the shock. However when shocks in nitrogen gas and helium gas with the same pressure change were sent past the interferometer, the amplitude of the irregular fluctuations in nitrogen were nearly ten times the amplitudes of those observed in helium as shown in the records of Fig. 14a and 14b. This result can readily be interpreted in terms of fluctuations in the flow, since the difference in amplitudes is roughly equal to the difference in densities of the two gases.[18] Finally, the interferometer response was observed while purposely introducing fluctuations in the flow with a small perforated bronze strip inserted across a diameter of the channel cross-section ahead of the interferometer. The irregular fluctuations on the trace (Fig. 14c) had the same character but were larger than the fluctuations ordinarily observed.

Fig. 15 shows the response of the interferometer to a small amplitude standing wave produced in the shock tube by acoustic means. The standing waves were produced as in Kundt's classic apparatus. The three records shown in Fig. 15 were obtained with a standing sound wave of constant amplitude and frequency. Trial 529 shows the response when the small induced density changes occur around a density such

---

18. The fringe shift is approximately the same for the same density change in all gases (Sec. 3.2).

TRIAL 529 RELATIVE PHASE AT $(2n+1)\pi/2$

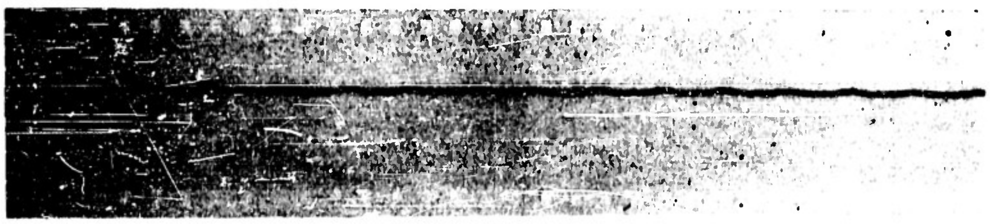

TRIAL 530 RELATIVE PHASE NEAR $n\pi$

TRIAL 531 RELATIVE PHASE AT $n\pi$

FIG. 15 CHRONO-INTERFEROMETER RESPONSE TO A SMALL AMPLITUDE STANDING WAVE that the interfering beams in the interferometer have a phase difference near an odd multiple of $\pi/2$, Trial 530 shows the response when the phase difference is near but does not change through a multiple of π, and Trial 531 shows the response when the phase difference oscillates about some multiple of π. This test illustrates that the error in measurement of the amplitude of a small density variation is greater when the phase difference of the interfering beams is near a multiple of π. Another illustration of this variation in sensitivity to small density changes is seen in Fig. 14a, where the small irregular fluctuations tend to be less pronounced when the trace is at the top or bottom.

PART B. DENSITY MEASUREMENTS IN SHOCK-TUBE FLOW

IV Experiment and Procedure

4.1 Scope

Primary[19] shock-tube flows resulting from initial diaphragm pressure ratios of approximately 2, 10, and 50 have been studied. The flows, all started from dry nitrogen gas at room temperature, are representative of the flow conditions employed in shock-tube studies of aerodynamic and blast phenomena. The initial conditioms and the theoretical flow conditions are summarized in Table III.

TABLE III

SUMMARY OF EXPERIMENTAL CONDITIONS

	Initial Diaphragm Pressure Ratio P_c/P_o		
	2	10	50
Flow in the hot gas region	subsonic	subsonic	supersonic
Flow in the cold gas region	subsonic	near sonic	supersonic
Flow in the rarefaction	all subsonic	sonic to subsonic	supersonic to subsonic
Rarefaction Occupies	part of chamber	all of chamber	all of chamber and part of channel
Initial Chamber Pressure P_c	1 atm	5 atm	5 atm
Initial Channel Pressure P_o	1/2 atm	1/2 atm	1/10 atm

19. Primary shock-tube flow is flow not affected by reflections from closed ends of the tube.

To achieve maximum accuracy of density measurement, high initial density is desirable; for a given gas--nitrogen in these tests--high initial density involves high initial pressure in the chamber. A limitation on initial chamber pressure lay in the strength of Lucite tubing used for the shock tube. Adequate safety to personnel was felt to exist by keeping initial pressures below 60 psig.

With the choice of initial pressures in Table III the entire flow in the chamber is predicted by the ideal shock-tube theory to be the same for the cases $P_c/P_o=10$, and $P_c/P_o=50$. The choice of $P_o=1/2$ atm was made for the case $P_c/P_o=2$ so that initial channel conditions would be the same for two of the cases under study.

4.2 Interferometer Positions

As described in the introduction and illustrated in Fig. 2, the chrono-interferometer was positioned at distances of 18, 85, 150, and 218 tube diameters from the diaphragm clamp during the study of the flows resulting from the three initial conditions chosen. At each interferometer-to-diaphragm distance, the chamber and channel lengths were chosen for the maximum duration of primary channel flow resulting from an initial diaphragm pressure ratio of 10; the maximum duration of channel flow is obtained when the reflected shock and rarefaction from the closed ends of the tube arrive at the interferometer at the same time. The basis for the choice of lengths is illustrated by the x-t plot of ideal shock-tube flow in Fig. 16. This idealized description was used in

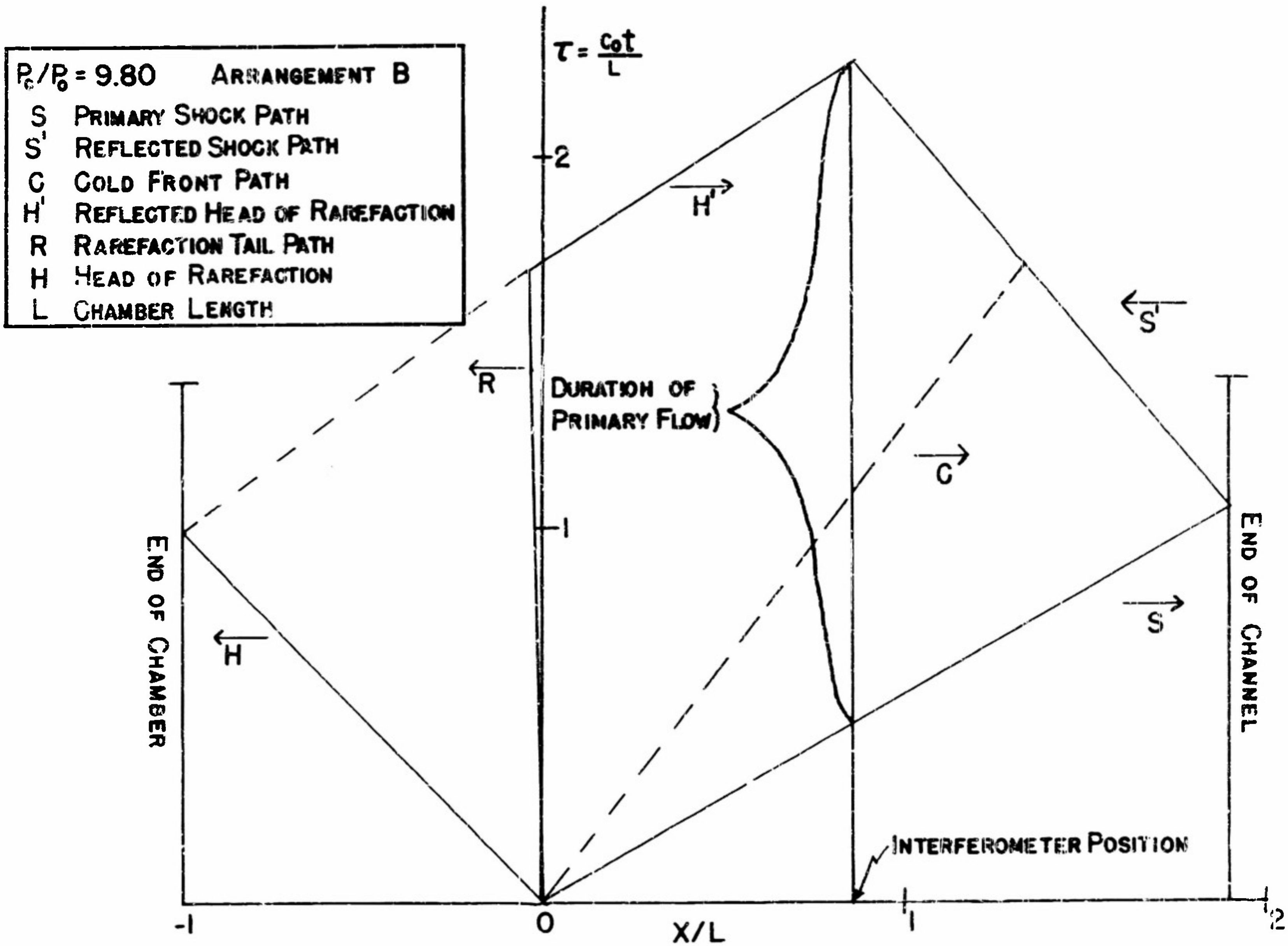

FIG. 16 x-t PLOT TO DETERMINE OPTIMUM SHOCK TUBE ARRANGEMENT determining the optimum arrangements of the shock tube, the alteration in speed of the reflected shock upon passing through the cold front being neglected for simplicity.

Both channel and chamber flows were studied for each arrangement of the shock tube. Channel flow is studied by arranging the initial low pressure on the interferometer side of the diaphragm and chamber flow is studied by arranging the initial high pressure on the interferometer side of the diaphragm. The distances between diaphragm clamp and interferometer, listed in Table IV, are slightly different for the chamber from those of the channel as it is necessary to always keep the diaphragm breaker in the low pressure end.

TABLE IV

INTERFEROMETER POSITIONS

Shock Tube Arrangement	Diaphragm-To-Interferometer Distance	
	Channel	Chamber
A	0.630 m	0.532 m
B	2.958 m	2.943 m
C	5.285 m	5.188 m
D	7.622 m	7.522 m

4.3 Experimental Procedure

For each arrangement of the shock tube, the tube axis is aligned to within ± 1 mm over the tube's 13 meter length. The internal diameter of all shock tube sections is constant to ± 0.001 inch, and aligning pins at all joints assure no discontinuities exceeding 0.001 inch. Nine sections of polished Lucite ranging in length from 0.24 m to 1.33 m, and two brass sections 0.86 m and 3.67 m in length, all of which are interchangeable, allow a choice of spacing between shock-tube parts and flow measuring apparatus.

In section 3.2 it was established that an experimental procedure which assures a knowledge of the composition of the gas used in the shock tube should be followed. The density measurements were carried out with commercial "water pumped" nitrogen, whose water vapor content is less than one part per million, and the following procedure for filling the shock tube was employed. First the tube is blown clear of all old shattered diaphragm material with an air blast and a new diaphragm inserted. The shock tube is evacuated by pumping for a 20-30 minute period; chamber and channel pressures were then below the saturated water vapor pressure at the ambient temperature. Nitrogen was then admitted into the channel and the chamber until the desired initial conditions were reached. The gas was allowed to come into thermal equilibrium with the shock tube walls. With careful assembly of the tube sections a leak rate of less than 4 mm of mercury per hour is obtained.

Static pressures above atmospheric are measured with a 0-60 psi Bourdon type dial gauge which is periodically calibrated against a dead weight gauge tester. Static sub-atmospheric pressures are measured with a mercury in glass barometer whose vacuum is maintained with a Cenco "Hyvac" pump.

In order to minimize initial temperature gradients along the shock tube, all light sources used with the flow measuring equipment are turned on only just prior to operating the shock tube. The initial temperature of the gas in the shock tube is constant within $\pm$ 0.6°C as measured by six mercury in glass thermometers placed in good thermal contact with the external tube wall at about two meter intervals.

The diaphragm materials used are near their rupture points at each of the initial conditions. For P_c/P_o = 10 and 50, two thicknesses of 0.002" thick laminated "Red Zip" cellophane are used. For P_c/P_o = 2 the diaphragm consists of one thickness of 0.001" Dupont 200 PHT cellophane which has been weakened by baking at 350°C for 30 minutes and kept desiccated. The diaphragm is punctured by a metal probe operating through a sliding seal at an oblique angle in the wall of a duralumi-num section of shock tube.

4.4 Flow Measuring Apparatus

A typical arrangement of the apparatus for measuring and recording the primary flow is illustrated by the block diagram in Fig. 17. The chrono-interferometer and the oscil-lograph designated Mark II have been described in Chapter 2.

Since the chrono-interferometer cannot resolve the steep density gradient at the shock, the strength of the shock front is determined by recording its arrival at eight optical de-tection stations. Of these detection stations, whose opera-ting principle will be described shortly, two can be mounted at any point along the tube, and the remaining six are per-manently arranged in two groups of three each. The positions of these detection stations are indicated for each shock tube arrangement in Fig. 2. The transient flow information is

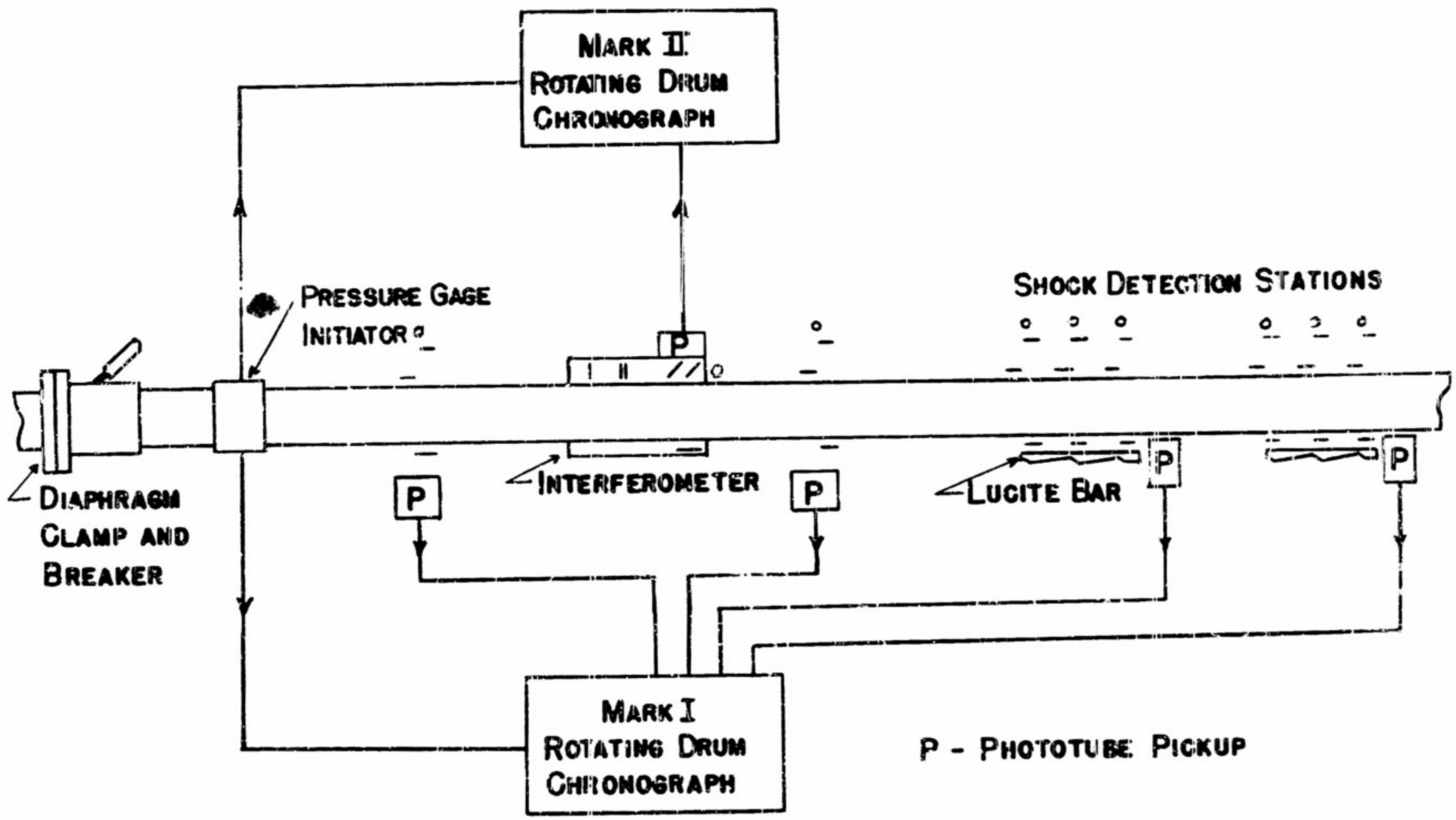

FIG. 17 MEASUREMENT AND RECORDING APPARATUS

recorded on the two rotating drum oscillographs which are designated Mark I and Mark II in the block diagram of Fig. 17. The oscillograph traces are initiated by an electrical signal from a piezoelectric gauge, which will be described shortly, located near the diaphragm clamp. Mark I oscillograph is used as a chronograph to record the shock arrival at the eight detection stations.

The shock detection stations[7] consist of an arrangement of three knife edges in a plane perpendicular to the shock tube axis as shown in Fig. 18. The knife edges are adjusted so that light cannot pass the third knife edge; however, as the shock front enters the light beam, portions normally intercepted by the third knife edge are reflected past it into a phototube. A Lucite bar is used to "pipe" the light from groups of these stations to a common phototube. The phototube output signal passes through an inverter and a cathode follower, and is transmitted to the Mark I chronograph on low impedance cable.

Signals from four phototube pickups are mixed in the Mark I chronograph and amplified sufficiently to deflect the beam of a cathode ray tube (Dumont 3JP15) whose short persistence screen is photographed on 35 mm. film held in a rotating drum. The Mark I oscillograph is provided with a sweep, synchronized to a 100 KC crystal controlled oscillator, which produces a deflection transverse to the direction of film motion for 50 microseconds in each direction successively. The motion of the film results in the zig-zag pattern shown on the typical shock time record in Fig. 19.

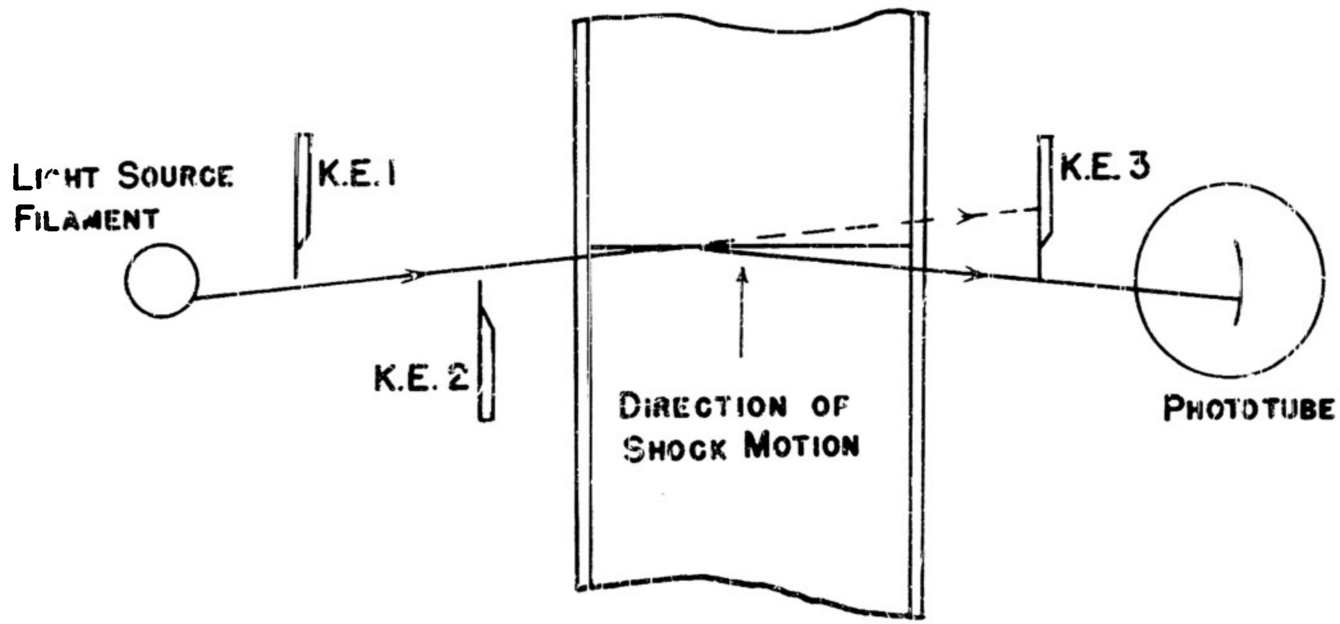

FIG. 18 SHOCK DETECTION STATION

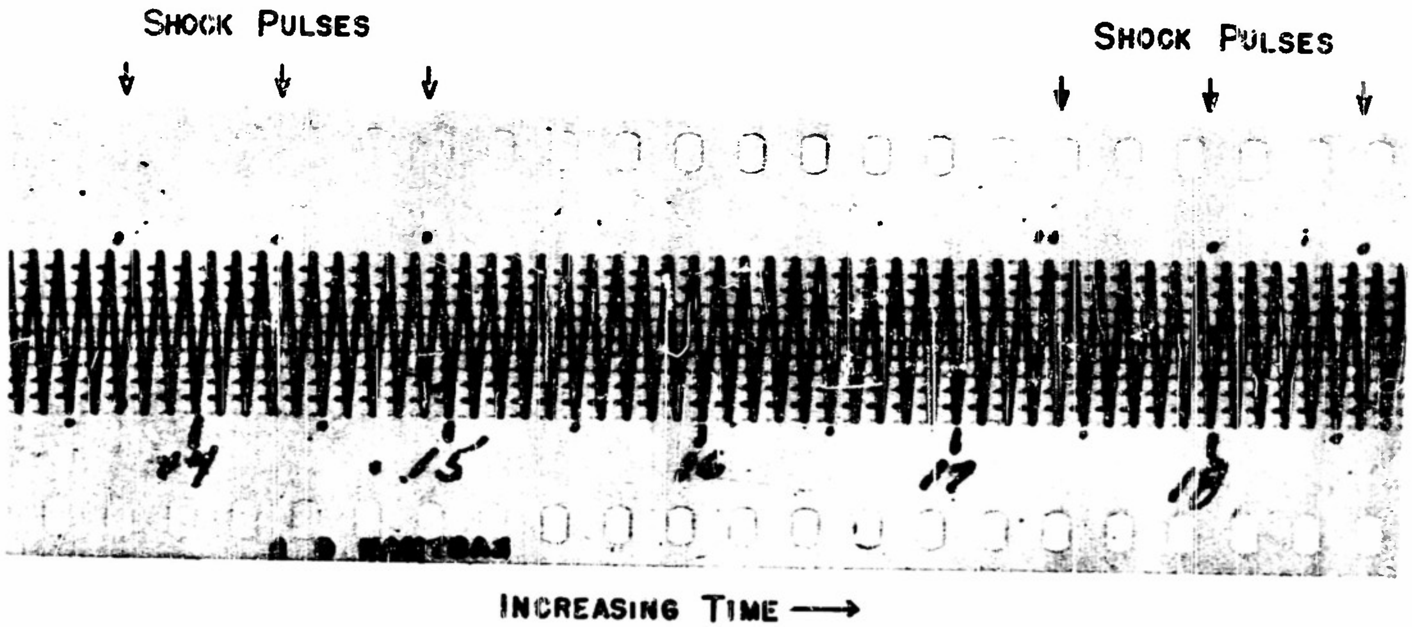

FIG. 19 SHOCK VELOCITY RECORD, MARK I CHRONOGRAPH. ARROWS INDICATE POSITIONS OF PULSES MARKING SHOCK ARRIVAL AT DETECTION STATIONS.

The sweep frequency multiplied by 20 is used to produce marker pips at five microsecond intervals; the pips are visible on the record of Fig. 19. The signals from the shock detection stations deflect the cathode ray spot in the direction opposite to the deflection of the marker pips. Six shock-detection-station pulses are visible on the portion of a record shown in Fig. 19. The Mark I chronograph provides a time base for recording sequential information within one microsecond over a 30,000 microsecond interval.

The initiator referred to earlier and indicated on Fig. 18 is a ring-type piezoelectric gauge constructed from barium titanate.[20] The gauge, whose inside diameter is 1-3/8 inches and which is 1/8" thick radially and 1/4" wide, is polarized radially. The inner and outer surfaces coated with a conducting paste serve as electrodes. The ring is mounted in a section of shock tube which can be inserted at any joint of the tube. The response of the gauge to either a shock or a rarefaction near the diaphragm position produces an initiating signal.

---

20. R. A. Shunk, et al, Rev. Sci. Instr. 24, 1069 (1953)

V Data and Results

5.1 Nature of the Data.

The data taken for each experiment in the density measurement of primary shock-tube flow are of both a static and a transient nature. The static data include the distances from the diaphragm position of the eight shock detection stations and the interferometer, the initial channel and chamber pressures, the temperature along the tube, and whenever the white-light-fringe technique (see Sec. 3.2) is used, the zeroth-fringe density. The transient data appear on the oscillographic record of the shock path and the record of chrono-interferometer fringe shift with time.

The survey of density in primary shock-tube flows is based on measurements whose range is shown in Table V. In addition to the 84 experiments listed in Table V, 30 experiments which did not yield all the required data due to malfunction of some part of the apparatus give supporting evidence.

TABLE V

CLASSIFICATION OF CHRONO-INTERFEROMETER

OSCILLOGRAPHIC RECORDS ACCORDING TO

EXPERIMENTAL CONDITIONS

Diaphragm-to Interferometer Distance	P_c/P_o=1.99				P_c/P_o=9.80				P_c/P_o=49.2			
	Channel		Chamber		Channel		Chamber		Channel		Chamber	
	F.	W.L.	F.	W.L.	F.	W.L.	F.	W.L.	F.	W.L.	F.	W.L.
A 0.630 m	1	0	1	0	2	7	2	2	1	4	2	1
B 2.958 m	1	0	1	0	2	4	1	2	2	7	2	1
C 5.285 m	1	0	1	0	2	2	2	0	2	2	2	0
D 7.622 m	3	0	1	0	5	2	1	0	6	4	2	0

Legend: P_c/P_o - average initial diaphragm pressure ratio.
Channel - Channel flow record
Chamber - Chamber flow record
F - Records taken with monochromatic filter
W.L. - Records taken with white light.

For the flows initiated from a pressure ratio P_c/P_o=1.99, all the information was obtained using the monochromatic filter. The irregular fluctuations noted under other conditions were not present, and a regular fringe count was possible throughout the flow. Flows initiated from pressure ratios P_c/P_o = 9.80 and 49.2 produced traces at the stations A and B nearer to the diaphragm which contained large amplitude "noise". Therefore it was necessary to perform a large number of experiments using the white-light-fringe technique to establish the time dependence of the average density in these flows. At stations C and D more distant from the diaphragm, the chrono-interferometer records were less "noisy" and less use of the white-light fringe technique was made, as may be seen in Table V.

5.2 Reduction of Shock Path Records.

The record of the shock motion in the channel serves the dual purpose of establishing zero time (diaphragm rupture) and of measuring the shock velocity for the determination of the density change across the shock. A plot of the shock arrival at each shock detection station, whose distance from the diaphragm is known, is made from each shock path record using an arbitrary time zero. The time intercept at the diaphragm position on these plots is used to establish zero time for each experiment.

The average shock speed V is determined at points midway between detection stations from the measured time and distance intervals. The shock Mach number $M_s = V/c_o$ can be computed, the sound speed c_o in the undisturbed gas[21] being known. A plot of M_s as a function of distance from the diaphragm position is used to determine shock Mach number

---

21. Sound speed in nitrogen gas is computed from $c_o = 337.7(1+0.00359t)^{1/2}$ m/sec where t is the Centigrade temperature. This value is taken from the International Critical Tables 6, 463, McGraw-Hill (1929).

at the interferometer station. The fractional density ratio across the shock discontinuity at the interferometer position is then calculated from this graphically determined value of M_s. The equation for this calculation resulting from the elimination of y between equations (B1) and (B4), appendix B, for $\gamma = 7/5$, is

$$\left(\frac{\Delta\rho}{\rho_0}\right)_s = \frac{5(M_s^2-1)}{M_s^2+5} \quad (5.1)$$

5.3 Reduction of Chrono-Interferometer Records.

A record of fringe shift vs. time is obtained directly from the interferometer records. The arrival of the shock in the case of channel flow, and the arrival of the rarefaction head in the case of chamber flow is used for time reference point for the fringe shift time measurement. In order to establish these references on records taken with the white light source, the output of a ring-type piezoelectric gauge near the interferometer is simultaneously recorded on the second channel of the Mark II oscillograph. By reference on the film record to the time between the pressure gauge detection of the shock or rarefaction and the chrono-interferometer response to white light, the desired reference point can be established by comparison with a record including the gauge response on a monochromatic trace taken with the same initial conditions. This procedure relies upon the reproducibility of shock-tube flows under the same initial conditions.

The small changes in initial conditions due to the daily variations of ambient temperature may be accounted for by expressing the data in a dimensionless form involving the sound speed c_0 in the undisturbed gas. The time-like parameter $\tau = \frac{c_0 t}{d}$ is used, where d is the interferometer-to-diaphragm distance and t is the time measured from the proper zero. For chamber flows, where t_1 is measured from the arrival of the rarefaction head at the interferometer, the formula

$$\tau = 1 + \frac{c_0 t_1}{d} \tag{5.2}$$

is used. For channel flows, where t_2 is the time relative to the shock arrival at the interferometer, the formula

$$\tau = \tau_s + \frac{c_0 t_2}{d} \tag{5.3}$$

is used. The value τ_s is determined from the shock path record described in Sec. 5.2.

The density ratio ρ/ρ_c, where ρ_c is the initial chamber density, is used to discuss the chamber flow. The ratio

$$\rho/\rho_c = 1 - \Delta\rho/\rho_c , \tag{5.4}$$

where $\Delta\rho$ is the density change from the value ρ_c, is obtained from the fringe shift ΔS, counted from the head of the rarefaction, by the equation

$$\Delta\rho/\rho_c = \frac{T_c}{T_i}\left(\frac{\Delta P}{\Delta S}\right)_i \frac{\Delta S}{P_c} \tag{5.5}$$

which makes use of the basic interferometric relation (3.2). In the preceding equation T_c and P_c are initial chamber temperature and pressure, and the subscript i refers to the isothermal interferometer calibration. The density in the channel flow is expressed in the form of fractional density change $\Delta\rho/\rho_o = (\rho - \rho_o)/\rho_o$, where ρ_o is the initial channel density. The value of $(\frac{\Delta\rho}{\rho_o})_s$ across the shock is calculated by (5.1) using the shock path data. The additional fractional density change behind the shock is calculated from the fringe shift ΔS counted from the shock. The formula for the fractional density change in the channel is

$$\Delta\rho/\rho_o = (\Delta\rho/\rho_o)_s + \frac{T_o}{T_i}\left(\frac{\Delta P}{\Delta S}\right)_i \frac{\Delta S}{P_o}, \tag{5.6}$$

where T_o and P_o are initial channel temperature and pressure.

An estimate, based on the ideal shock-tube flow theory, of the effect on the density of a small variation in the initial pressure ratio P_c/P_o indicates that the density variation due to variations in P_c/P_o among trials would be less than the experimental error in density measurement except in the hot gas region between shock and cold front. Therefore, a correction was applied only to the values of $\Delta\rho/\rho_o$ and τ between shock and cold front to reduce the experimental values to those expected at the average P_c/P_o.

A sample reduction of data is outlined in appendix D.

5.4. Results.

The density measurements made in primary shock-tube flows are presented in graphical form. The time variation of density at eight different positions in three flows started from different initial pressure ratios has been recorded. Of the 24 density-time measurements, all four channel positions at P_c/P_o=1.99, and all four chamber positions for each initial pressure ratio are grouped together, with the remaining 8 studies of channel flow presented separately. These 12 graphs appear as Figures 20 to 31.

The density variation with time at the channel positions is presented as a plot of fractional density change $\Delta\rho/\rho_o = (\rho - \rho_o)/\rho_o$ against the time-like variable $\tau = c_o t/d$, and at the chamber positions the dimensionless variables ρ/ρ_c and τ are used. The reference densities ρ_o and ρ_c are respectively the undisturbed channel gas and chamber gas density, c_o is the sound velocity in the undisturbed gas in both channel and chamber, t is the time after diaphragm rupture, and d is the distance between interferometer windows and diaphragm. The use of these variables permits corrections to standard conditions to be made for measurements made under slightly different initial conditions, as

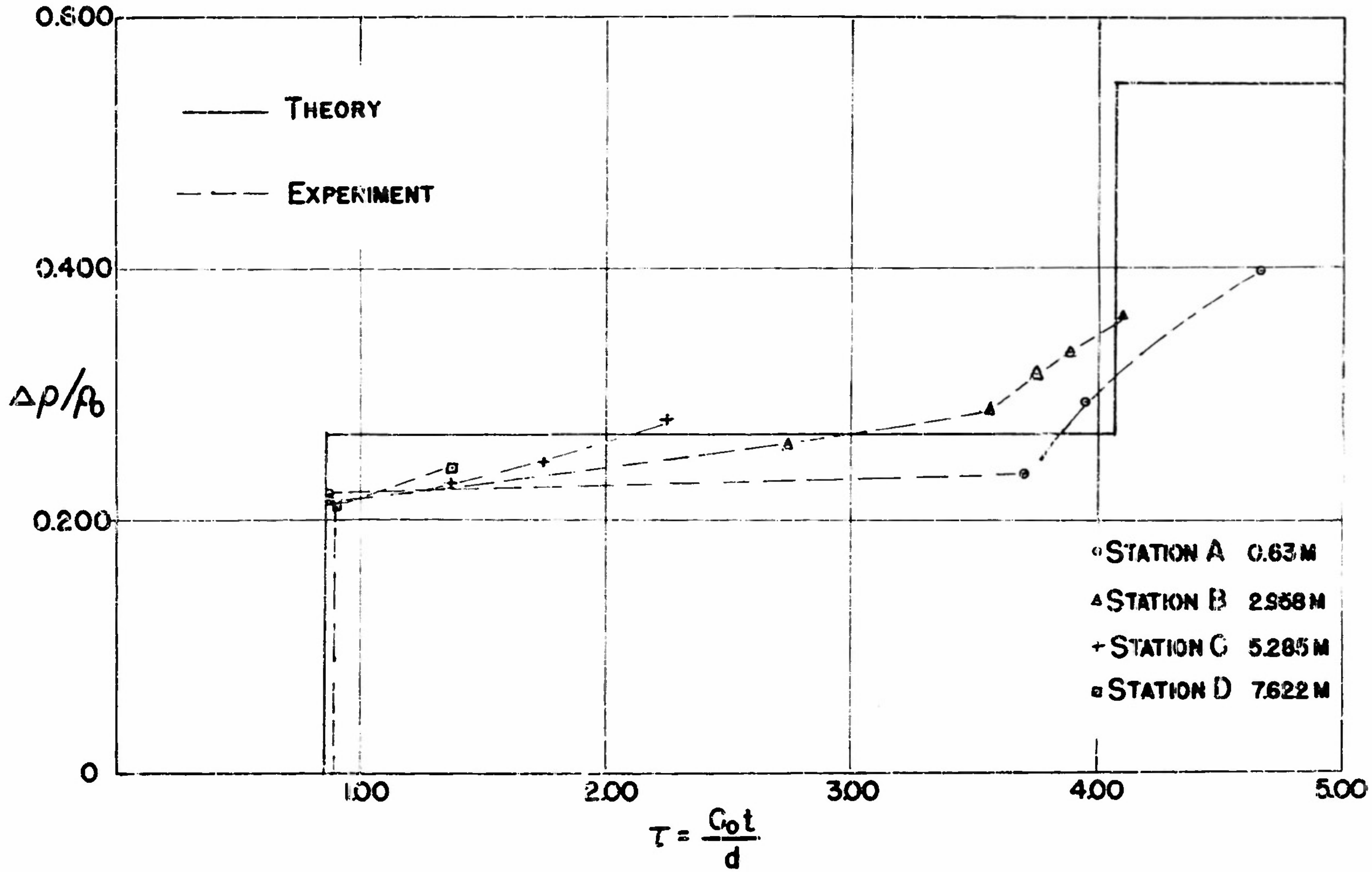

FIG. 20 CHANNEL FLOW $P_c/P_0 = 1.99$

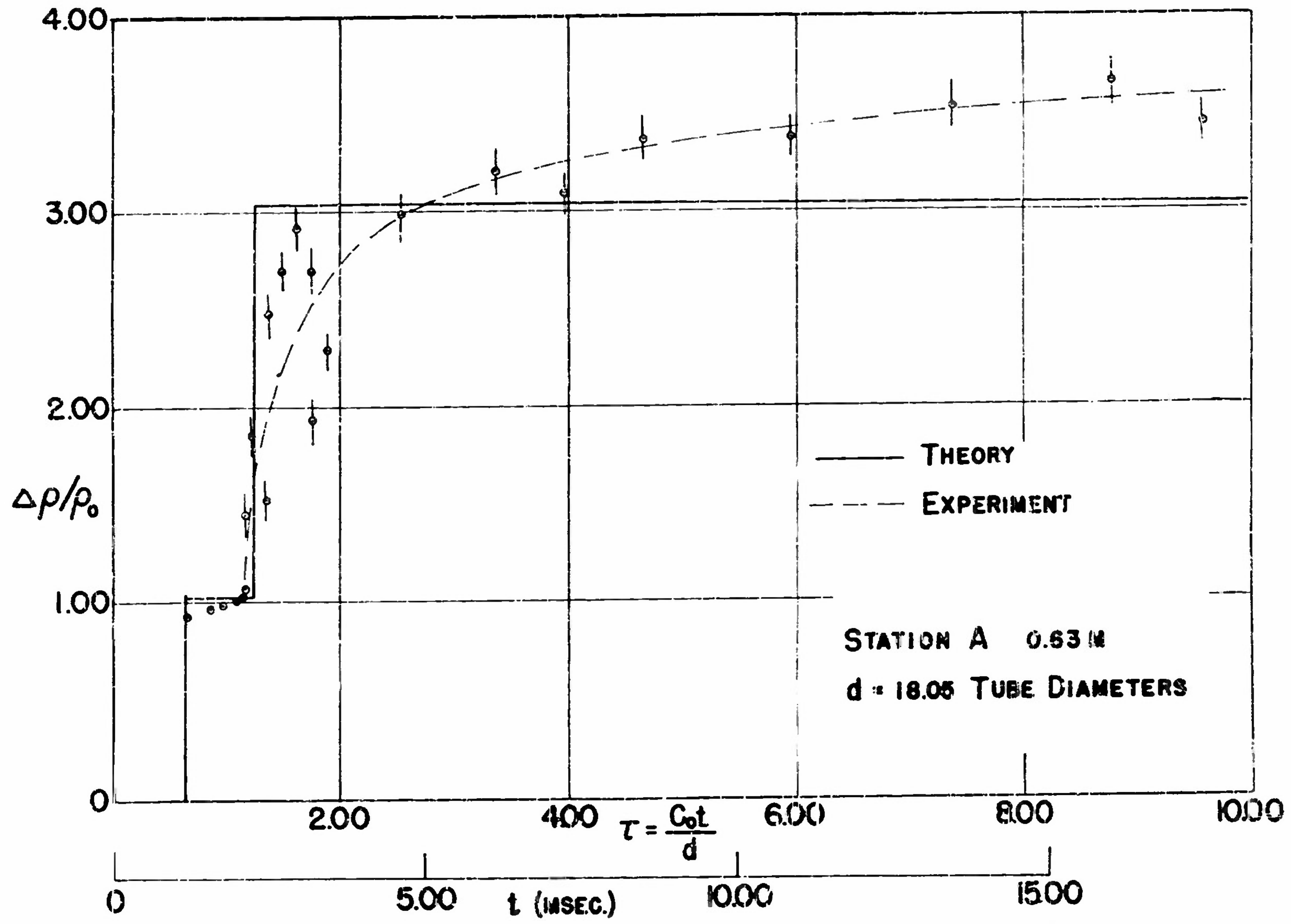

FIG. 21 CHANNEL FLOW $P_c/P_o = 9.80$

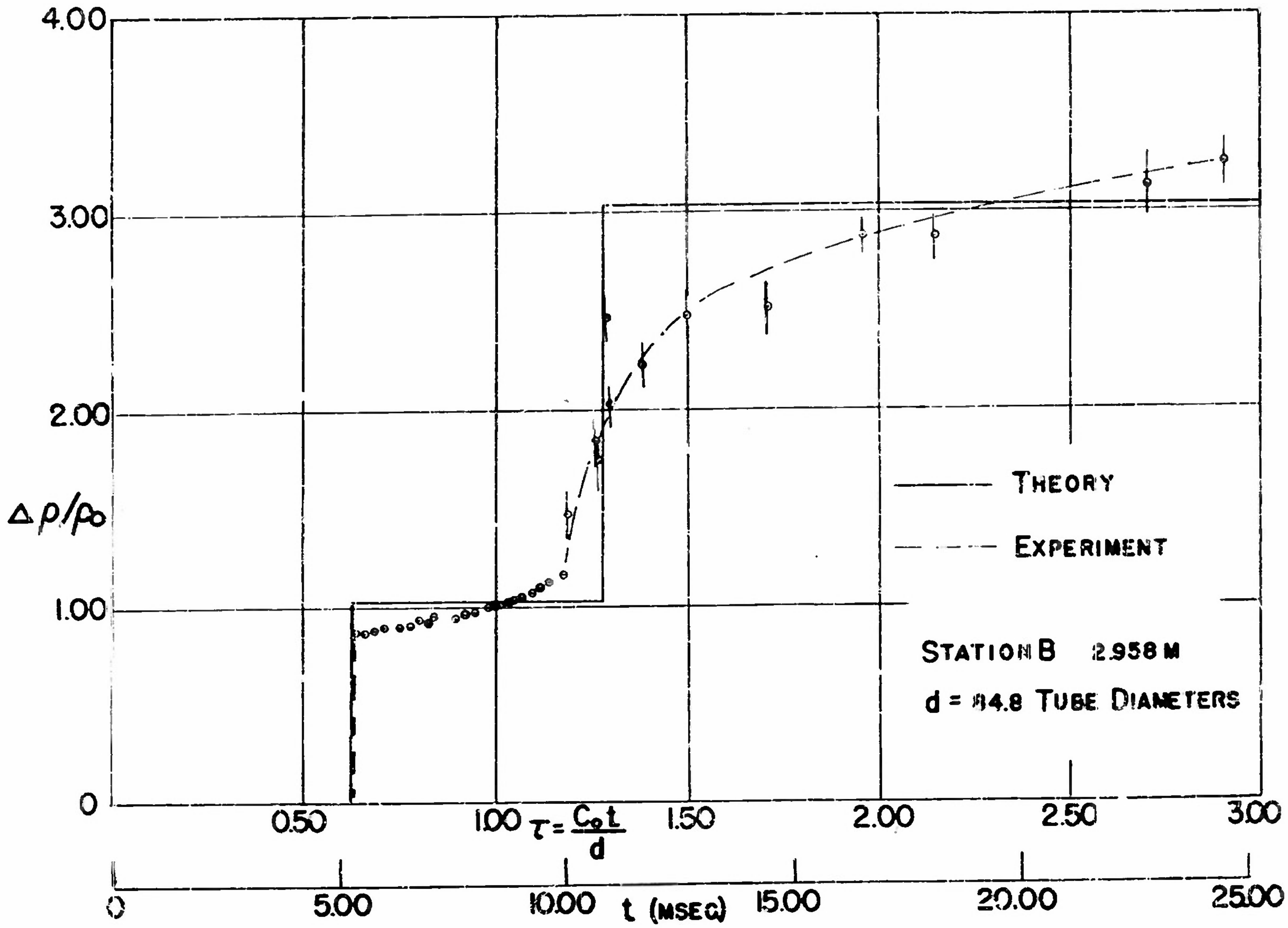

FIG. 22 CHANNEL FLOW $P_c/P_0 = 9.80$

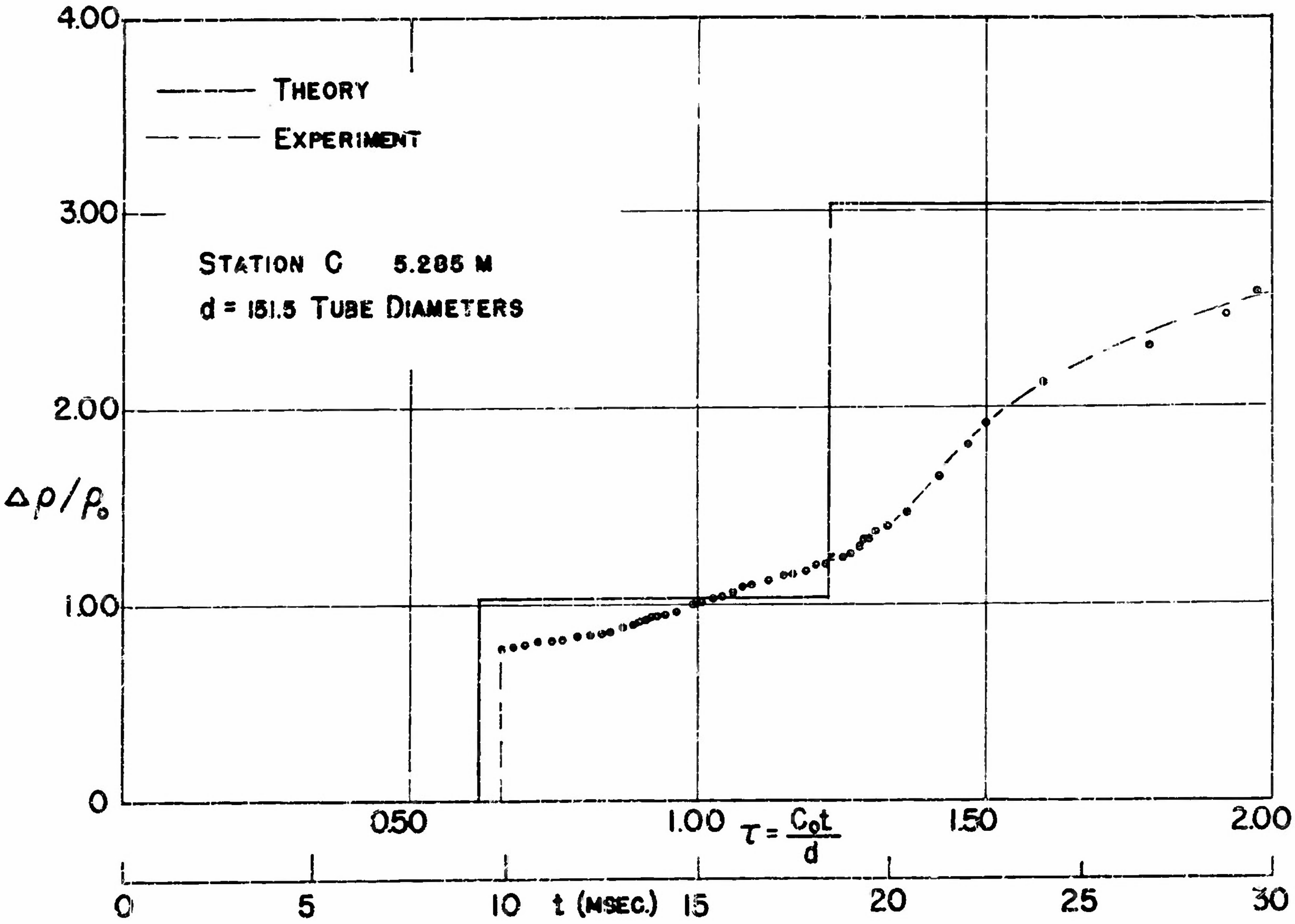

FIG. 23 CHANNEL FLOW $P_c/P_0 = 9.80$

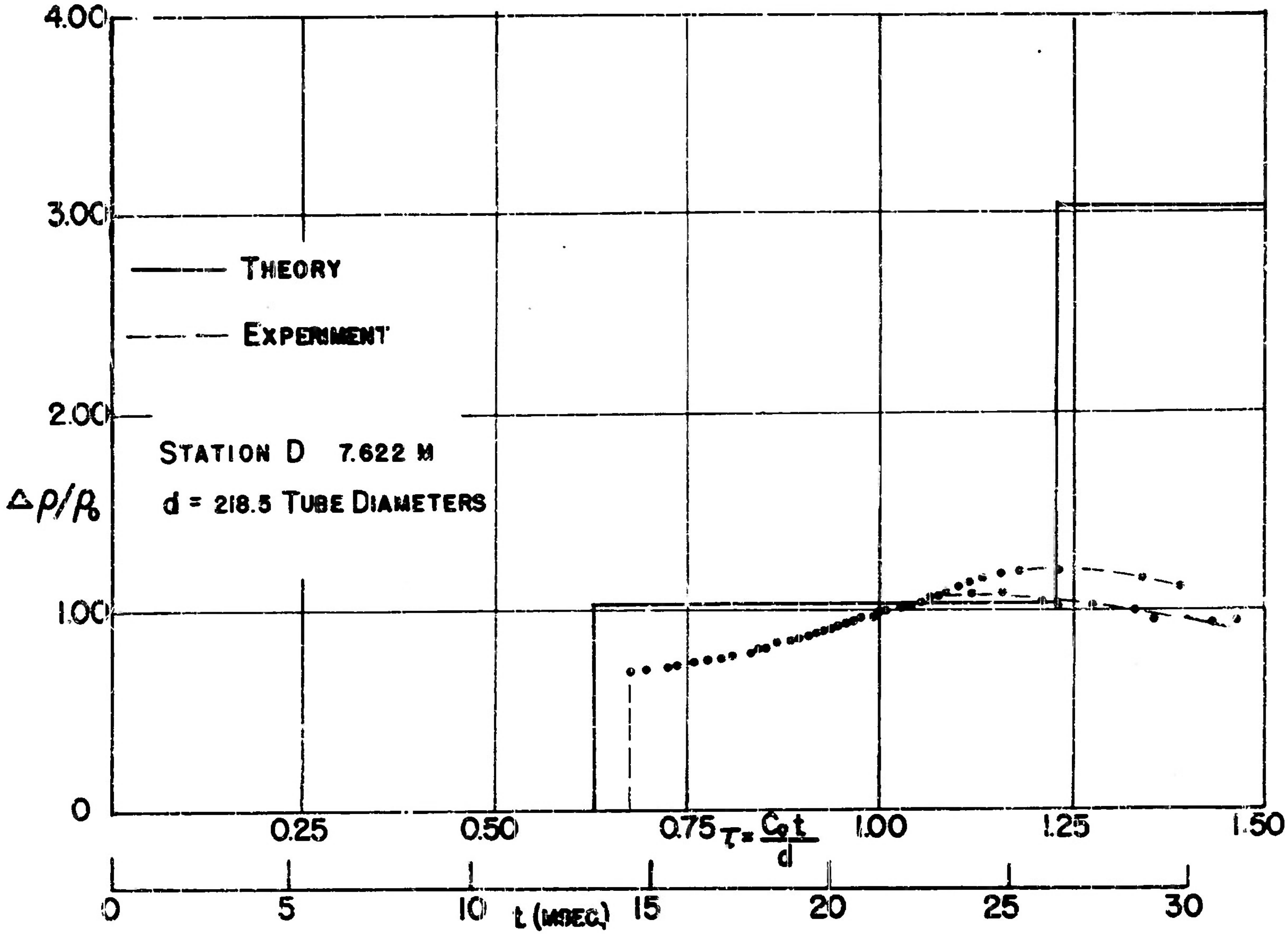

FIG. 24 CHANNEL FLOW $P_c/P_a = 9.80$

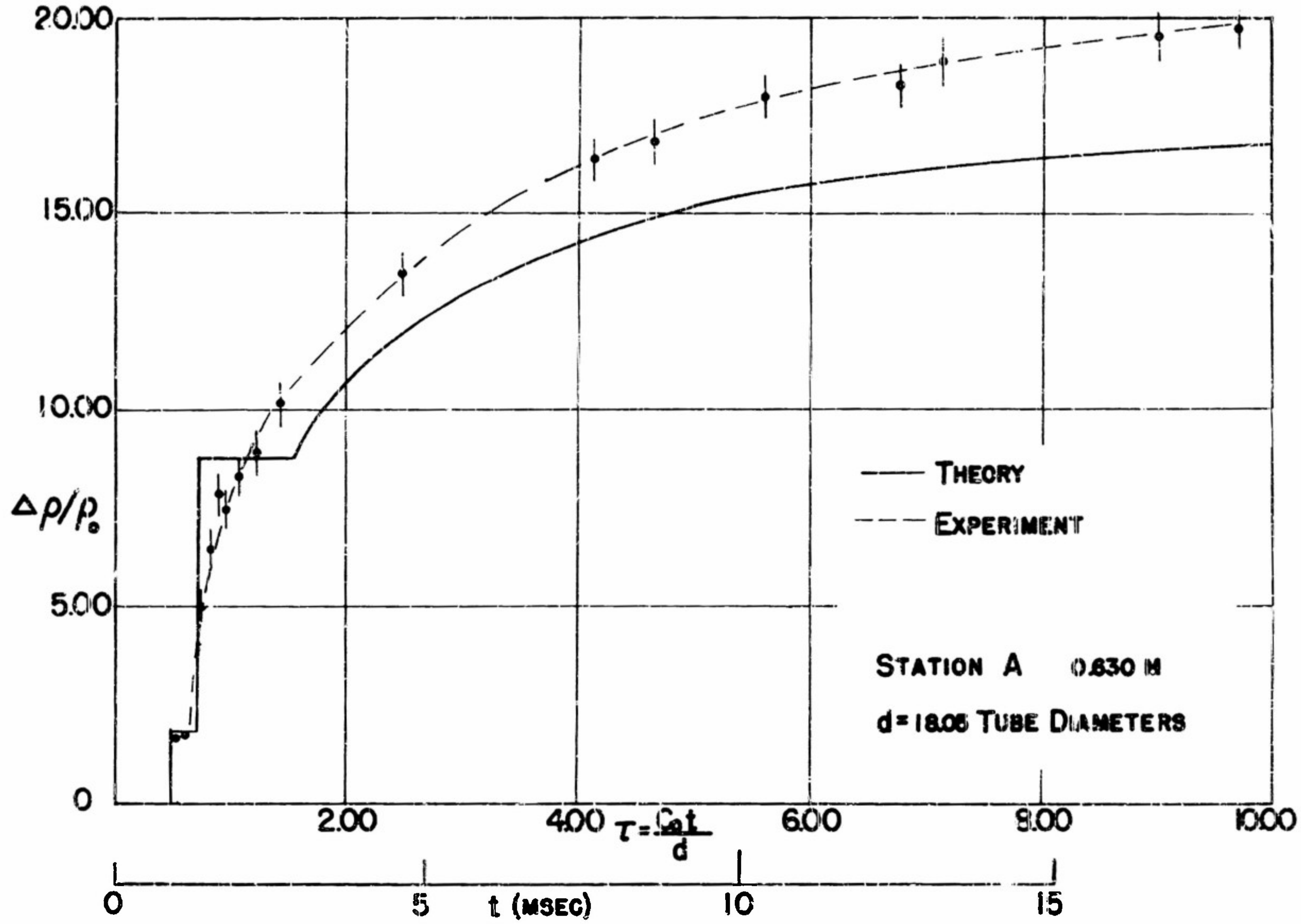

FIG. 25 CHANNEL FLOW $P_c/P_0 = 49.2$

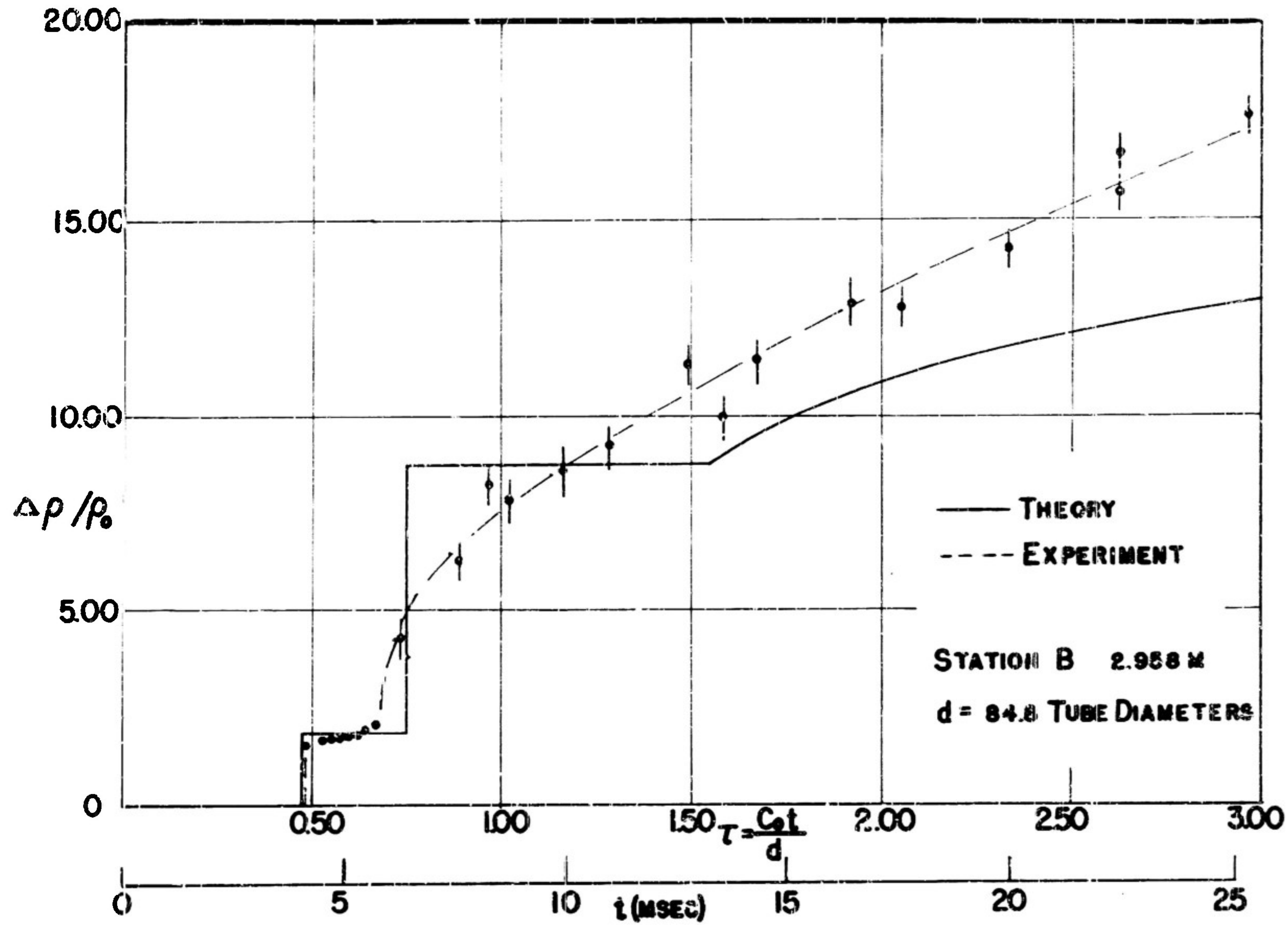

FIG. 26 CHANNEL FLOW $P_c/P_o = 492$

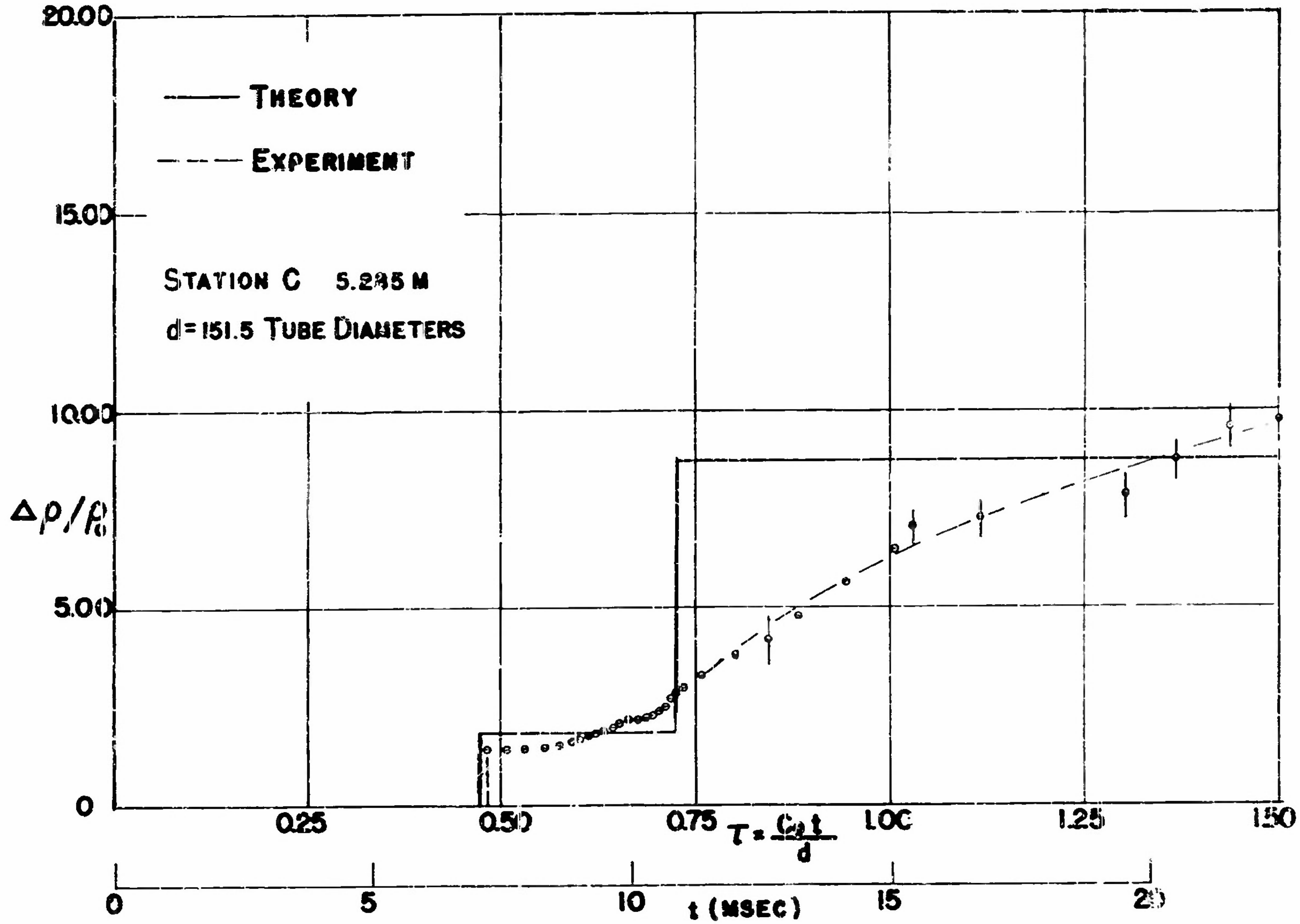

Fig. 27 Channel Flow $P_c/P_0 = 49.2$

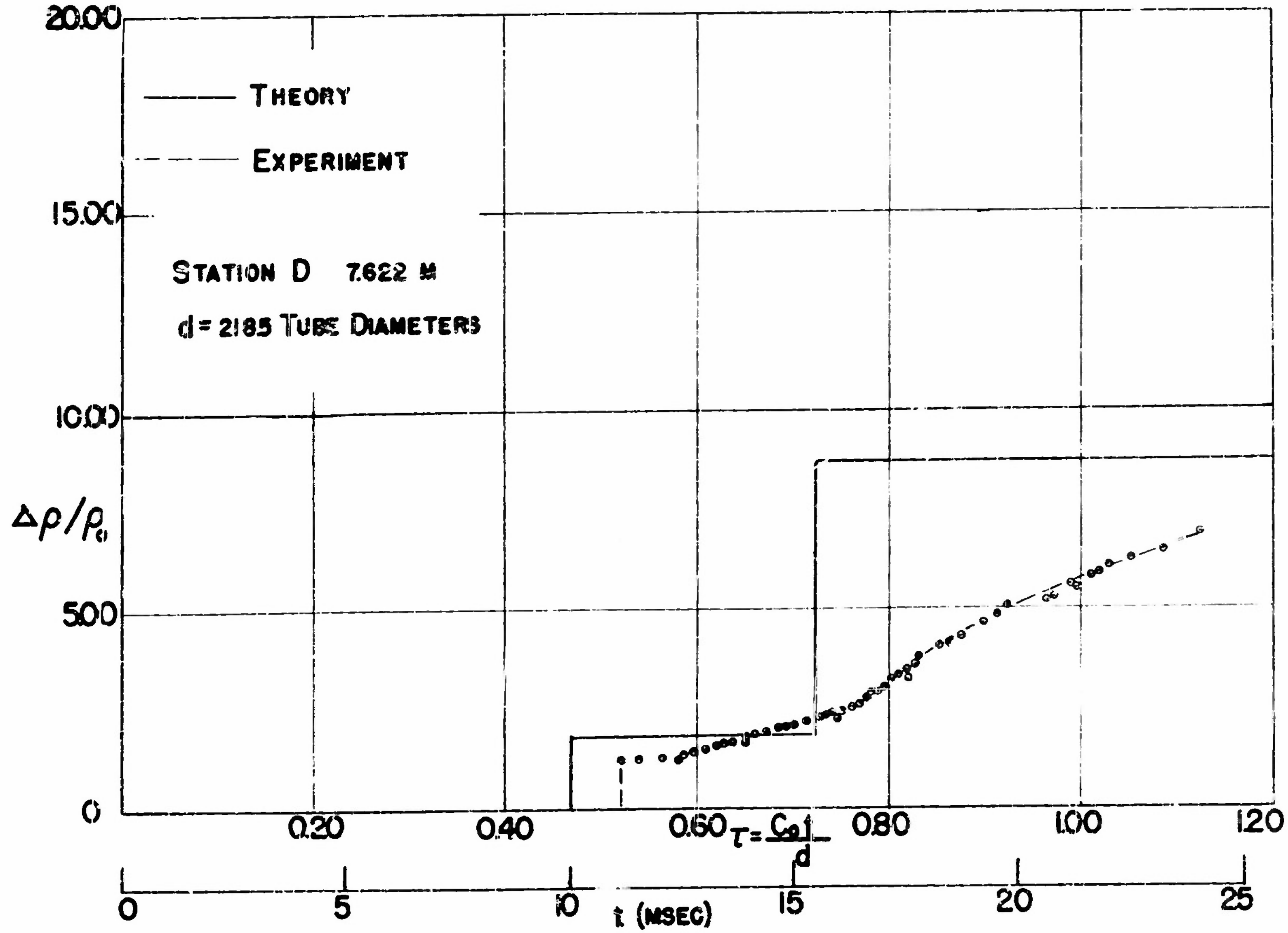

FIG. 28 CHANNEL FLOW $P_c/P_0 = 49.2$

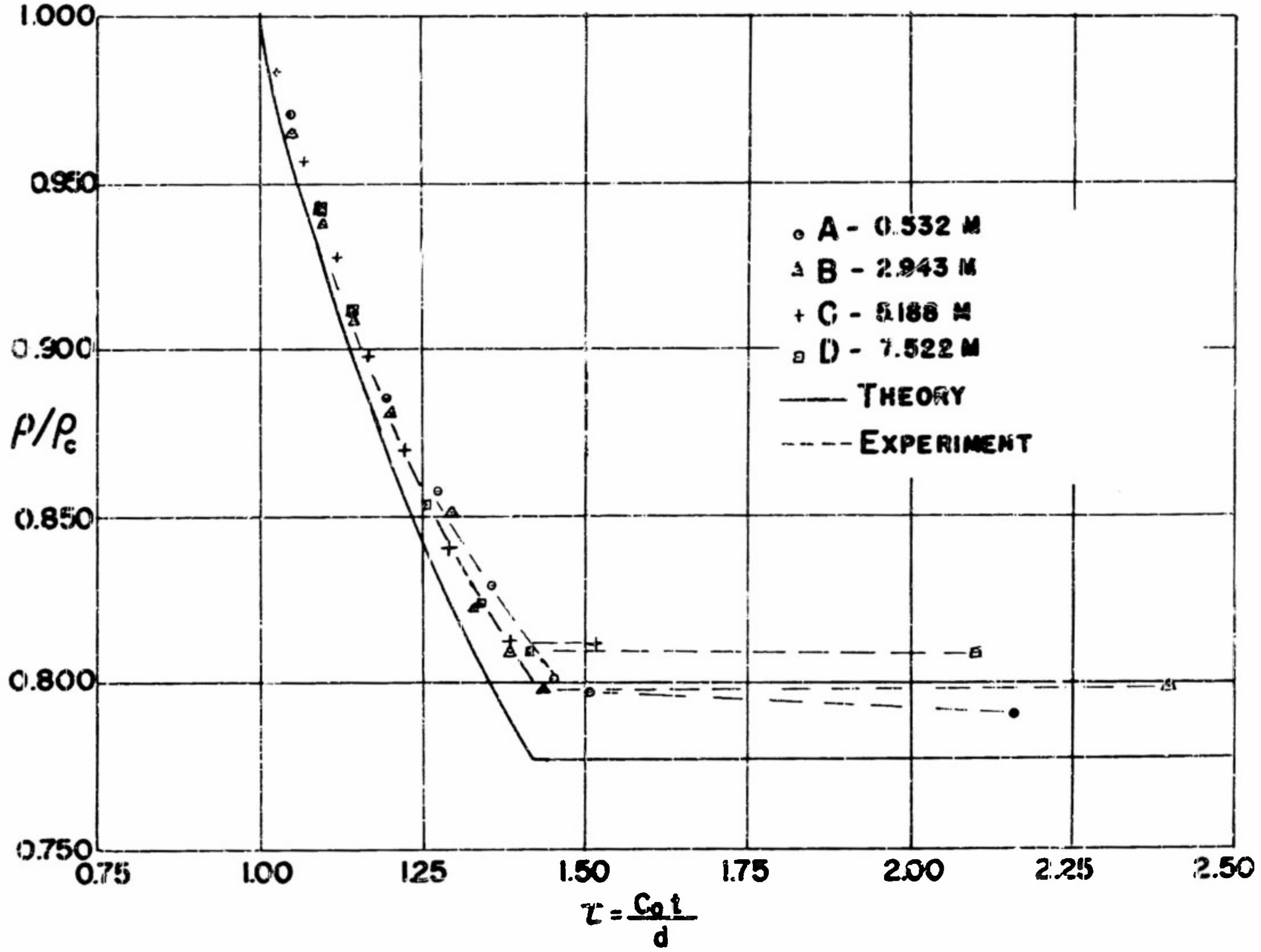

FIG. 29 CHAMBER FLOW $P_c/P_0 = 1.99$

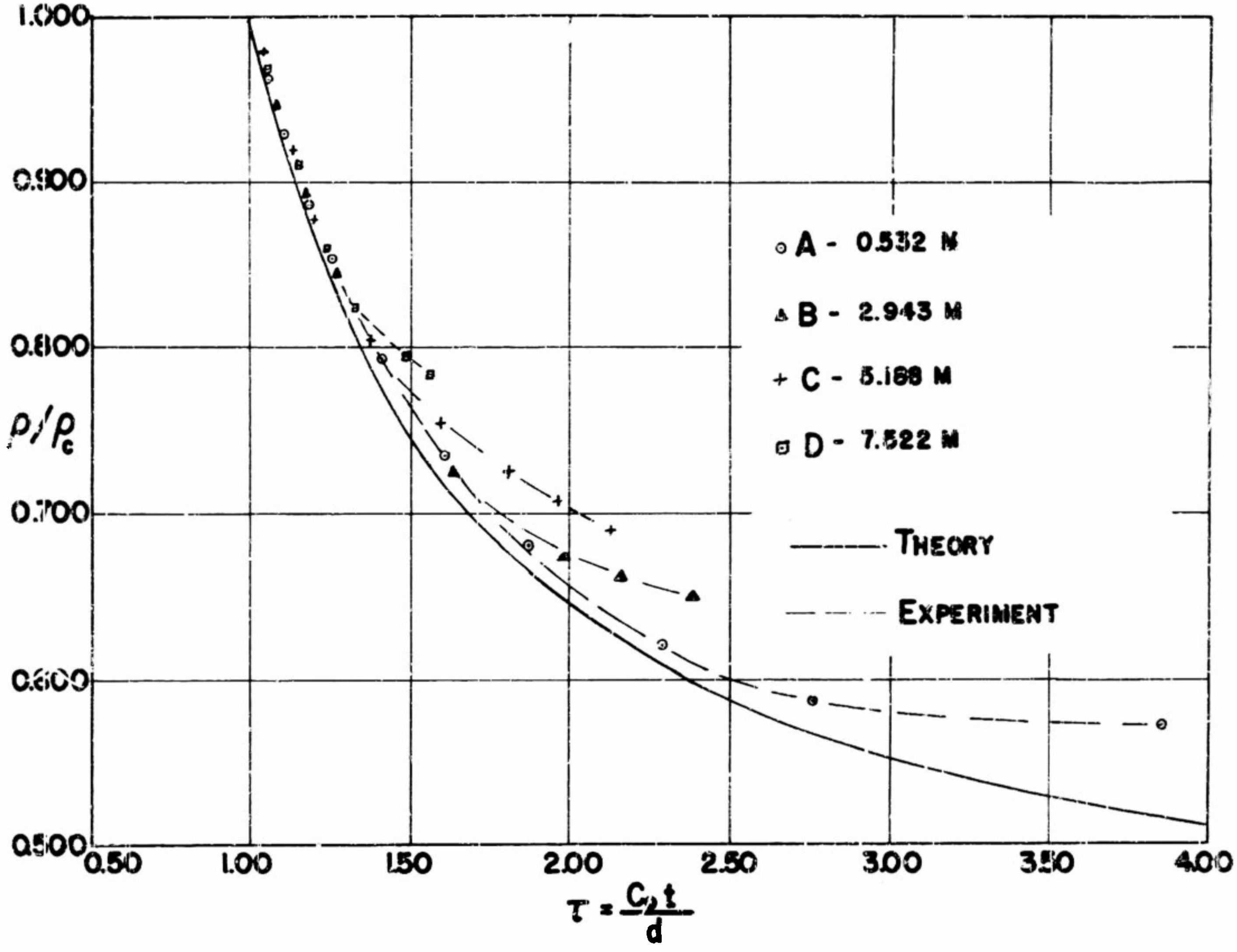

FIG. 30 CHAMBER FLOW $P_c/P_o = 9.80$

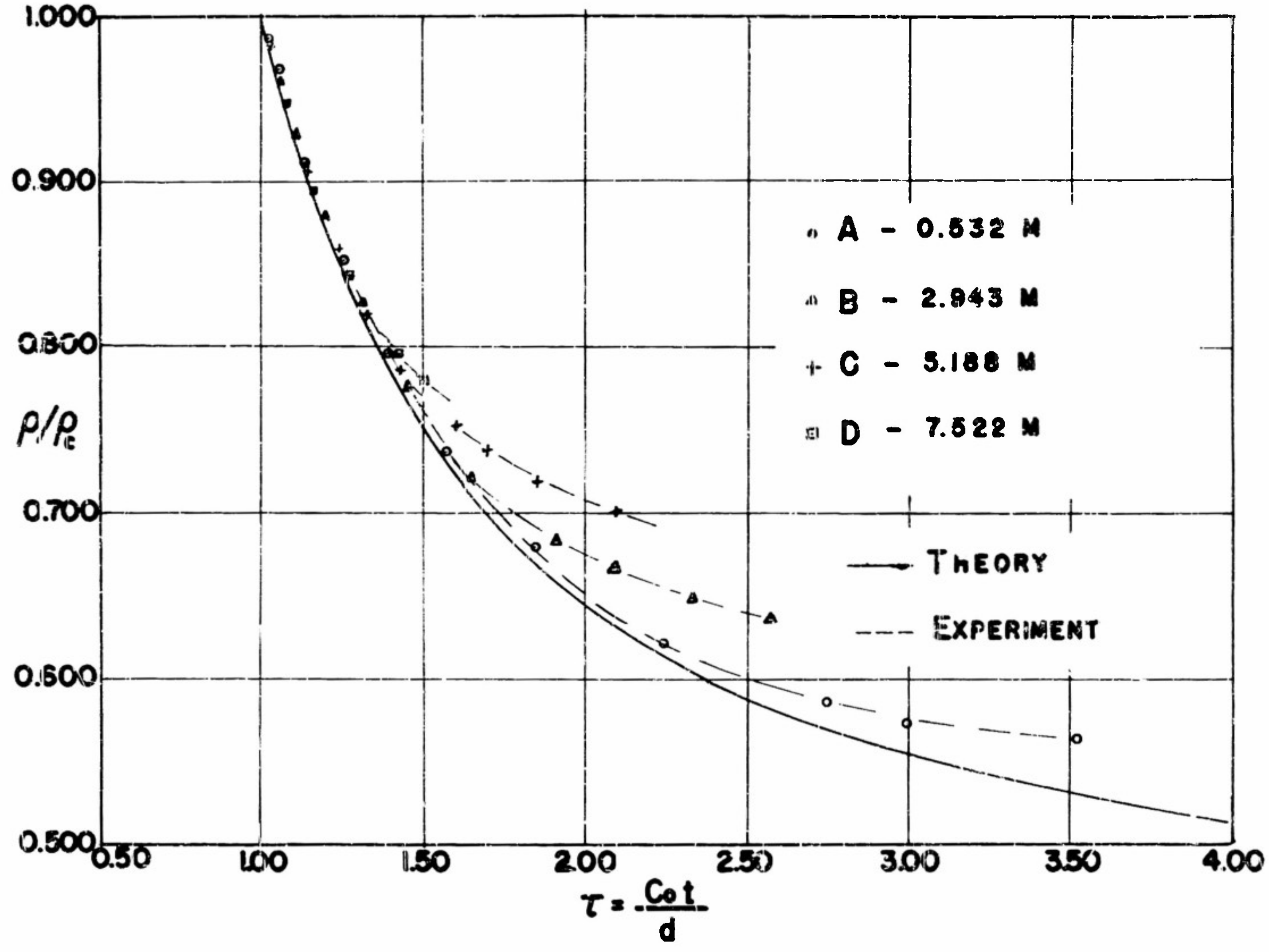

FIG. 31 CHAMBER FLOW $P_c/P_0 = 49.2$

described in the preceding section; the use further facilitates the comparison of experimental results with the idealized theory.

The channel flow results are presented in Figures 20 to 28. The time dependence of density at all four interferometer stations is given in Fig. 20 for P_c/P_o=1.99. Figures 21, 22, 23, and 24 for P_c/P_o=9.80 and Figures 25, 26, 27, and 28 for P_c/P_o=49.2 present the density variation with time at the successively more remote interferometer stations A, B, C, and D respectively. Freehand curves through experimental points are shown dashed. The idealized shock-tube theory predicts constant density behind the shock until the arrival of the contact surface (cold front), constant density behind the contact discontinuity, and, in the case of P_c/P_o=49.2, increasing density as the rarefaction spreads over the station under study. These quantitative predictions of the idealized theory are drawn on each graph to permit comparison with the actual flow.

In each case, the duration of the measurement was approximately 30 milliseconds from diaphragm rupture. The variable $\tau = \frac{c_o t}{d}$ thus terminates at smaller values for larger distances d of the measuring station from the diaphragm, and it appears that a smaller fraction of the flow is studied at greater distances. Actual times in milliseconds are shown on Figures 21 through 28 corresponding to a sound speed of 752.5 m/sec in the undisturbed gas.

The duration of the measurements of channel flows was sufficient to observe the cold front at all stations except C and D for P_c/P_o=1.99, and station D for P_c/P_o=9.80. In these cases the rarefaction reflected from the end of the chamber reached the interferometer before the cold front arrived. In Fig. 24 (P_c/P_o=9.80 at station D) the two reflected rarefactions shown illustrate the effect of delaying the arrival of the reflected wave by making a small increase in chamber length.

The chamber flow measurements for all stations are shown on Figures 29, 30, and 31 for the flows initiated from P_c/P_o= 1.99, 9.80, and 49.2 respectively. The measured rarefactions are compared with the centered rarefaction postulated in the ideal shock-tube theory.

5.5 Reliability of the Density Measurements

Since more interest exists in relative density changes than in values of absolute density, the reliability of measured values of the former will be discussed. Actually the known initial pressures and temperatures in chamber and channel, and the known thermodynamic properties of nitrogen gas would permit relative density values to be transformed into absolute density values with high precision.

In preceding sections of this chapter it has been mentioned that the relative density values are determined from equations repeated here for reference.

$$\left(\frac{\Delta\rho}{\rho_o}\right)_s = \frac{5(M_s^2 - 1)}{M_s^2 + 5}$$ Fractional density increase across shock. (5.1)

$$\frac{\Delta\rho}{\rho_o} = \left(\frac{\Delta\rho}{\rho_o}\right)_s + \frac{T_o}{T_i}\left(\frac{\Delta P}{\Delta S}\right)_i \frac{\Delta S}{P_o}$$ Relative channel density in terms of measured fringe shift. (5.6)

$$\frac{\rho}{\rho_c} = 1 - \frac{T_c}{T_i}\left(\frac{\Delta P}{\Delta S}\right)_i \frac{\Delta S}{P_c}$$ Relative chamber density in terms of measured fringe shift. (5.5)

As stated in preceding sections, the density determinations made with the white-light-fringe technique yield density values directly.

The determination of time at which a density measurement is made is also subject to error. Since all graphical comparison in Figures 20-31 involve the "relative" time parameter,

$$\tau = c_o t/d$$

the reliability of this quantity is of interest. The uncertainties in the values of τ relative to those in the relative density values are so small that no indication of their magnitude can be made on the graphs. Error intervals in relative density values are shown by vertical lines through data points in Figures 20-31; the accuracy of data points without vertical lines is such that the error interval would be less than indicated by the size of the symbols.

Now consider the influence of errors in measured quantities on the precision of the plotted data points in turn. The variation, among repeated trials of flows started from identical conditions, of the measured shock Mach number $M_s = \frac{V}{c_0}$ is larger than can be attributed to errors in the measured time and distance intervals or to the sound speed c_0. Groups of five or more repetitions (P_c/P_o=9.80, 49.2) yield in no case a sample standard deviation for M_s exceeding 1%. Through equation (5.1), the calculated values of $(\Delta\rho/\rho_o)_s$ are thus found to be reliable to within 2% for P_c/P_o=9.80, 49.2. Similar considerations involving fewer repetitions show values for the case P_c/P_o = 1.99 to be reliable within 1%.

In section 3.2 the quantity $\frac{1}{T_1}\left(\frac{\Delta P}{\Delta S}\right)_1$ was shown to be constant to 0.4% over a pressure range from 1/2 to 5 atmospheres. In measuring the initial conditions, the reading and instrumental errors are such that the quantities T_o/P_o and T_c/P_c will be correct to within 0.5%. The reading error from the chrono-interferometer records of the fringe shift ΔS are conservatively estimated to be $\pm$ 1/10 fringe for "quiet" chamber flow and $\pm$ 1/8 fringe for the "quiet" hot gas region of channel flow. The accumulated errors in the relative densities calculated by equations (5.5) and (5.6) are less than the size of the symbols indicating experimental points in Figures 20 through 31.

The larger error involved in measurements made by the white-light-fringe technique arises from two sources. First, with the care taken in this work the zeroth-fringe-density setting is known only to ± 1 fringe. Secondly, in noisy flow regions where noise amplitude exceeds 1/2 fringe, the average fringe amplitude cannot be accurately determined, so that the fringe number can be identified only to ± 1 fringe.

The errors in the time parameter $\tau = c_o t/d$ are small and involve only errors in c_o and in the determination of the initial time zero. The sound velocity is known to within ± 0.5 m/sec. The time origin as determined from the x-t plot of the shock path has an estimated error of ± 50 microseconds.

VI Discussion

The density measurements presented in the preceding chapter show that, with the exception of flow near the head of the rarefaction, the density distribution in time and space in the 1-3/8 inch diameter shock tube is not accurately described by the ideal theory. Rough outlines of the ideally predicted regions of constant density hot gas, constant density cold gas, and a rarefaction wave are evident in most of the measurements, however. In this chapter, some details of the deviations in the flow from that predicted by the ideal theory are discussed and certain mechanisms are suggested which might need be taken into account to develop a more satisfactory theory of shock tube flow.

6.1 Features of Primary Shock Tube Flow

a) Spreading of the Cold Front.

One of the most marked deviations observed in the flow from that predicted by the ideal theory is the absence of a contact surface between hot and cold gas. In every case studied, as may be seen in Figures 20-27, the density increases gradually as the cold gas region approaches and passes the interferometer windows. Nearer the diaphragm a rather rapid increase in density with time is observed (Figs. 21, 22, 25, 26). On these graphs the scatter in the white-light-fringe points, which is outside experimental error, indicates that there is initially, with the arrival of the cold gas, a narrow region of rapidly fluctuating density. At more distant interferometer stations the density increases quite gradually without such violent fluctuations and the cold front is greatly extended. (Fig. 23, 27, 28). Although the cold front region was observed only at stations A and B for $P_c/P_o = 1.99$ it is evident even in this case that the front is spreading out both into the predicted hot gas and the cold gas regions and occupies a region extending over approximately four tube diameters (Fig. 20).

b) Non-Uniform Hot Gas Region.

In every case studied deviation from a constant density in the hot gas region exists. The density increases continuously with time after the shock passes. In the case of $P_c/P_o = 1.99$ this density increase is 30% of the initial density change across the shock, and for $P_c/P_o = 9.80$ and 49.2, this density increase exceeds 50% of the density change across the shock at more distant stations.(Figs. 23, 24, 27, 28). The shock velocity records show a decrease in shock strength with distance in agreement with previous measurements in this tube.[3] Furthermore, the duration of the hot gas region becomes progressively less than theoretically predicted with increasing interferometer-to-diaphragm distance.

c) Non-Uniform Cold Gas Region.

As the cold gas region passes, the average density is observed to increase with time. At interferometer stations near the diaphragm, density values higher than theoretically predicted are achieved. The shattering diaphragm material is carried along with this gas and the observed particles are more numerous and more compact at shorter distances from the diaphragm position. There is no evidence of a constant density region in the cold gas. Only in the case of $P_c/P_o = 49.2$ is the tail of the rarefaction predicted to pass the interferometer stations in the channel, and there is no marked indication of the arrival of the leading edge (Fig. 25, 26).

d) Deviation from a Centered Rarefaction.

The postulated centered rarefaction in the chamber is a good approximation to the observed rarefaction initially. As the flow develops the latter portions of the rarefaction begin to deviate from the centered rarefaction. In the case $P_c/P_o = 1.99$ the rarefaction tail which is fairly clearly marked, occurs at successively higher densities as the interferometer-to-diaphragm distance increases; the tail density is 3% higher at station A and 5% higher at station D (Fig. 29). In the cases $P_c/P_o = 9.80$, and 49.2 the density decrease in the rarefaction is much less than that of the postulated wave (Figs. 30, 31). The rarefaction resulting from $P_c/P_o = 49.2$ follows the postulated centered rarefaction for slightly longer times at each station.

e) Irregular Density Fluctuations

The records obtained in flows resulting from $P_c/P_o = 1.99$ are free from irregular fluctuations. However, the flows resulting from $P_c/P_o = 9.80$ and 49.2 give evidence of irregular density fluctuations (Figs. 11b and 12b) which in general are most prevalent in the flow following the cold front in the channel and in the flow at the later portions of the rarefaction in the chamber. At station A (nearest the diaphragm) the hot gas region produces signals characteristic of shock passage which appear after the passage of the primary shock. However, at the more distant stations B, C, and D small irregular density fluctuations appear which grow in magnitude as the hot gas region passes. These fluctuations appear at successively longer times after the shock passes stations B, C, and D respectively and they have the same order of absolute magnitude for both initial conditions at each interferometer station. At the nearer stations A and B the fluctuations attain an amplitude exceeding one half fringe immediately upon the arrival of the cold gas. At the more distant stations C and D the irregular fluctuations in the channel never attain a half-fringe amplitude in the cold gas region. As the rarefaction passes a chamber position, small irregular density fluctuations appear and increase in magnitude in a regular fashion until a half-fringe amplitude or greater exists. The appearance of these fluctuations in the rarefaction is not simply correlated with either density, or time of flow.

6.2 Composite Representations of the Results.

The measurements of density in primary shock tube flows can be presented by two additional graphical methods as an aid toward visualizing the extent of the deviation from the ideal flows. In Fig. 32 the density distribution at the eight stations along the shock tube at a particular time after diaphragm rupture is presented, together with the theoretical distribution (Appendix C). The second method consists of a plot of lines of constant density for the primary flow on the x-t plane. This latter method, yielding the plots of Figs. 33, 34, and 35, is most elegantly suggested by the wave speed camera investigations of shock tube flow carried out at the University of Toronto.[22]

---

22. Glass, I. I., Institute of Aerophysics Report No. 6, University of Toronto (1950)

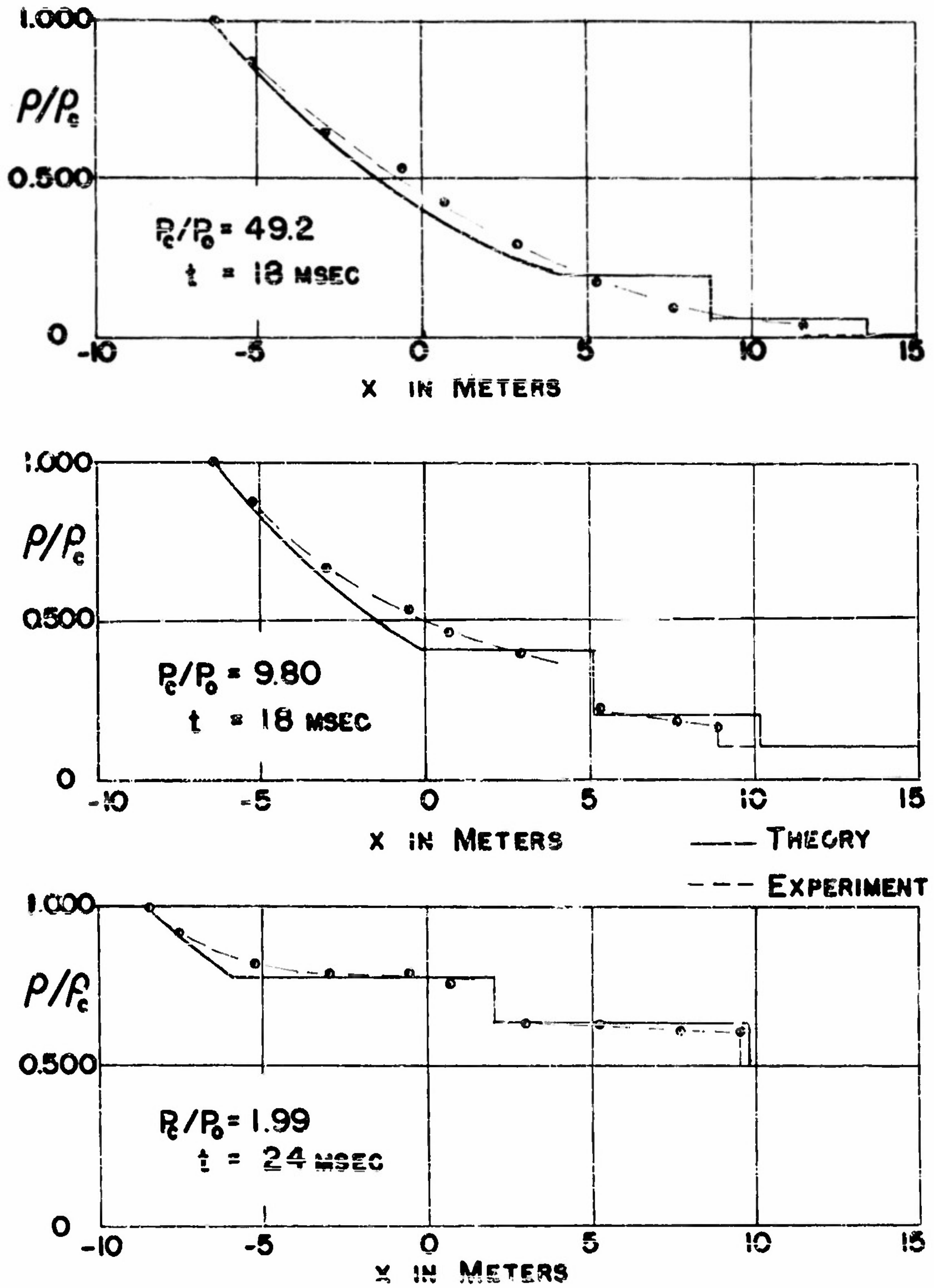

FIG. 32 SPATIAL DENSITY DISTRIBUTION IN PRIMARY SHOCK-TUBE FLOW AT A PARTICULAR TIME

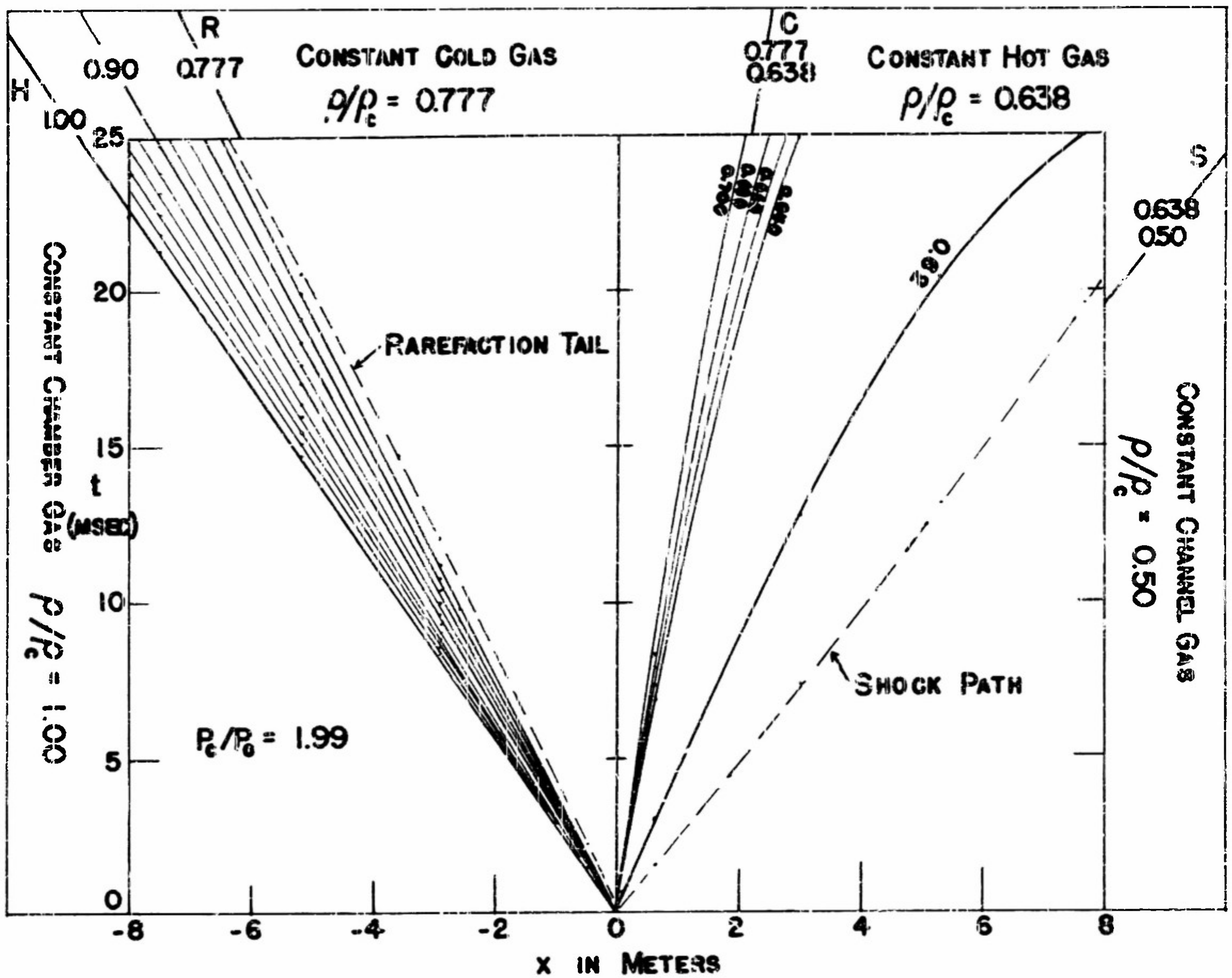

FIG. 33 X-t PLOT OF LINES OF CONSTANT DENSITY. BORDER SHOWS IDEALLY PREDICTED FLOW

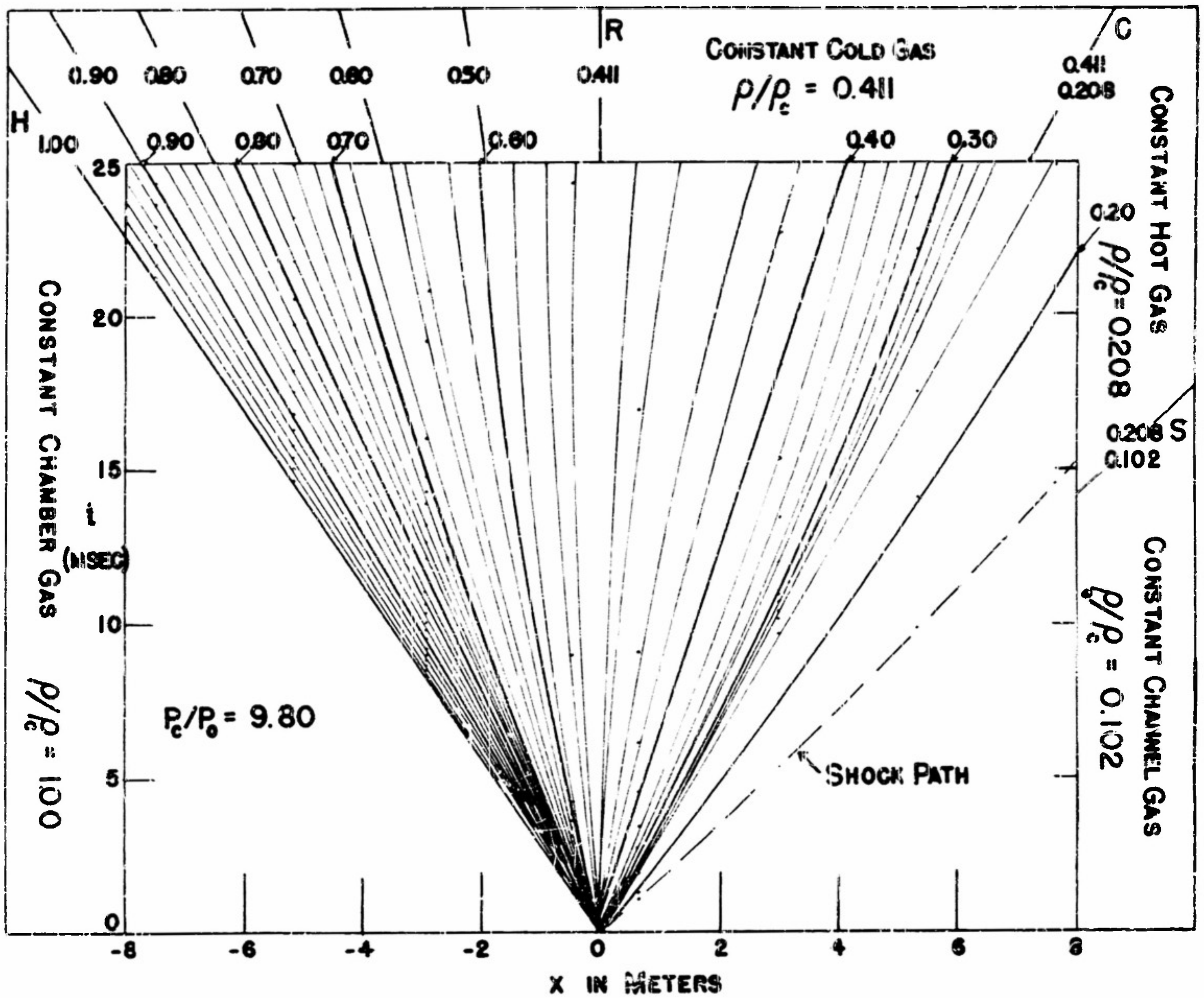

FIG. 34 x-t PLOT OF LINES OF CONSTANT DENSITY (ρ/ρ_c). BORDER SHOWS IDEALLY PREDICTED FLOW

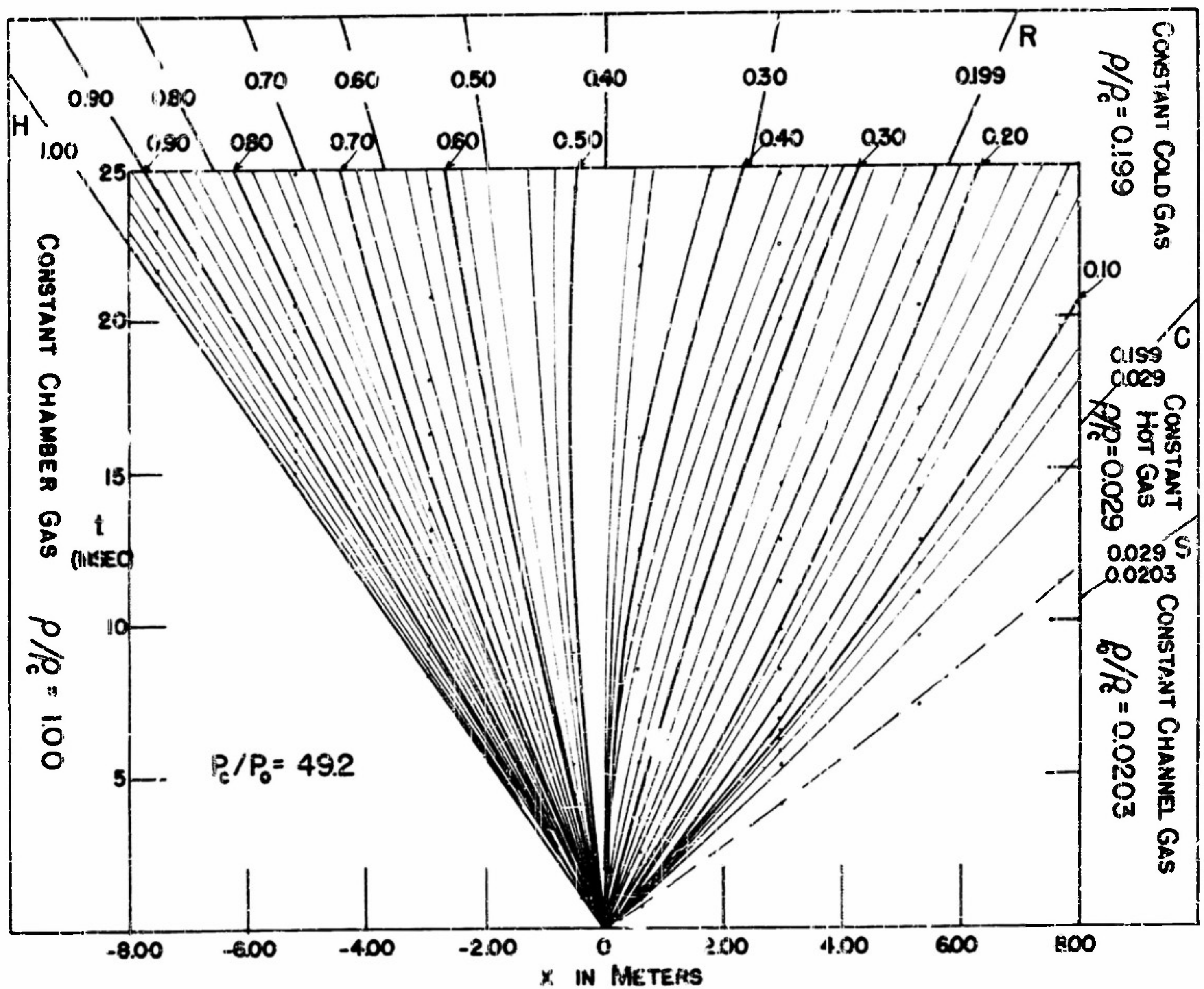

FIG. 35 x-t PLOT OF LINES OF CONSTANT DENSITY (ρ/ρ_c). BORDER SHOWS IDEALLY PREDICTED FLOW

The x-t plots of primary shock tube flows in Figs. 33, 34, and 35 are for the initial conditions P_c/P_o = 1.99, 9.80 and 49.2 respectively. The predictions of ideal theory are shown on the border of each plot; in the interior of the plots, density lines are drawn for density increments of $\rho/\rho c$ = 0.02. Since the shock paths and the path of the rarefaction tail in the case of P_c/P_o = 1.99 are not lines of constant density experimentally, they are shown dotted. After 20 milliseconds of flow the cold front seems to be spread out over 60 tube diameters for P_c/P_o = 9.80 and 49.2.

An x-t plot of the lines of constant density for the rarefaction resulting from the initial condition P_c/P_o = 9.80 is presented on Fig, 36 in order to indicate in another way the large deviation from the postulated centered rarefaction. The theoretical straight line C^- characteristics (Appendix A) are lines of constant density. The shift of the observed lines of constant density from the ideal straight lines is indicated by the small arrows. On this plot are also shown by additional contours the time and the positions at which the amplitude of the irregular density fluctuations attains a value of 0.06 and 0.2 fringe. Density values lying above and to the right of the 0.2 fringe amplitude fluctuation contour were established by the white-light-fringe technique. Contours of equal size fluctuations do not follow a line of constant density.

6.3 Speculation on Dissipative Mechanisms.

a) Hot Gas Region

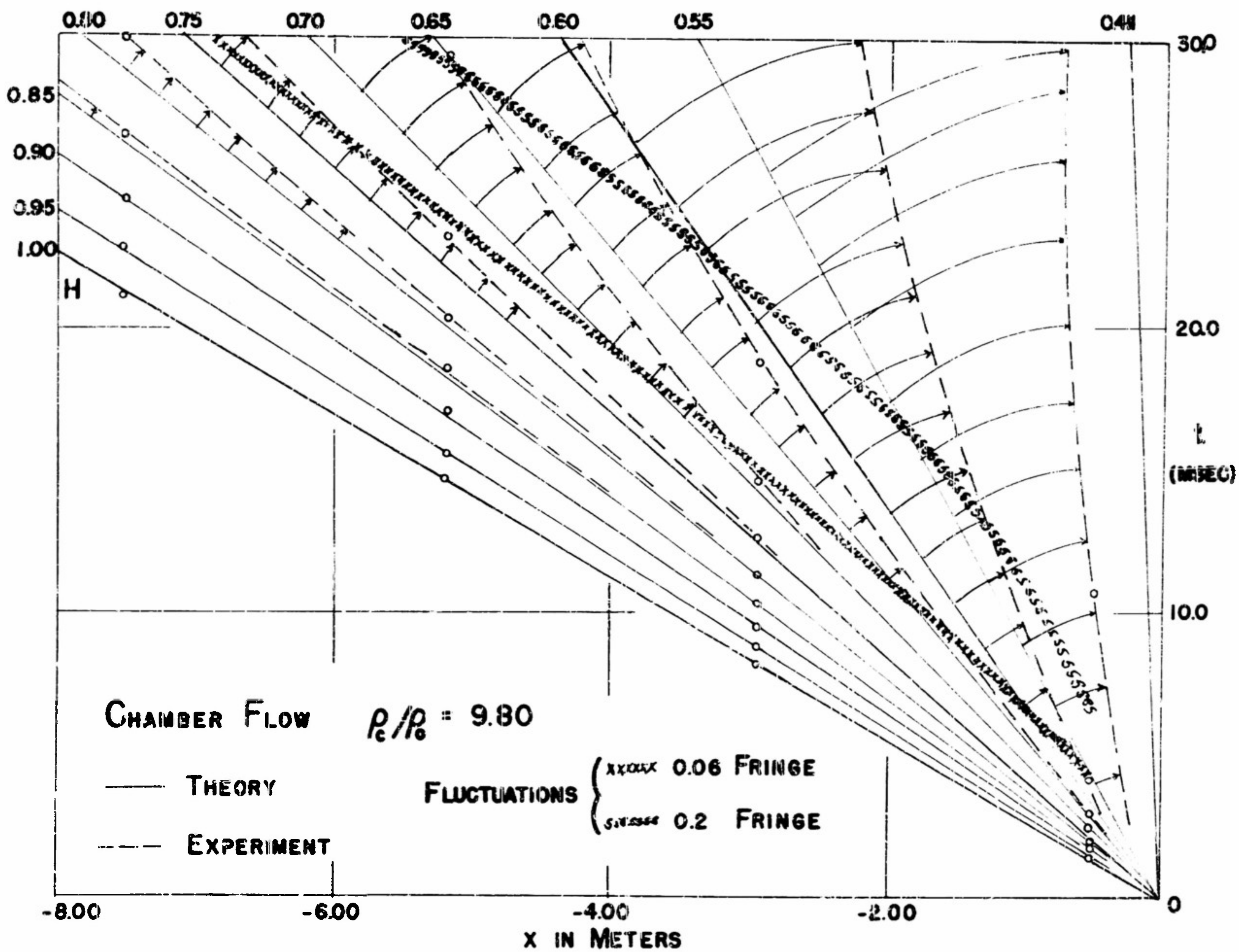

FIG. 36 x - t PLOT OF LINES OF CONSTANT DENSITY

The growth of a boundary layer has been proposed[3-5,23,24,25] as a mechanism for causing deviation from the ideal shock tube flow. Of the various proposals which have been made for attributing non-ideal shock tube behavior to boundary layer growths only that by Hollyer is in a form permitting a prediction to be made of density variation as a function of time. This theory permits the calculation of the average density in the hot gas region as a function of the time t_2 after shock passage from the knowledge of a single parameter y, the shock pressure ratio. The average density in the hot gas region is predicted to increase in proportion to $\sqrt{t_2}$. A direct comparison with the density measurements presented here appears in Fig. 37 for the case $P_c/P_o = 49.2$ at interferometer stations B, C, and D where $y = z + 1 = 4.3$, 3.8, and 3.4 respectively. The theoretical straight lines are calculated from the formula[26]:

$$\delta\rho = \frac{\sqrt{\lambda_o \rho_o}}{2R} \; \frac{y^{1/2}(1 + \mu y)^{1/2}}{\mu(y-1)(\mu + y)^{1/2}} \left[(y-\mu-2)A_2 + 2y(\mu + 1)\frac{\theta'(0)}{\sigma} \right] t_2^{1/2}$$

$$= \frac{\sqrt{\lambda_o \rho_o}}{12R} \; \frac{y^{1/2}(1 + 6y)^{1/2}}{(y-1)(6 + y)^{1/2}} \left[(y-8)A_2 + 14y\frac{\theta'(0)}{\sigma} \right] t_2^{1/2}$$

---

23. Donaldson, and Sullivan, NACA Technical Note 1942 (1949)

24. R. K. Lobb, Phys. Rev. 84, 612 (A) (1951)

25. Huber, McFarland, and [illegible]vine, NACA Research Memorandum SL53D13a (1953)

26. This formula is derived by carrying out the suggested integration of equation (150) on p. 140 of reference 4. As shown in reference 4 the assumption of $\sigma = 1$ leads to a somewhat smaller estimate of heat transfer at the shock tube wall, than results from the more nearly correct value 0.75 for σ.

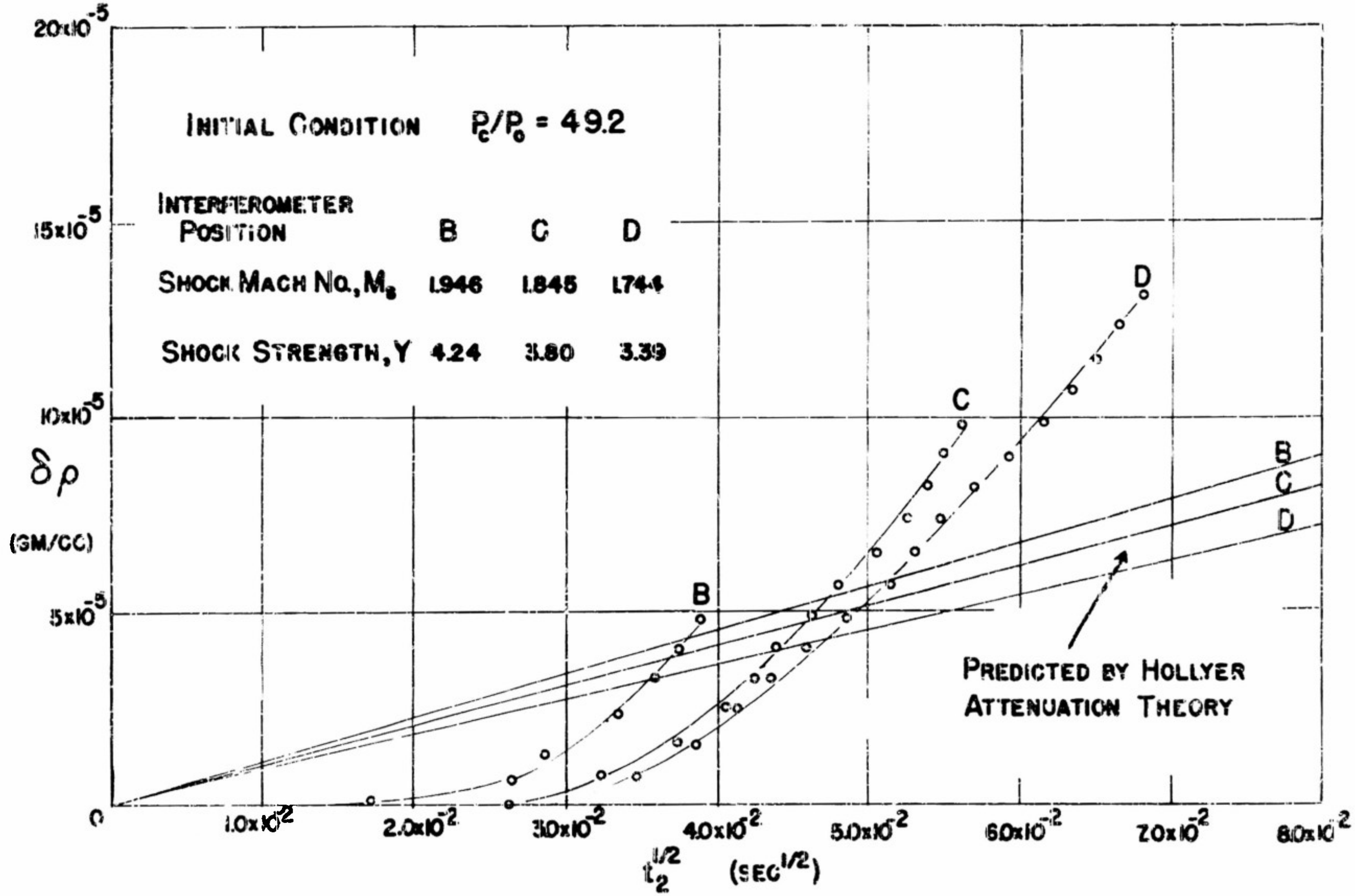

FIG. 37 DENSITY INCREASE IN HOT GAS FOLLOWING PASSAGE OF SHOCK

here:

$\mu = \frac{\gamma-1}{\gamma+1} = 6$ for nitrogen gas,

$R = 0.873$ cm, hydraulic radius of the shock tube,

$\lambda_o = 178.1$ micropoises, viscosity of the undisturbed channel gas,

$\rho_o = 1.154 \times 10^{-4}$ gm/cc, density of the undisturbed channel gas,

σ Prandtl number (assumed constant at 1),

$y = z + 1$, the shock pressure ratio.

The quantity A_2 is given graphically in the reference as a function of y and for the case of $\sigma = 1$ the quantity $\theta'(0)$ is calculated from A_2 and y.

The lack of quantitative agreement between theory and experiment is probably partly attributable to three features observed in the shock tube flow which are not taken into account in the attenuation theory. These features will be mentioned in turn.

In the attenuation theory the flow outside the hot gas region is assumed to be that of the ideal shock tube theory which has adjusted to the perturbed region at the contact surface. Since the cold front spreads out into a region large in comparison to the tube diameter, since there is no region of uniform flow between cold front and rarefaction, and since the rarefaction deviates markedly from a centered rarefaction, this assumption is seriously violated.

The duration of the flow studied may be too great to permit application of the Prandtl boundary layer approximation since the "boundary layer" may fill the tube rather early and free stream flow values may not exist. At Princeton University, Bershader[27] has studied the growth of a transient boundary layer over a flat plate by obtaining flash interferograms at successive times after shock passage. The interferograms show a boundary layer which develops a thickness of about 0.3 inch in a time t_2 = 735 microseconds. The flow conditions (nitrogen gas, z = 4.6) are similar to the case P_c/P_o = 49.2 at station B of this work. If a boundary layer of a similar nature occurs in the cylindrical tube, about half the tube's cross-section would be filled with boundary layer in 1 millisecond.

The assumption of laminar flow in the attenuation theory may not be applicable to a significant fraction of the affected gas.

b) Cold Front Region

The marked change in chrono-interferometer response to the passage of the cold front region with increasing interferometer-to-diaphragm distance can be explained if the surface between hot and cold gas is assumed to acquire an extended paraboloidal shape in the cylindrical tube. As this elongated shape moves across the interferometer position, the chrono-interferometer would yield the observed regular fringe intensity variation with time.

c) Rarefaction Wave

The deviation of the chamber flow from that of a centered rarefaction suggests the action of a dissipative mechanism such

---

27. Bershader, D., Private Communication. Also see Bershader, D., Phys. Rev. <u>91</u>, 470 (A) (1953)

as a boundary layer. The deviations most certainly cannot be accounted for by the assumption that an isentropic non-centered wave is produced as though by an accelerated piston, for an isentropic wave would still be described by straight constant-density lines on an **x-t plot.**

d) Irregular Density Fluctuations

The density fluctuations which begin with small amplitude behind the shock and during the later portions of the rarefaction may represent an instability developing in the flow. It should be noted that the tests upon interferometer windows in the shock tube walls did not conclusively prove that fluctuations were not induced locally by the small remaining recesses in the tube walls. However, observed fluctuations may not be attributable entirely to this cause, and other sources may be mentioned.

The larger fluctuations in the hot gas and the cold gas region which become less noticeable at greater distances from the diaphragm could be attributed to processes associated with diaphragm rupture. In particular the noisy flow conditions at station A for the conditions P_c/P_o = 9.80 and 49.2 could be attributed to secondary waves catching up to the main shock.

By Schlieren spark photographs of the shock reflected from the closed end of the channel, which is moving back into the gas set in motion by the primary shock Hollyer[4] has studied the growth of the boundary layer in the hot gas. On the basis of the shock-boundary layer interaction he classifies the boundary layer as laminar or turbulent and correlates the results with the "Reynold's number per cm", $Re/cm = u\rho/\lambda(T)$; where μ, ρ, and T are calculated from the shock relations and λ the viscosity is obtained from T through Sutherland's formula.[28] Hollyer finds the boundary layer in the 2" x 7" Michigan shock tube to be turbulent for Re/cm > 1.5×10^4 cm^{-1}. All of the flows studied in the presently reported density measurements have Re/cm > 1.5×10^4cm^{-1}. On the basis of this classification the boundary layer would be turbulent, and the prominent fluctuations so consistently observed on the chrono-interferometer records for P_c/P_o = 9.80 and 49.2 flows may represent density fluctuations characteristic of turbulence. The absence of density fluctuations in the P_c/P_o = 1.99 flow and in the early portions of the rarefactions may indicate that the appearance of turbulence in these less rapid flows has a time dependence.

- -

28. $\lambda/\lambda_o = (T/T_o)^{3/2} \dfrac{T_o + 114}{T + 114}$

Sutherland, W. Phil. Mag. 5th series 36, 507 (1893)

VII Conclusions

The chrono-interferometer has been applied successfully to a study of primary shock tube flows. The instrument developed is especially well adapted to the study of waves of finite amplitude and, although it is restricted to use on one-dimensional flows with relatively small density gradients, the instrument has the advantage that there is no effective limitation to the time over which measurements can be made. Two dimensional flows and limited portions of one dimensional flows containing steep density gradients are better studied with a field interferometer employing flash photography.

Compared to field interferometers, the chrono-interferometer is relatively simple to construct and is much less costly since small optical components are employed. However, the optical components must be free of vibration over a relatively long time period during a measurement.

The density measurements of the primary shock-flow have provided a quantitative detailed picture of density distribution in space and time throughout the tube. Measures of the departure from the predicted flow of ideal theory are provided. Although more detail of shock tube flow has been obtained there is still insufficient information available to show conclusively what mechanisms are present and what role they play. When the density measurements were undertaken it seemed possible that a one dimensional description of shock tube flow based upon a perturbation to the ideal theory could be made; however, in view of the large extent of the observed deviations this does not seem feasible for a shock tube of the size in which these measurements were taken.

The author wishes to express his gratitude to Dr. R. J. Emrich for his valuable assistance in initiating and directing this investigation and to Dr. C. W. Curtis for many excellent suggestions and interest in the work described.

In addition, particular thanks are due to Mr. A. Leeming, not only for his excellent machine work but for many helpful suggestions relative to the design of the chrono-interferometer, and to Mr. R. A. Shunk for his help in constructing electronic apparatus and in making the measurements.

APPENDIX A

CENTERED RAREFACTION

The description of finite one-dimensional waves moving in a polytropic gas without dissipation may be found in a number of books and reports[29,30]. Certain relations applying to a centered rarefaction are listed below for convenience.

A centered leftward-facing rarefaction is described by straight-line characteristics C^- drawn in the x-t plane intersecting at the origin. Along any one characteristic, all flow variables (e.g. pressure P, density ρ, local sound speed c, particle speed u) are constant. Among the flow variables there are the following relations:

$$P = A\rho^{\gamma}$$ (isentropic process in ideal gas; γ is ratio of specific heats) (A1)

$$c^2 = \frac{dP}{d\rho} = \gamma A \rho^{\gamma-1}$$ (definition of sound speed) (A2)

$$\frac{u}{2} + \frac{c}{\gamma-1} = \frac{c_0}{\gamma-1}$$ (simple wave; c_o is sound speed in undisturbed gas where u = 0) (A3)

$$\frac{u}{c_0} = \frac{2}{\gamma-1}\left[1 - \left(\frac{P}{P_0}\right)^{\frac{\gamma-1}{2\gamma}}\right]$$ (P_o is pressure in undisturbed gas where u = 0) (A4)

$$\frac{u}{c_0} = \frac{2}{\gamma-1}\left[1 - \left(\frac{\rho}{\rho_0}\right)^{\frac{\gamma-1}{2}}\right]$$ (ρ_o is density in undisturbed gas) (A5)

---

29. For example, Courant and Friedrichs, "Supersonic Flow and Shock Waves", Interscience Publishers, New York (1949)
30. I. I. Glass, Institute of Aerophysics Report No. 9, University of Toronto (1951)

Equation of a characteristic line C^- on which density value is ρ :

$$\frac{x}{t} = u - c = c_0 \left[\frac{2}{\gamma-1} - \frac{\gamma+1}{\gamma-1} \left(\frac{\rho}{\rho_0} \right)^{\frac{\gamma-1}{2}} \right] \tag{A6}$$

which may be solved for the explicit dependence of ρ on x and t

$$\frac{\rho}{\rho_0} = \left(\frac{2}{\gamma+1} - \frac{\gamma-1}{\gamma+1} \frac{x}{c_0 t} \right)^{\frac{2}{\gamma-1}} \tag{A7}$$

valid in the domain $t > 0$, $-c_0 t < x < \dfrac{2c_0}{\gamma-1} t$.

At the point $x = 0$, the flow is sonic ($u = c$) and the density is constant in time with the value

$$\rho_d = \left(\frac{2}{\gamma+1} \right)^{\frac{2}{\gamma-1}} \rho_0 \tag{A8}$$

APPENDIX B

SHOCK RELATIONS

Across a normal shock, such as is created in a shock tube, there are the Rankine-Hugoniot relations which relate all flow variables behind the shock to the flow ahead of the shock through a single "shock strength parameter". Following are the relations which employ the shock strength parameter $y = 1 + z = P/P_o$ the ratio of pressures behind and in front of the shock.[29,31,32]

$$\frac{\rho}{\rho_o} = \frac{(\gamma+1)y + (\gamma-1)}{(\gamma+1) + (\gamma-1)y} \tag{B1}$$

$$\frac{u}{c_o} = \frac{y-1}{\left[\frac{\gamma}{2}\left[(\gamma+1)y + (\gamma-1)\right]\right]^{\frac{1}{2}}} \tag{B2}$$

$$\frac{c}{c_o} = \left[y\,\frac{(\gamma+1) + (\gamma-1)y}{(\gamma+1)y + (\gamma-1)}\right]^{\frac{1}{2}} \tag{B3}$$

The so-called "shock Mach number" $M_s = V/c_o$, the ratio of propagation speed of the shock into undisturbed gas and sound speed in the undisturbed gas is

$$M_s = \frac{V}{c_o} = \left[\frac{(\gamma+1)y + (\gamma-1)}{2\gamma}\right]^{\frac{1}{2}} \tag{B4}$$

---

31. R. N. Hollyer and Otto Laporte, Am. Journ. Phys. 21, 610 (1953)
32. Liepmann and Puckett, "Aerodynamics of a Compressible Fluid", Wiley, New York (1949)

APPENDIX C

SUMMARY OF THE IDEAL SHOCK TUBE THEORY

The idealized theory is summarized in this appendix to emphasize the theoretical density distribution in the shock tube; other treatments[2,5,6,33,34,35] of the flow emphasize pressure or flow Mach number. The mathematical treatment is based upon the following simple wave model. A plane shock and a plane rarefaction form instantly upon bursting of the diaphragm between the chamber and the channel. Subsequently, the rarefaction and the shock propagate from the diaphragm into the chamber and the channel. A contact surface, which is the boundary between the cold gas expanded by the rarefaction and the hot gas compressed by the shock, moves from the diaphragm position with the gas. The theory treats the one-dimensional, adiabatic, and inviscid flow of an ideal polytropic gas.

The wave model of shock-tube flow is fitted by satisfying the discontinuity conditions at the contact surface. This is accomplished by matching both the particle velocity and the pressure between the hot gas behind the shock and the cold gas at the rarefaction tail. We need only equate equation (A4) to equation (B2) thus imposing the conditions

- -

33. Bleakney and Taub, Revs. Modern Phys. 21, 584 (1949)
34. Huber, Fitton, and Delpino, NACA Technical Note 1903 (1949)
35. C. W. Lampson, Tech Note 139, Ballistics Res. Lab. (1950)

that the pressure P and particle speed u behind the shock are equal to the pressure and particle speed respectively at the rarefaction tail. In general the chamber and channel gases need not be the same. Therefore, we will denote channel gas parameters by the subscript o and chamber gas parameters by the subscript 1. Upon equating equations (A4) and (B2) we find that

$$\left(y\frac{P_o}{P_c}\right)^{\frac{\gamma_1-1}{2\gamma_1}} = 1 - \frac{c_o(\gamma_1-1)(y-1)}{c_1\left[2\gamma_o\left[(\gamma_o+1)y+(\gamma_o-1)\right]\right]^{\frac{1}{2}}} \qquad \text{(C1)}$$

where $y = P/P_o$, the shock pressure ratio. From this equation the initial diaphragm pressure ratio needed theoretically to produce a shock with a pressure ratio y can be calculated. If the channel and chamber gases are the same, we have

$$\frac{P_c}{P_o} = \frac{z+1}{\left\{1-\frac{(\gamma-1)z}{\sqrt{2\gamma\left[(\gamma+1)(z+1)+(\gamma-1)\right]}}\right\}^{\frac{2\gamma}{\gamma-1}}} = \frac{z+1}{\left\{1-\frac{z}{\sqrt{7(6z+7)}}\right\}^{7}} \qquad \text{(C2)}$$

where $z = (P-P_o)/P_o$ and in the latter equation the value $\gamma = 7/5$ has been introduced for the ratio of specific heats. The excess pressure ratio z, which we prefer as the shock strength parameter, can be used for expressing the relationship between the flow variations across the shock.

For the same gas composition of known γ in chamber and and channel, the initial diaphragm pressure ratio P_c/P_o, and the initial temperature of the gas in the tube are the only initial data required to determine the density distribution after diaphragm rupture. The formulae necessary to determine the density distribution from a known z are tabulated in Table VI. These formulae determine only the primary flow, i.e., the flow existing before reflection at the closed ends of the shock tube. A more general discussion of shock-tube flow would include the reflected waves; however, since the studies described in this thesis are concerned only with the primary shock-tube flow, the reflected waves are not discussed. A discussion of the reflected phenomena has been given.[36]

The appropriate formulae from Table VI can be used to plot the theoretical density distributions for the initial conditions $P_c/P_o = 50$, and $P_c/P_o = 2$ as shown in Fig. (38a) and (38b), respectively. The tail of the rarefaction (R) moves forward into the channel for the former case and backward into the chamber in the latter case. The density ρ_d is attained at the diaphragm position for the case $P_c/P_o=50$. The shock and contact discontinuities are labeled (S) and (C) respectively. Each of the plots in Fig. 38 are to scale; however the scales are different for the two cases. Figs. (38c) and (38d) are representations of the flow on the (x,t) plane, the dotted lines are typical particle paths which illustrate the difference between the processes occurring in the channel and the chamber. These plots apply to a diatomic gas whose $\gamma = 7/5$.

- -

36. R. K. Lobb, Institute of Aerophysics, Report No. 4, University of Toronto (1950)

TABLE VI

IDEAL THEORY FORMULAE FOR THE DENSITY DISTRIBUTION IN PRIMARY SHOCK TUBE FLOW

$$\frac{\rho_s}{\rho_0} = \frac{(\gamma+1)z + 2\gamma}{(\gamma-1)z + 2\gamma} = \frac{6z+7}{z+7} \qquad \text{(C3)}$$

$$\frac{\rho_h}{\rho_c} = \left(\frac{p}{p_c}\right)^{\frac{1}{\gamma}} = \left[(z+1)\frac{p_0}{p_c}\right]^{\frac{1}{\gamma}} = \left[(z+1)\frac{p_0}{p_c}\right]^{\frac{5}{7}} \qquad \text{(C4)}$$

$$\frac{\rho}{\rho_c} = \left[\frac{2}{\gamma+1} - \frac{\gamma-1}{\gamma+1}\frac{x}{c_0 t}\right]^{\frac{2}{\gamma-1}} = \left[\frac{1}{6}\left(5 - \frac{x}{c_0 t}\right)\right]^{5} \qquad \text{(C5)}$$

where $t > 0$; $-c_0 t < x < \left(\frac{\gamma+1}{2}u - c_0\right)t = \left(\frac{6}{5}u - c_0\right)t$

$$\frac{V}{c_0} = \left(\frac{\gamma+1}{2\gamma}z + 1\right)^{\frac{1}{2}} = \left(\frac{6}{7}z + 1\right)^{\frac{1}{2}} \qquad \text{(C6)}$$

$$\frac{u}{c_0} = \frac{z}{\sqrt{\frac{\gamma}{2}\left[(\gamma+1)z + 2\gamma\right]}} = \frac{5z}{\sqrt{7(6z+7)}} \qquad \text{(C7)}$$

$$\frac{c_{T_h}}{c_0} = \frac{\gamma+1}{2}\frac{u}{c_0} - 1 = \frac{6}{5}\frac{u}{c_0} - 1 \qquad \text{(C8)}$$

The numerical forms of the equations are for a diatomic gas where $\gamma = 7/5$.

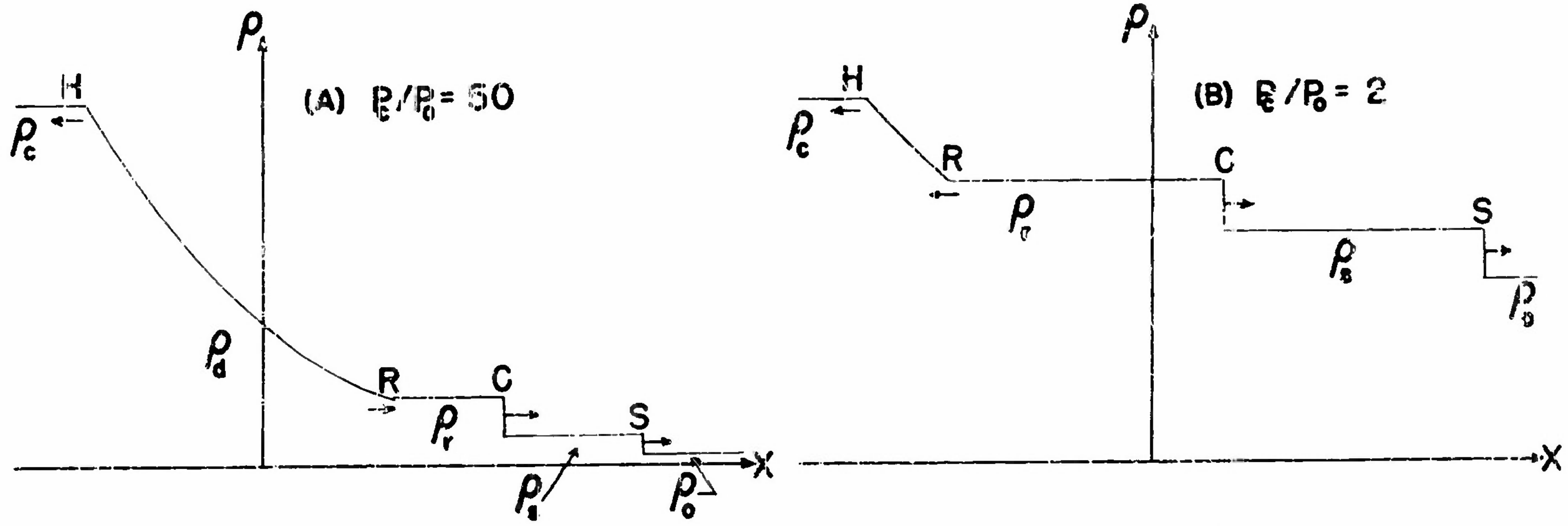

DENSITY DISTRIBUTION AT TIME, t_0, AFTER DIAPHRAGM RUPTURE

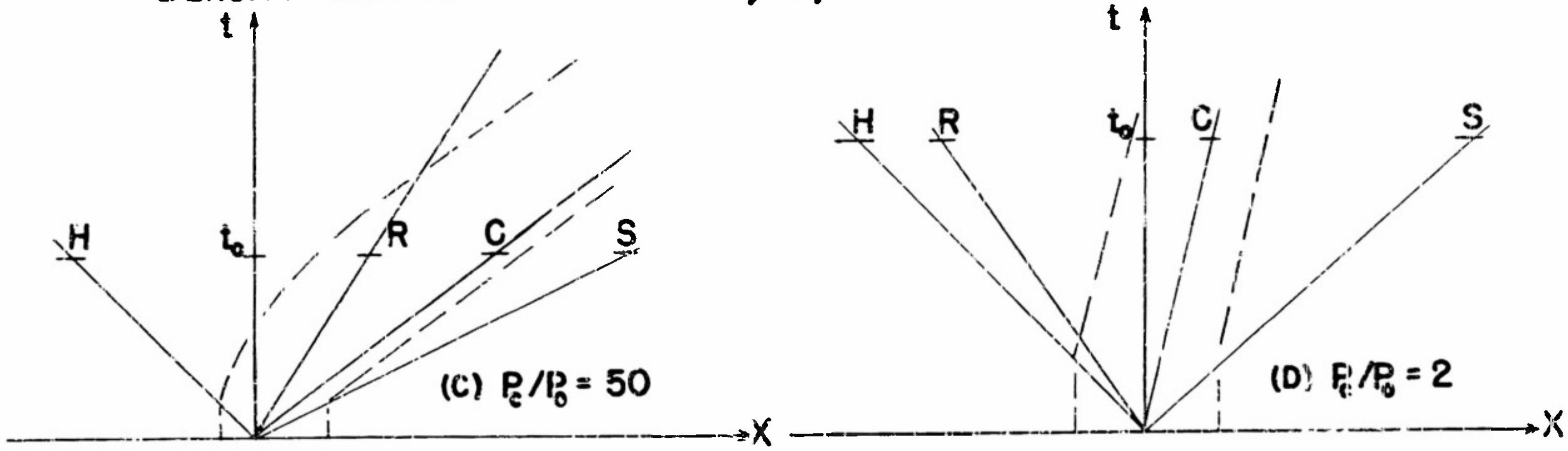

PARTICLE PATHS IN FLOW FOLLOWING DIAPHRAGM RUPTURE

FIG. 38 THEORETICAL PRIMARY SHOCK TUBE FLOW

TABLE VII

SUMMARY OF NOTATION OF APPENDIX C.

c_o	sound speed in the medium ahead of a rarefaction or shock wave.
P	pressure in flow region between shock and tail of rarefaction.
P_o	initial channel pressure ahead of the shock.
P_c	initial chamber pressure.
t	time after diaphragm bursts.
u	particle velocity in flow region between shock and tail of rarefaction.
V	shock velocity.
v_r	velocity of tail of rarefaction.
x	distance along tube, origin at diaphragm position, positive in the channel.
y	pressure ratio, P/P_o, across shock.
z	excess pressure ratio, $(P-P_o)/P_o$ across shock.
γ	ratio of specific heat at constant pressure to that at constant volume.
γ_o	ratio of specific heats of channel gas.
γ_1	ratio of specific heats of chamber gas.
ρ	gas density.
ρ_o	initial channel gas density.
ρ_c	initial chamber gas density.
ρ_r	density of cold gas between cold front and tail of rarefaction.
ρ_s	density of hot gas between shock and cold front.

APPENDIX D

SAMPLE REDUCTION OF DATA

The case of $P_c/P_o = 9.80$ with the interferometer at station B has been chosen for a sample data reduction to illustrate the nature of the data analysis. The results of the reduction illustrated are plotted in Figs. 22 and 30. The initial data for this representative case are given in Table VIII.

TABLE VIII

INITIAL DATA FOR $P_c/P_o = 9.80$, STATION B

	Film Number		P_c	P_o	P_c/P_o	T_o	$\Delta S_{w.l.f.}$
	C.I.F.	Shock Time	cm. of Hg.	cm. of Hg.		°C	
	L114	646	378.4	38.43	9.85	24.5±0.6	
Channel	L117	649	378.5	38.72	9.78	25.1±0.3	18.0
	L118	650	378.3	38.67	9.78	25.3±0.2	50.8
Flow	L119	651	378.3	38.86	9.73	25.5±0.4	39.8
	L120	652	378.3	38.82	9.74	23.8±0.2	31.2
	L134	668	378.6	38.51	9.83	22.9±0.3	
Chamber	L138	672	378.5	38.44	9.85	24.9±0.3	65.9
Flow	L139	673	378.5	38.44	9.85	24.9±0.3	65.9

Legend. C.I.F. - Chrono-Interferometer record
Shock Time-Shock arrival record
P_c - Initial Chamber Pressure
P_o - Initial Channel Pressure

T_o - Average of temperature along tube with mean deviation

$\Delta S_{w.l.f.}$ - Zeroth fringe density with o and c respectively channel and chamber reference.

The results obtained from the plots of the shock path data and the derived shock Mach number are summarized in Table IX. These data determine $(\Delta\rho/\rho_o)_s$, and τ_s for the case of channel flow.

TABLE IX

DATA FROM SHOCK PATH RECORDS

Film Number	Shock Arrival Time t (msec)	Shock Mach No. at B M_s	$\tau_s = \frac{c_o t}{d}$	$(\Delta\rho/\rho_o)_s$
646	5.40	1.514	0.6426	0.886
649	5.39	1.510	0.6425	0.879
650	5.38	1.511	0.6413	0.881
651	5.41	1.513	0.6454	0.884
652	5.41	1.512	0.6433	0.883

$$(\Delta\rho/\rho_o)_s = \frac{5(M_s^2-1)}{M_s^2+5} \qquad c_o = 352.5 \text{ m/sec}$$

$$d = 2.965 \text{ m}$$

Some of measurements from the interferometer records of channel flow, along with the derived values of $\Delta\rho/\rho_o$ and τ are given in Table X. In the hot gas region between shock and cold front a linear correction for the deviation of the initial P_c/P_o from the average value 9.80 was applied. The correction to $\left(\frac{\Delta\rho}{\rho_o}\right)_s$ is given by

$$\delta\left(\frac{\Delta\rho}{\rho_o}\right)_s = 0.050\ (9.80 - P_c/P_o)$$

The correction to τ at the shock is

$$\delta\tau_s = 0.012\ (P_c/P_o - 9.80)$$

The correction to τ at the cold front is

$$\delta\tau_c = 0.054\ (P_c/P_o - 9.80)$$

These linear corrections are based upon the idealized shock tube theory.

TABLE X

REDUCTION OF CHANNEL FLOW DATA

Film Number	Fringe Count ΔS	Time t_2	$\Delta\rho/\rho_o$	τ
	Relative to shock	Relative to shock (m sec)		
L114	0	0	0.8835	0.6432
	2 1/2	3.05	1.0253	1.008
	4 1/2	4.15	1.138	1.139
	cold front arrival	4.25	-	1.175
L117	0	0	0.8835	0.6423
	2 1/5	2.96	1.003	0.9945
	4 1/5	4.21	1.116	1.143
	cold front arrival	4.26	-	1.155
L118	50.8$\pm$1	12.0	2.874	2.27
L119	39.8$\pm$1	6.2	2.234	1.381
L120	31.2$\pm$1	5.3	1.756	1.270

$$\frac{\Delta\rho}{\rho_c} = \left(\frac{\Delta\rho}{\rho_c}\right)_s + \frac{T_c}{T_1}\left(\frac{\Delta P}{\Delta S}\right)_1 \frac{\Delta S}{P_c} \quad , \tau = \tau_s + \frac{c_o t_2}{d}$$

Representative measurements from the interferometer records of chamber flow with the derived values of ρ/ρ_c and τ are given in Table XI.

TABLE XI

REDUCTION OF CHAMBER FLOW DATA

Film Number	Fringe Count ΔS from wave head	Time t_1 (m sec) from wave head	ρ/ρ_c	τ
L134	0	0	1.000	1.000
	12	0.84	0.9314	1.1003
	24	1.85	0.8627	1.2209
	36	3.20	0.7941	1.3821
	48	5.33	0.7254	1.6364
	57	8.23	0.6740	1.9824
	61	11.58	0.6511	2.3810
L138	65.9$\pm$2	21.4	0.620	3.58
L139	65.9$\pm$2	21.5	0.620	3.59

$$\frac{\rho}{\rho_c} = 1 - \frac{T_c}{T_1}\left(\frac{\Delta P}{\Delta S}\right)_1 \frac{\Delta S}{P_c} \quad , \tau = 1 + \frac{c_o t_1}{d}$$

Bibliography

Barrell, H. and Sears, J. E., "The Refraction and Dispersion of Air for the Visible Spectrum," Phil. Trans. A238, 1 (1939)

Bershader, D., "Interferometric Study of Supersonic Channel Flow," Rev. Sci. Instr. 20, 260 (1949)

Bershader, D., "Shock Tube Studies of Transient Boundary Layers in Compressible Flow" Phys. Rev. 91 470 (A) (1953)

Bleakney, W., Weimer, D. K., and Fletcher, C. H. "The Shock Tube: A Facility for Investigations in Fluid Dynamics," Rev. Sci. Instr. 20 807 (1949)

Courant, R. and Friedrichs, K. O., "Supersonic Flow and Shock Waves," Interscience Publishers, New York (1948)

Curtis, C. W., Emrich, R. J., and Mack, J., "A Chrono-Interferometer for Measuring Gas Density During Transient Flow," to be published

Emrich, R. J. and Curtis, C. W., "Attenuation in the Shock Tube," J. Appl. Phys. 24, 360 (1953)

Gale, H. G., "On the Relation Between Density and Index of Refraction of Air", Phys. Rev. 14, 1 (1902)

Geiger, F. W. and Mautz, C. W., "The Shock Tube as an Instrument for the Investigation of Transonic and Supersonic Flow", Engineering Institute Report, University of Michigan (1949)

Gladstone, J. H. and Dale, T. P. "Researches on the Refraction, Dispersion, and Sensitiveness of Liquids", Phil. Trans. 153 317 (1863)

Glass, I. I., "An Experimental Determination of the Speed of Sound in Gases from the Head of a Rarefaction Wave", Institute of Aerophysics Report No. 9, University of Toronto (1951)

Glass, I. I., "The Design of a Wave Interaction Tube", Institute of Aerophysics Report No. 6, University of Toronto (1950)

Hollyer, R. N., Jr., "A Study of Attenuation in the Shock Tube", Engineering Research Institute Report, University of Michigan (1953)

Huber, P. W., Fitton, C. W., Jr., and Delpino, F., "Experimental Investigation of Moving Pressure Disturbances and Shock Waves and Correlation with One-Dimensional Unsteady-Flow Theory," NACA TN 1903, (1949)

Laponsky, A. B., "Observation of Shock Formation and Growth", Institute of Research Report TR1, Lehigh University (1951)

Lobb, R. K., "A Study of Supersonic Flows in a Shock Tube," Institute of Aerophysics Report No. 8, University of Toronto (1950)

Shunk, R. A., Dranetz, A. I., and Budenstein, P. P., "Ring Shaped Piezoelectric Gauge for Shock Tube," Shop Note, Rev. Sci. Instr. 24 1069 (1953)

Winckler, J., "Mach Interferometer Applied to Studying an Axillary Symmetric Supersonic Air Jet," Rev. Sci. Instr. 19, 307, (1948)

Collateral References

Bleakney, W. and Taub, A. H., "Interaction of Shock Waves," Revs. Modern Phys. 21, 584 (1949)

Chapman, D. R., and Rubesin, M. W., "Temperature and Velocity Profiles in the Compressible Laminar Boundary Layer with Arbitrary Distribution of Surface Temperature," J. Aero. Sci. 16, 547 (1949)

Donaldson, C. duP., and Sullivan, R. D., "The Effect of Wall Friction on the Strength of Shock Waves in Tubes and Hydraulic Jumps in Channels," NACA Technical Note 1942 (1949)

Elmore, W. C. and Sands, M., "Electronics", McGraw-Hill, New York (1949)

Huber, P, W., McFarland, D. R., and Levine, P., "Investigation of the Attenuation of Plane Shock Waves Moving Over Very Rough Surfaces," NACA Technical Memorandum SL53D13a, (1953)

Ladenburg, R., Winckler, J., and Van Voorhis, C. C., "Interferometric Studies of Faster than Sound Phenomena Part I." Phys. Rev. 73, 1359 (1948)

Lamb, H., "Hydrodynamics" Dover Publications, New York (1945)

Lampson, C. W., "Resume of the Theory of Plane Shock and Adiabatic Waves with Applications to the Theory of the Shock Tube," Tech. Note 139 Ballistic Res. Lab. (1950)

Liepmann, H. W. and Puckett, A. E., "Aerodynamics of a Compressible Fluid," Wiley, New York (1947)

Lobb, R. K., "On the Length of a Shock Tube", Institute of Aerophysics Report No. 4, University of Toronto (1950)

Lobb, R. K., "Growth of a Laminar Boundary Layer Behind a Shock Wave," Phys. Rev. 84, 612 (A) (1951)

Sutherland, W., "Viscosity of Gases and Molecular Force," Phil. Mag. 5th Series 36 507 (1893)

Taylor, G. I. and Maccoll, J. W., "The Mechanics of Compressible Fluids", Aerodynamic Theory Vol. III, Durand Reprint Committee, California Institute of Technology (1943)

Wegener, P. and Lundquist, G. "Condensation of Water Vapor in the Shock Tube Below 150°K," Letter, J. Appl. Phys. 22, 233 (1951)

Zimm, B. H., "Apparatus and Methods for Measurement and Interpretation of the Angular Variation of Light Scattering" J. Chem. Phys. 16, 1099 (1949)

APPROVED DISTRIBUTION LIST FOR

UNCLASSIFIED TECHNICAL REPORTS ISSUED UNDER

CONTRACT N7onr 39302

PROJECT NR 061-063

Chief of Naval Research
Department of the Navy
Washington 25, D. C.
Attn: Code 438 (2)

Commanding Officer
Office of Naval Research
Branch Office
150 Causeway Street
Boston, Mass. (0)

Commanding Officer
Office of Naval Research
Branch Office
The John Crerar Library Bldg.
86 East Randolph Street
Chicago 1, Illinois (1)

Commanding Officer
Office of Naval Research
Branch Office
346 Broadway
New York 13, New York (1)

Commanding Officer
Office of Naval Research
Branch Office
1030 East Green Street
Pasadena 1, California (1)

Commanding Officer
Office of Naval Research
Branch Office
[illegible] Geary Street
San Francisco 24, Calif. (1)

Commanding Officer
Office of Naval Research
Navy no. 100, Fleet Post Office
New York, New York (2)

Director
Naval Research Laboratory
Washington 25, D. C.
Attn: Code 2021 (6)

Documents Service Center
Armed Services Technical
Information Agency
Knott Building
Dayton 2, Ohio (5)

Chief, Bureau of Aeronautics
Department of the Navy
Washington 25, D. C.
Attn: Research Division (1)

Chief, Bureau of Ordnance
Department of the Navy
Washington 25, D. C.
Attn: Research and Development Division (1)

Office of Ordnance Research
Department of the Army
Washington 25, D. C. (1)

Commander
Air Research and Development Com.
Office of Scientific Research
P. O. Box 1395
Baltimore 18, Maryland
Attn: Fluid Mechanics Div. (1)

Director of Research
National Advisory Committee
for Aeronautics
1724 F Street, Northwest
Washington 25, D. C. (1)

Director
Langley Aeronautical Laboratory
National Advisory Committee
for Aeronautics
Langley Field, Virginia (1)

Director
National Bureau of Standards
Washington 25, D. C.
Attn: Fluid Mechanics Sec. (1)

Professor R. Courant
Institute for Mathematics and
Mechanics
New York University
45 Fourth Avenue
New York 3, New York (1)

Professor G. Kuerti
Department of Mechanical
Engineering
Case Institute of Technology
Cleveland, Ohio (1)

Professor W. R. Sears, Director
Graduate School of Aeronautical
Engineering
Cornell University
Ithaca, New York (1)

Commanding Officer
Naval Ordnance Laboratory
White Oak, Maryland
Attn: Aeroballistics Research
Department (1)

Commanding Officer and Director
David Taylor Model Basin
Washington 7, D. C.
Attn: Aerodynamics Lab. (1)

Ballistics Research Laboratory
Department of the Army
Aberdeen Proving Ground
Aberdeen, Maryland
Attn: Mr. R. H. Kent (1)

Professor F. H. Clauser
Department of Aeronautics
Johns Hopkins University
Baltimore 18, Maryland (1)

Professor J. R. Markham
Department of Aeronautical
Engineering
Mass. Institute of Technology
Cambridge 39, Mass. (1)

Professor J. F. Ludloff
Guggenheim School of Aeronautics
New York University
New York 53, New York (1)

Professor A. Kantrowitz
Graduate School of Aeronautical
Engineering
Cornell University
Ithaca, New York (1)

Dr. R. W. Perry
ARO Inc.
Arnold Engineering Development
Center
Tullahoma, Tennessee (1)

Dr. A. T. Ellis
Hydrodynamics Laboratory
California Institute of Tech.
Pasadena, California (1)

Commanding General
Hdqs., Air Materiel Command
Wright-Patterson Air Force Base
Dayton, Ohio
Attn: MCHIXD4 (1)

Chief, Bureau of Ordnance
Department of the Navy
Washington 25, D. C.
Attn: Code Re2c (1)

Commanding Officer
Naval Ordnance Laboratory
White Oak, Maryland
Attn: Hyperballistics Div. (1)

Ballistics Research Laboratory
Department of the Army
Aberdeen Proving Ground
Aberdeen, Maryland
Attn: Mr. C. W. Lampson (1)

Exterior Ballistics Laboratory
Department of the Army
Aberdeen Proving Ground
Aberdeen, Maryland
Attn: Mr. F. D. Bennett (1)

Professor J. Kestin
Division of Engineering
Brown University
Providence 12, Rhode Island (1)

Graduate Division of Applied
Mathematics
Brown University
Providence 12, Rhode Island (1)

Professor D. F. Hornig
Metcalf Research Laboratory
Brown University
Providence 12, Rhode Island (1)

Professor Hsue-Shien Tsien
Guggenheim Jet Propulsion Center
California Institute of Tech.
Pasadena 4, California (1)

Professor M. S. Plesset
Hydrodynamics Laboratory
California Institute of Tech.
Pasadena 4, California (1)

Professor A. B. Arons
Department of Physics
Amherst College
Amherst, Mass. (1)

Professor Walker Bleakney
Palmer Physical Laboratory
Princeton University
Princeton, New Jersey (1)

Professor George F. Carrier
Department of Engin. Sciences
Harvard University
Pierce Hall
Cambridge 38, Mass. (1)

Dr. R. N. Hollyer, Jr.
Applied Physics Laboratory
Johns Hopkins University
8621 Georgia Avenue
Silver Spring, Maryland (1)

Professor H. G. Stever
Department of Aeronautical Engineering
Mass. Institute of Technology
Cambridge 39, Mass. (1)

Professor R. G. Stoner
Department of Physics
Pennsylvania State University
State College, Pennsylvania (1)

Professor S. F. Borg
Department of Civil Engin.
Stevens Institute of Technology
711 Hudson Street
Hoboken, New Jersey (1)

Professor E. L. Resler
Institute for Fluid Dynamics and Applied Mathematics
University of Maryland
College Park, Maryland (1)

Professor Otto Laporte
Engineering Research Institute
East Engineering Building
University of Michigan
Ann Arbor, Michigan (1)

Professor J. G. Kirkwood
Department of Chemistry
Yale University
New Haven, Conn. (1)

Mr. K. L. Sandefur
Department of Physics
Midwest Research Institute
4049 Pennsylvania Avenue
Kansas City, Missouri (1)

Dr. S. J. Fraenkel
Armour Research Institute
Illinois Institute of Technology
Chicago 16, Illinois (1)

Chief, Bureau of Aeronautics
Department of the Navy
Washington 25, D. C.
Attn: Airframe Design Div. (1)

Chief, Bureau of Ordnance
Department of the Navy
Washington 25, D. C.
Attn: Code Re9a (1)

Commanding Officer
Naval Ordnance Laboratory
White Oak, Maryland
Attn: Aerophysics Division (1)

Commander
Naval Ordnance Test Station
Inyokern
China Lake, California (1)

Director
Ames Aeronautical Laboratory
National Advisory Committee for Aeronautics
Moffett Field, California (1)

Director
Lewis Flight Propulsion Laboratory
National Advisory Committee for Aeronautics
21000 Brookpark Road
Cleveland 11, Ohio (1)

Professor A. Ferri
Department of Aeronautical Engineering and Applied Mechanics
Polytechnic Institute of Brooklyn
99 Livingston Street
Brooklyn 2, New York (1)

Brown University
Graduate Division of Applied Mathematics
Providence 12, Rhode Island (1)

Professor P. F. Maeder
Division of Engineering
Brown University
Providence 12, Rhode Island (1)

California Institute of Tech.
Guggenheim Aeronautical Lab.
Pasadena 4, California
Attn: Prof. P. A. Lagerstrom(1)
Prof. L. Lees (1)
Prof. H. W. Liepmann(1)

Professor S. Corrsin
Department of Aeronautical Eng.
Johns Hopkins University
Baltimore 18, Maryland (1)

Dr. F. N. Frenkiel
Applied Physics Laboratory
Johns Hopkins University
8621 Georgia Avenue
Silver Spring, Maryland (1)

Professor C. C. Lin
Department of Mathematics
Mass. Institute of Technology
Cambridge 39, Mass. (1)

Mass. Institute of Technology
Department of Mechanical Eng.
Cambridge 39, Mass.
Attn: Prof. J. Kaye (1)
Prof. A. H. Shapiro(1)
Prof. E. S. Taylor (1)

Professor H. G. Lew
Department of Aeronautical
Engineering
Pennsylvania State University
State College, Pennsylvania(1)

Stanford University
Guggenheim Aeronautical Lab.
Stanford, California (1)

Professor S. A. Schaaf
Low Pressures Research Project
University of California
Berkeley, California (1)

Dean L. M. K. Boelter
University of California
Los Angeles 24, California(1)

Institute for Fluid Dynamics
and Applied Mathematics
University of Maryland
College Park, Maryland (1)

Professor A. M. Kuethe
Department of Aeronautical Eng.
University of Michigan
Ann Arbor, Michigan (1)

Professor J. D. Akerman
Department of Aeronautical Eng.
University of Minnesota
Minneapolis 14, Minnesota (1)

University of Washington
Department of Aeronautical Eng.
Seattle, Washington (1)

Professor C. H. Fletcher
Department of Aeronautical Eng.
University of Illinois
Urbana, Illinois (1)

Professor M. J. Thompson
Defense Research Laboratory
University of Texas
Austin, Texas (1)

Professor R. P. Harrington
Department of Aeronautical Eng.
Rensselaer Polytechnic Institute
Troy, New York (1)

Director
Jet Propulsion Laboratory
California Institute of Technology
Pasadena 4, California (1)

Professor J. V. Charyk
Forrestal Research Center
Princeton University
Princeton, New Jersey (1)

Professor S. M. Bogdonoff
Department of Aeronautical Eng.
Princeton University
Princeton, New Jersey (1)

Professor M. U. Clauser
Department of Aeronautical Eng.
Purdue University
Lafayette, Indiana (1)